COMPARATIVE STUDY OF NANOPARTICLES AND ALCOHOLIC FUEL ADDITIVES WITH OPTIMIZED SYNTHESIS OF PALM-SESAME BIODIESEL USING TRIBOLOGICAL AND INTERNAL COMBUSTION ENGINE TESTING

MUHAMMAD MUJTABA ABBAS

FACULTY OF ENGINEERING
UNIVERSITY OF MALAYA
KUALA LUMPUR

2021

COMPARATIVE STUDY OF NANOPARTICLES AND ALCOHOLIC FUEL ADDITIVES WITH OPTIMIZED SYNTHESIS OF PALM-SESAME BIODIESEL USING TRIBOLOGICAL AND INTERNAL COMBUSTION ENGINE TESTING

MUHAMMAD MUJTABA ABBAS

THESIS SUBMITTED IN FULFILMENT OF THE REQUIREMENTS FOR THE DEGREE OF DOCTOR OF PHILOSOPHY

FACULTY OF ENGINEERING
UNIVERSITY OF MALAYA
KUALA LUMPUR

2021

UNIVERSITY OF MALAYA

ORIGINAL LITERARY WORK DECLARATION

Name of Candidate: Muhammad Mujtaba Abbas

Matric No: KVA180053

Name of Degree: Doctor of Philosophy

Title of Thesis: Comparative study of nanoparticles and alcoholic fuel additives with optimized synthesis of Palm-Sesame biodiesel using tribological and internal combustion engine testing

Field of Study: Energy

I do solemnly and sincerely declare that:

(1) I am the sole author/writer of this Work;
(2) This work is original;
(3) Any use of any work in which copyright exists was done by way of fair dealing and for permitted purposes and any excerpt or extract from, or reference to or reproduction of any copyright work has been disclosed expressly and sufficiently and the title of the Work and its authorship have been acknowledged in this Work;
(4) I do not have any actual knowledge nor do I ought reasonably to know that the making of this work constitutes an infringement of any copyright work;
(5) I hereby assign all and every rights in the copyright to this Work to the University of Malaya ("UM"), who henceforth shall be owner of the copyright in this Work and that any reproduction or use in any form or by any means whatsoever is prohibited without the written consent of UM having been first had and obtained;
(6) I am fully aware that if in the course of making this Work I have infringed any copyright whether intentionally or otherwise, I may be subject to legal action or any other action as may be determined by UM.

Candidate's Signature Date: 10-11-2021

Subscribed and solemnly declared before,

Witness's Signature Date: 10-11-2021

Name:

Designation

COMPARATIVE STUDY OF NANOPARTICLES AND ALCOHOLIC FUEL ADDITIVES WITH OPTIMIZED SYNTHESIS OF PALM-SESAME BIODIESEL USING TRIBOLOGICAL AND INTERNAL COMBUSTION ENGINE TESTING

ABSTRACT

The demand for renewable energy is steadily increasing due to the rise in population, economic development, and environmental issue globally. Renewable energy sources are now considered better replacements for fossil fuels. Meanwhile, up to 20% of liquid fuels such as methyl esters are currently being blended with petroleum fuels. Recently, the commercialization of biodiesel is a significant challenge due to its poor cold flow properties and oxidative stability. Poor cold flow properties and oxidative stability can be improved by selecting suitable vegetable oils for producing different blends. Among all available vegetable oils, sesame seed oil (SSO) has unique cold flow properties and oxidation stability. This research aimed to improve the cold flow, lubricity, and diesel engine characteristics of biodiesel produced from the palm-sesame oil blends. Response Surface Methodology (RSM) and Extreme Learning Machine (ELM) techniques were used to develop the production process, and the input variables (time, catalyst amount, methanol to oil ratio, and duty cycle) were optimized. The optimum yield of P50S50 (50% palm + 50% sesame) biodiesel obtained was 96.61 % under operating parameters such as time (38.96 min), duty cycle (59.52 %), methanol to oil ratio (60 V/V %), and catalyst amount (0.70 wt.%). The cold flow characteristics of P50S50 biodiesel were significantly improved, such as cloud point (7.89 ℃), pour point (3.80 ℃), and cold filter plugging point (− 1.77 ℃) with better oxidation stability of 6.89 h. During the test run, the friction coefficient was measured directly using the high-frequency reciprocating rig (HFRR). The results exhibited that B10 (Malaysian commercial diesel) demonstrated a poor coefficient of friction and wear scar diameter compared with other tested fuels. The addition of ethanol as a fuel additive in the B30 fuel sample reduced fuel lubricity and

increased the wear and friction coefficient compared with other fuel additives. B30 fuel with titanium oxide (TiO_2) nanoparticles exhibited improved results with the minimum wear scar diameter and lowest friction coefficient among all other fuel samples. Dilution of engine oil with unburned fuels changes its lubricity and tribological properties. Lubricating oil diluted with B10 showed a high coefficient of friction (COF) with severe abrasive and adhesive wear compared with mineral lubricant, among other fuels. Lubricant+B30+TiO_2 showed the minimum increase in COF value among all other modified fuels compared to SAE-40 mineral lubricant. Engine performance and emissions characteristics were studied using a compression ignition (CI) diesel engine with variable engine rpm at full load conditions. The results were compared with B30 and B10 fuels. The main findings indicated that the B30+TiO_2 ternary blend showed an overall decrease in brake-specific fuel consumption compared with other tested fuels. B30+DMC produced higher brake thermal efficiency, among other fuels. B30+DMC ternary blend showed a reduction in carbon monoxide (CO) and hydrocarbons (HC) emissions compared to B30. B30+CNT ternary blend showed a slight decrease in nitrogen oxide (NO_x) emissions compared to B30. The research suggests that Palm-Sesame biodiesel with fuel additives is a suitable replacement for diesel fuel in compression ignition engines without engine modification.

Keywords: Palm-sesame biodiesel; Tribology; Engine characteristics; Fuel additives; optimization

KAJIAN PERBANDINGAN NANOPARTIKEL DAN TAMBAHAN BBM ALKOHOLIK DENGAN SINTESIS OPTIMAL BIODIESEL PALM-SESAME DENGAN MENGGUNAKAN UJIAN ENGINE TRIBOLOGI DAN DALAMAN

ABSTRAK

Permintaan terhadap tenaga boleh dibaharui semakin meningkat berikutan peningkatan populasi, perkembangan ekonomi, dan isu berkenaan alam sekitar seluruh dunia. Sumber tenaga boleh dibaharui sekarang dianggap sebagai pengganti yang lebih baik kepada bahan api fosil. Selain itu, sehingga 20% bahan api cecair seperti ester metil kini digaul Bersama bahan api petroleum. Baru-baru ini, pemerdagangan biodiesel adalah cabaran besar oleh kerana sifat aliran sejuk dan juga stabiliti pengoksidaannya yang lemah. Sifat aliran sejuk dan stabiliti pengoksidaan yang lemah boleh dipertingkatkan dengan memilih minyak sayuran yang sesuai untuk menghasilkan campuran yang berbeza. Antara minyak sayuran yang tersedia, minyak bijan mempunyai sifat aliran sejuk dan juga stabiliti pengoksidaan yang unik. Tujuan kajian ini adalah untuk meningkatkan sifat aliran sejuk, pelinciran dan juga ciri-ciri enjin diesel menggunakan biodiesel yang dihasilkan dari campuran minyak kelapa sawit-bijan. *Respond Surface Methodology (RSM)* dan juga *Extreme Machine Learning (ELM)* telah digunakan untuk membangunkan proses penghasilan, dan pembolehubah input (masa, jumlah pemangkin, nisbah minyak kepada methanol, dan kitaran tugas) telah dioptimumkan. Hasil yang optimum bagi biodiesel P50S50 (50% kelapa sawit + 50% bijan) didapati adalah 96.61% menggunakan parameter operasi seperti masa (38.96 min), kitaran tugas (59.52 %), nisbah methanol kepada minyak (60 V/V%) dan jumlah pemangkin (0.70 wt.%). Ciri-ciri aliran sejuk bagi biodiesel P50S50 telah ditingkatkan secara signifikan seperti titik kabus (7.89 °C), titik tuang (3.80 °C), dan titik penyumbat penapis sejuk (1.77 °C) dengan stabiliti pengoksidaan yang lebih baik iaitu 6.89 jam. Menerusi ujian tribologi, pekali geseran telah diukur secara terus menggunakan rig resiprokasi frekuensi tinggi. Keputusan menunjukkan bahawa B10 (diesel komersil di Malaysia) mempunyai pekali

geseran dan diameter parut haus yang teruk berbanding bahan-bahan api lain yang turut dikaji. Penambahan ethanol sebagai bahan tambah ke dalam sampel bahan api B30 telah menerukkan sifat pelinciran dengan meningkatkan kadar haus dan juga pekali geseran jika dibandingkan dengan bahan tambah bahan api yang lain. Bahan api B30 dengan nanopartikel titanium oxide (TiO_2) menunjukkan hasil penambahbaikan dengan diameter parut haus yang minimum dan juga pekali geseran yang paling rendah diantara semua sampel-sampel bahan api. Pencairan minyak pelincir dengan bahan api belum dibakar telah mengubah sifat-sifat pelinciran dan juga tribologi minyak pelincir. Minyak pelincir yang dicairkan dengan biodiesel B10 menunjukkan pekali geseran yang tinggi diiringi kesan hausan yang teruk berbanding minyak pelincir mineral, antara semua bahan api. Minyak pelincir+B30+TiO_2 menunjukkan peningkatan pekali geseran yang minimum diantara semua bahan api yang telah diubahsuai jika dibandingkan dengan minyak pelincir mineral SAE-40. Prestasi enjin dan sifat-sifat pelepasan telah dikaji menggunakan enjin diesel pencucuhan mampatan dengan kelajuan enjin berubah-ubah pada kondisi beban penuh. Keputusan ujian telah dibandingkan dengan bahan api B30 dan B10. Penemuan utama menunjukkan bahawa campuran ternar B30+TiO_2 menghasilkan penurunan bagi penggunaan bahan api tentu brek berbanding bahan api yang lain. B30+DMC menghasilkan kecekapan haba brek yang lebih tinggi berbanding bahan api yang lain. Campuran ternar B30+DMC menunjukkan penurunan bagi pelepasan karbon monoksida (CO) dan hidrokarbon (HC) berbanding B30. Campuran ternar B30+CNT menunjukkan penurunan yang sedikit bagi pelepasan nitrogen oksida (NOx) berbanding B30. Kajian ini mensyorkan bahawa biodiesel kelapa sawit-bijan bersama bahan tambah bahan api adalah merupakan pengganti yang sesuai kepada bahan api diesel di dalam enjin pencucuhan mampatan tanpa memerlukan pengubahsuaian.

Kata kunci: Biodiesel kelapa sawit-bijan; Tribologi; Sifat-sifat engine; Bahan tambah bahan api; pengoptimuman

ACKNOWLEDGMENTS

In the name of Allah, the most beneficent and merciful. ‘‘My success can only come from Allah. In Him I trust, and unto Him I look’’. Therefore, all credit should be directed at Him for providing me with the courage and competence to accomplish my research work.

I would like to extend the words of thanks and acknowledgment towards my supervisors, **Emeritus Prof. Dr. Masjuki Haji Hassan, Prof. Dr. Md. Abul Kalam and Dr. Ong Hwai Chyuan** for their great supervision, brilliant ideas, guidance, and support throughout the research. Completion of research would not be an easy task without consistent support, guidance, and encouragement from my beloved supervisors. I also extend my sincere gratitude to the Higher Education Commission (HEC), Islamabad, Pakistan, for their financial assistance [Grant No. 5-1/HRD/UESTPI (Batch-VI)/4954/2018/HEC]. I would also like to extend my gratitude to my research collaborators Mustabshirha Gul, Manzoore Elahi M. Soudagar, Waqar Ahmed, Shahid Bashir Baig, Haris Mahmood Khan and Luqman Razzaq for their valuable suggestions and creative thoughts.

Finally, I owe my deepest gratitude to my parents, wife, lovely son and siblings for their composure, support, love, and positivity during this challenging time.

TABLE OF CONTENTS

LIST OF FIGURES

LIST OF TABLES

LIST OF SYMBOLS AND ABBREVIATIONS

ANOVA	:	Analysis of variance
ANN	:	Artificial neural network
APE	:	Allylic position equivalent
ASTM	:	American society for testing and materials
B30	:	70% Diesel and 30% biodiesel
$Ba(OH)_2$	:	Barium hydroxide
BAPE	:	Bis-allylic position equivalent
BP	:	Brake power
BSFC	:	Brake specific fuel consumption
BTE	:	Brake thermal efficiency
BT	:	Brake torque
CCD	:	Central composite design
CFPP	:	Cold filter plugging point
CH_3ONa	:	Sodium methoxide
CI	:	Compression ignition
CN	:	Cetane number
CNT	:	Carbon nanotubes
CO	:	Carbon monoxide
COF	:	Coefficient of friction
CO2	:	Carbon dioxide
CP	:	Cloud point
CPO	:	Crude palm oil
CPCSO	:	Crude palm-crude sesame oil
CPR	:	Cold-pressed rapeseed

CSO	:	Crude sesame oil
CV	:	Calorific value
DEE	:	Diethyl ether
DMC	:	Dimethyl carbonate
EIA	:	Energy information administration
ELM	:	Extreme learning machine
EN	:	European
EU	:	European union
EN	:	European
FA	:	Fatty acid
FAME	:	Fatty acid methyl ester
FAO	:	Food and agricultural organization
FP	:	Flash Point
GC	:	Gas chromatography
GHG	:	Greenhouse gas
HC	:	Hydrocarbon
HCL	:	Hydrochloric acid
HFRR	:	High-frequency reciprocating rig
H_2SO_4	:	Sulphuric acid
KOH	:	Potassium hydroxide
KV	:	Kinematic viscosity
MAPE	:	Mean average percentage error
MPOB	:	Malaysian palm oil board
NaOH	:	Sodium hydroxide
NOx	:	Nitrogen oxide
P50S50	:	50% Palm - 50% Sesame biodiesel

P60S40	:	60% palm – 40% sesame
PP	:	Pour point
POME	:	Palm oil methyl ester
ppm	:	Parts per million
R^2	:	Coefficient of determination
RIP	:	Rancimat induction period
RMSE	:	Root mean square error
RSM	:	Response surface methodology
SD	:	Standard deviation
SEP	:	Standard error of prediction
SEM	:	Scanning electron microscopy
SME	:	Sesame methyl ester
SSO	:	Sesame seed oil
TiO_2	:	Titanium oxide
ULSD	:	Ultra-low sulfur diesel
USA	:	United States of America
WSD	:	Wear scar diameter

CHAPTER 1: INTRODUCTION

Rapid population growth has increased energy consumption around the globe. The demand for energy in every sector (transport, agricultural, domestic, etc.) is increasing gradually and will face a shortage of fuel due to a gradual decline in fossil fuel reserves (Wakil, Kalam, Masjuki, Atabani, & Rizwanul Fattah, 2015). Currently, the global annual energy usage of 12.2 billion tons is fulfilled by crude oil. This energy utilization will rise to 1.75 billion tons of crude oil by 2035 (Cecrle et al., 2012). In 2020, world oil consumption was reduced due to the COVID-19 pandemic. The COVID-19 global pandemic and its related economic consequences have witnessed two distinct cycles of worldwide production and the use of liquid fuels in 2020, as shown in Figure 1.1.

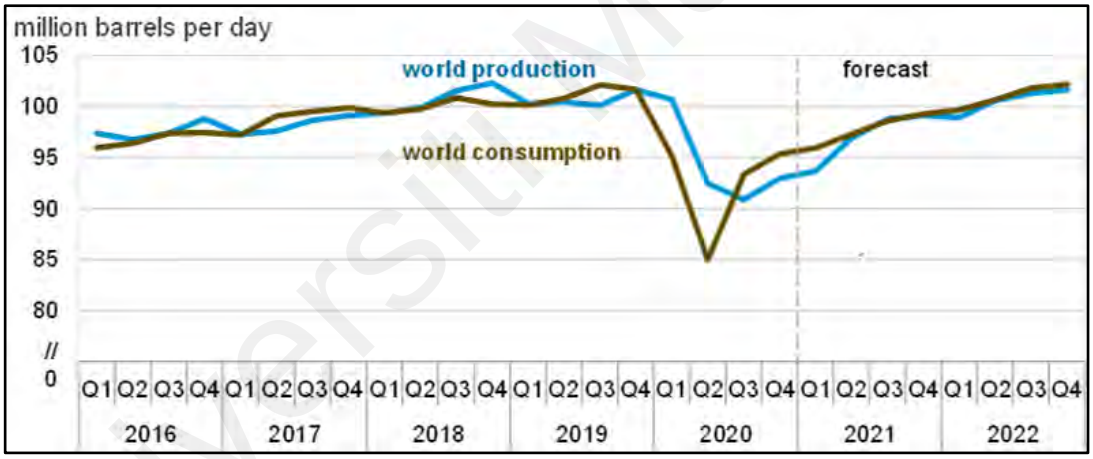

Figure 1.1: World liquid fuels production and consumption balance (EIA, 2021)

Preliminary statistics and projections suggest that in 2020 the global consumption of liquid fuels decreased by 9.0 million barrels daily (b/d), the highest decrease of the Energy Information Administration (EIA) statistics earliest known in 1980. EIA predicts that oil consumption will grow by 5.6 million b/d in 2021 and by 3.3 million b/d in 2022 (EIA, 2021). Asia is leading with 41% energy consumption up to 2040 among other countries around the globe (EIA, 2019). The depletion of fossil fuels poses a serious threat to oil and gas companies to meet the energy demand for all sectors in the future. Oil and gas

producers meet energy needs by using available fossil fuel reserves, which significantly increase carbon dioxide emissions (CO_2) globally (Absi Halabi, Al-Qattan, & Al-Otaibi, 2015). The primary concern in replacing fossil fuels with alternative renewable fuels is eradicating combustion emissions directly linked to climate change, global warming, and various diseases (Aransiola, Ojumu, Oyekola, Madzimbamuto, & Ikhu-Omoregbe, 2014). A high concentration of particulate matter in the air can cause cancer, allergies, respiratory diseases such as asthma, and brochities (Vardoulakis et al., 2015). According to Global Status Report on Renewable Energy (2018), the global proportion of energy generated from different sources is as follows: 10.4 % (modern sources of renewable energy), 7.8 % (traditional biomass), 2.2 % (nuclear energy), and 79.5 % (fossil fuels).

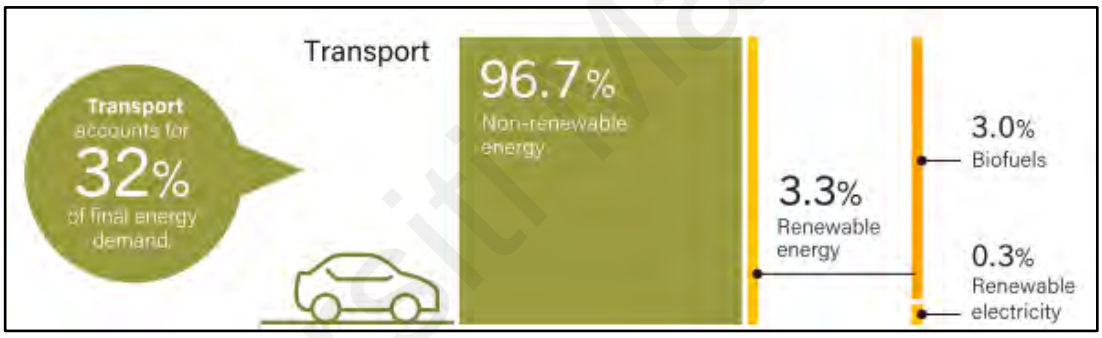

Figure 1.2: Renewable Share of Total Final Energy Consumption in Transport, 2017 (REN21, 2019)

The share of renewable energy in the transport sector accounts for 3.3% of global energy consumption, as shown in Figure 1.2. Forty-six (46) countries worldwide have set national targets to increase the share of renewable energy in transport by 20% by 2020 and 40% by 2030 (REN21, 2019). The three major categories of biofuels are first-generation biofuels (biofuel (bioethanol) - derived from sugar and starch like corn, sugar cane, etc.), second-generation biofuels (biofuel (biodiesel) - derived from vegetable oils such as palm oil, jatropha oil, neem oil, rapeseed oil, sesame oil, etc.) and third-generation biofuels (biofuel–derived from algae) (Silitonga et al., 2019). Second and third-

generation biofuels can produce biofuels for the transport sector because first-generation biofuels severely impact the food supply. The most suitable replacement for fossil fuels is biodiesel. It is quite similar and has better physicochemical properties like more excellent lubricity, higher cetane, and low sulfur content than fossil fuel diesel. In addition, biodiesel can be used as an alternative fuel without modifications to an existing diesel engine.

1.1 Research Background

The transport sector consumes fossil fuels abruptly to meet energy requirements. Almost 50% of fossil fuels are used to meet the energy requirements of the transport sector, due to this factor, fossil fuels are on the verge of exhaustion. About one-third (32%) of the total global energy consumption is attributed to the transport sector. The global energy demand of the transport sector itself has increased by 39% over the past decade (REN21, 2019). This is due to the increase in freight and overall transport demand in emerging countries globally. In 2018, road transport accounted for about 75% of the global energy consumption of transport by passenger vehicles (REN21, 2020). Therefore, there is a serious concern related to energy demand and environmental pollution. Mostly, the transport sector consumed fossil fuels, which are the leading cause of greenhouse gas emissions. By 2030, the transport sector would account for 50% of greenhouse gas emissions (REN21, 2018). Fossil fuels will be replaced with renewable biofuels to eradicate environmental pollution (carbon emissions) as well as to fulfill the transport sector energy demand. Environmental health is mainly affected by carbon emissions emitted by the transport sector (Uusitalo, Leino, Kasurinen, & Linnanen, 2017). Environmental issues like climate change, global warming, and human health concerns have been jeopardized by the harmful gases from petroleum fuel combustion. The increased usage of fossil fuels and the negative impact of exhaust gases on human health and climate change has led researchers to find renewable fuels to eradicate combustion

emissions (Aransiola et al., 2014). Air is polluted by exhaust gases released from the burning of fossil fuels in diesel engines like NO_x, CO, minute particulate matter, and HC (S Gavhane et al., 2020). Severe medical health issues like cancer, respiratory diseases (allergies, asthma, etc.) can occur due to the large quantity of particulate matter in the air (Vardoulakis et al., 2015). To comply with the Kyoto Protocol, renewable and sustainable fuels can overcome the reliance on fossils fuels.

Biodiesel is a potential candidate as an alternative fuel for a compression ignition engine. Biodiesel fuel captures a prominent place among all the other alternative fuels. Biodiesel is used directly or as a blend with diesel in CI engines without any fuel or engine modification. It is observed from the previous literature that there is a significant reduction in HC, CO, and particulate emissions during the combustion of biodiesel due to its superior properties such as cetane number, oxygen content, flash point, etc. to those of petroleum-based diesel fuel. It has also been found that, in diesel/biodiesel blend, particle emissions reduce consistently with fuel oxygen content (Hedayat et al., 2016). This significant decrease is due to a lack of aromatic content and a high quantity of oxygen in biodiesel (Lapuerta, Armas, & Rodriguez-Fernandez, 2008). Therefore, biodiesel is a significant potential biofuel to substitute crude diesel due to its similar physicochemical properties. Furthermore, its utilization is safe for engines because biodiesel has a lower ignition delay time, higher combustion efficiency, provides better lubricity, etc. (Wakil, Kalam, et al., 2015).

1.2 Problem statement

The conversion of vegetable oil into biofuel is not a new idea. In 1900, Rudolph Diesel was the first to test his newly invented diesel engine (i.e., compression-ignition engine) with renewable biofuel extracted from peanut oil instead of petroleum diesel, without any modifications to the engine (Dixit, kanakraj, & Rehman, 2012). Biodiesel is safe to use,

non-toxic, biodegradable, higher cetane number, higher combustion efficiency and provides better lubricity with a lower sulfur content (Wakil, Kalam, et al., 2015). Biodiesel synthesis from high saturated fatty acid oils limits its usage in cold weather conditions due to its poor cold flow characteristics. Biodiesel handling of transportation or long-term storage is another crucial issue, and biodiesel shows poor oxidative stability due to high unsaturation (Pullen & Saeed, 2014). The primary problem with biodiesel commercialization and industrialization is its poor oxidation stability and cold flow characteristics. Soybean is mainly used in the United States, palm biodiesel in Asia, and rapeseed biodiesel in Europe (Silitonga et al., 2013). Indonesia and Malaysia use their crude palm oil as a potential feedstock for the production of biodiesel. Indonesia is the leading producer of palm-based biodiesel (approx. 12 billion liters), followed by Malaysia (1.5 billion liters). Malaysia is expected to adopt B30 (30% palm biodiesel in diesel) by 2025 (Latiff, 2020). Indonesia has already introduced the B30 biodiesel since 2020 (Elisha, Fauzi, & Anggraini, 2019). Indonesia and Malaysia are exporting palm oil to Asia and Europe to produce biodiesel to meet energy demands, which is expected to increase in the future (Coca, 2020). However, palm oil has poor cold flow properties due to saturated fatty acids (Fattah, Masjuki, Kalam, Mofijur, & Abedin, 2014).

Palm contains 35 to 55% oil content. The high percentage of saturated fatty acids resulted in better oxidative stability than other feedstocks used for biodiesel production. However, palm oil-based biodiesel has poor cold flow characteristics such as cold filter plugging (12 ℃), pour point (15 ℃). Cloud point (16 ℃) due to low unsaturated fatty acids (Atabani et al., 2012b). Various researchers have identified the problems associated with engine operation during low-temperature climate as the result of clogging of filters, incomplete combustion, starting problem, and fuel starvation (Dwivedi & Sharma, 2014). Most researchers improved the cold flow properties by adding synthetic antioxidants but now many researchers blend the oils before transesterification to improve the cold flow

characteristics. In the past, some researchers blended biodiesel obtained from different feedstocks to improves these properties. A high degree of unsaturation in biodiesel results in poor oxidation stability and better cold flow properties. Conversely, a high percentage of saturated fatty acids results in good oxidation stability and poor cold flow properties (Lanjekar & Deshmukh, 2016). Therefore, feedstock selection is critical for blending with palm oil to improve its cold flow properties. Vegetable oils with a high degree of unsaturation can be used for blending with palm oil. However, at the same time, the oxidation stability of palm oil will be decreased. According to the literature, sesame seed oil (SSO) can be the most suitable option for blending with palm oil compared with all other feedstock oils. SSO has a high degree of unsaturation (up to 85%) and thus has good cold flow properties. Furthermore, it also exhibits high oxidative stability due to naturally occurring antioxidants (i.e., sesamin, sesamol, and sesamolin) with tocopherols (i.e., vitamin E) (Pullen & Saeed, 2014).

The lubricity of fuel is a very important parameter that should be accounted for when selecting fuel for engine applications. Most diesel engine components are self-lubricated with fuel, such as fuel pumps, fuel injectors, etc. Petroleum diesel has very low lubricity due to eliminating polar compounds (polyaromatic and nitrogen) during the desulfurization process (Gul et al., 2020). These compounds produce a lubricating film (protective layer) between the metal mating surface to minimize wear and friction. High-pressure fuel injection systems can also reduce engine emissions, so fuel lubricity is a key parameter to protect the injection system and other engine components' fuel lubricity (Lapuerta, Garcia-Contreras, & Agudelo, 2010). Many researchers used different fuel additives (nanoparticles and oxygenated alcohols) to improve diesel engine performance and emission characteristics (Soudagar et al., 2018). However, few researchers explored the effect of fuel additives on the lubricity of the fuel. The lubricity of fuel is a critical parameter related to the durability of diesel engines. Therefore, fuel additive lubricity

should be analyzed prior to engine testing. The lubricity of diesel injectors is crucial during the supply of diesel fuel in the combustion chamber. Lubricant film reduces friction and wear; consequently, efficiency increases. According to previous literature, the lubricant is contaminated with fuel up to 5% due to crankcase dilution (Arumugam & G. Sriram, 2013). After dilution, lubricant properties will be altered, which directly affect tribological properties. Few researchers investigated the effect of biodiesel dilution with lubricant on its tribological characteristics. Many researchers did not give any attention to lubricant degradation due to dilution with diesel-biodiesel-fuel additives. A tribological study of ternary fuel blends should be conducted before engine application to ensure its effect on the degradation of the lubricant.

The drawbacks of palm biodiesel, such as poor cold flow properties, and higher NO_x emission, can be overcome by using palm-sesame biodiesel with fuel additives (nanoparticles and oxygenated alcohols) in diesel engines. However, the literature review suggests that there are no previous studies reported on the application of oxygenated alcohols (dimethyl carbonate (DMC) and diethyl ether (DEE)) and nanoparticles (carbon nanotubes (CNT) and titanium oxide (TiO_2)) as fuel additives in diesel-palm and sesame biodiesel in diesel engines.

1.3 Scope of work

Malaysia and Indonesia are the largest producer and exporters of palm oil. Palm oil contains poor cold flow characteristics due to its high saturated fatty acid composition. In a cold climate, handling palm oil or palm biodiesel is complicated. This study was conducted to improve the cold flow characteristics and the oxidation stability of palm oil before transesterification. The critical review suggested the most feasible feedstock sesame oil for blending with palm oil to improve its physicochemical characteristics. In the current investigation, process variables were optimized using RSM and ELM to maximize the optimum yield of palm-sesame biodiesel. An HFRR test is conducted with

a ball-on-plate combination to analyze the lubricity of diesel fuel with biodiesel and fuel additives mixture for fuel injector application. For this research work, ethanol and dimethyl carbonate have been chosen as an oxygenated distilled fuel additive and CNT and TiO_2 as nanoparticle additives. Scanning electron microscopy (SEM) tool utilized to analyze the plate and ball scars used in HFFR tests.

According to my best knowledge, none have investigated the effect of different diesel-biodiesel blends with fuel additives on the tribology of contaminated lubricant. Therefore, six different types of fuels, B10, palm-sesame biodiesel blend (B30), B30 with alcohol (DMC and Ethanol), and nanoparticle (CNT and TiO_2) additives, were selected to investigate their effects on tribological characteristics of lubricating oil by four-ball tribo-tester.

In the current investigation, the drawbacks of palm biodiesel, such as cold weather starting of diesel engines, poor cold flow properties, and higher NO_x emission, can be overcome by using palm-sesame biodiesel with fuel additives nanoparticles and oxygenated alcohols in diesel engines. First, the B30 fuel blend is prepared by mixing palm-sesame methyl ester in the 50:50 ratio and blended with CNT (100 ppm), TiO_2 (100 ppm), DMC (10%), and DEE (5%) to form ternary fuel blends for diesel engine application. Then, a comprehensive investigation is carried out on the engine performance brake power (BP), brake thermal efficiency (BTE), and brake specific fuel consumption (BSFC) and emission (CO, NO_x, and HC) characteristics as well as compared with B10 and B30 blends without fuel additives. Hence, the effect of nanoparticles and alcoholic fuel additives with diesel-biodiesel blends on diesel engine performance and emission characteristics are carried out.

1.4 The objectives of the study

The main objective of this research was to optimize the operating transesterification process parameters for maximizing the yield of palm-sesame biodiesel using response surface methodology and to utilize palm-sesame biodiesel as a potential alternative biofuel in internal combustion engines. Tribological studies were carried out to analyze the effect of different fuel additives on engine parts. The effect of fuel additives on diesel engine characteristics was observed using diesel engine testing. The objectives of this research work are discussed as follows:

1. To optimize biodiesel synthesis from palm-sesame oil mixture using ultrasound technique by applying the response surface methodology.
2. To investigate test fuel's physicochemical properties with and without nanoparticle and alcoholic fuel additives.
3. To investigate the lubricity characteristics of synthesized palm-sesame biodiesel using HFRR and fuel dilution effect using four-ball tribo tester.
4. To investigate the diesel engine characteristics using synthesized palm-sesame biodiesel with fuel additives.

1.5 Organization of Thesis

This dissertation consists of five chapters and is organized as follows.

Chapter 1 is the introduction that provides background about the area of this study, highlights the current problems that motivated this research, and clarifies the objectives through which the aim of the present study can be achieved.

Chapter 2 is the literature review that briefly surveys the previously published work related to this field of study, which can be categorized as a selection of feedstock, importance of sesame oil, biodiesel production techniques, optimization tools for process

variables, the lubricity of fuel blends, contamination of the mineral lubricant and diesel engine performance and emission characteristics.

Chapter 3 is a methodology that concerns materials, devices, and methods used in this study to prepare biodiesel, optimize process variables, characterize biodiesel, a tribological analysis using HFRR, the tribological study of contaminated lubricant using four-ball tribo tester, and single-cylinder diesel engine testing.

Chapter 4 is a result and discussion which presents the experimental data obtained from biodiesel production, process optimization, characterization, the lubricity of ternary fuel blends, the effect of ternary fuel blends on mineral lubricant, and the effect of fuel additives on diesel engine performance and emission characteristics. All data are presented in the form of tables and figures.

Chapter 5 is the conclusion of the study, which consists of the end of the present work. Besides, the conclusion achieved in this study is summarized in this section.

CHAPTER 2: LITERATURE REVIEW

Vegetable oils are potential feedstock for the production of biodiesel. Biodiesel commercialization in few parts of the world is limited due to the poor physicochemical properties of biodiesel. According to literature, sesame oil has unique physicochemical properties which can be used as a potential feedstock for blending with different vegetable oils for the improvement of biodiesel properties. This chapter highlights the importance and potential of sesame oil among other vegetable oils. Optimization techniques are also discussed for the production of biodiesel. RSM and ELM techniques are effective to optimize the input process variables of biodiesel. This section highlighted the critical analysis of lubricity, engine performance, and emission characteristics.

2.1 Introduction

This section covers the importance of sesame as a promising feedstock for improving the physicochemical properties of palm oil. First, the physicochemical properties of sesame oil are discussed in detail. Then, different production and optimization techniques are discussed. Finally, this chapter reviews the significance of fuel, lubricant contamination, and diesel engine characteristics (performance and emission).

2.2 Selection of feedstock

2.2.1 Overview of sesame seed plantation

Sesame (*Sesamum indicum L.*) belongs to the *Pedaliaceae* family and is widespread in tropical and sub-tropical regions of Asia, Africa, and South America. The word "sesame" is derived from the Arabic word "simsim" (Moazzami & Kamal-Eldin, 2009). Globally, it is known as sesame, til in Asia and as benniseed or simsim in Africa. According to prehistory studies, cultivation of sesame was discovered in South Asian wild populations, and cultivation originated in South Asia before 2000 B.C from the time of the Harappan civilization (Fuller, 2003). The major crop cultivated in the Indus valley

civilization was sesame and cultivated in west Mesopotamia (Hegde, 2012). Assyrians used SSO in medicines, food, and salves (ointments).

Sesame is commonly called the 'queen of oilseeds,' and SSO was the first oil discovered and consumed by humans; it is also referred to as an 'orphan crop' (Moazzami & Kamal-Eldin, 2009). However, sesame has been rarely studied and has not been given a crop mandate by any research institute (Bhat, Babrekar, & Lakhanpaul, 1999). Few researchers have been researched sesame, and it has not been given a crop mandate by any research institute. Sesame is listed among neglected and underutilized crop species and is described as "a crop with high potential" by International Plant Genetic Resources Institute (Were, Onkware, Gudu, Welander, & Carlsson, 2006).

Sesame is very well-known and oldest oilseed crop due to its high-quality seed oil. Sesame is an erect, annual and herbaceous plant that grows 1–2 m tall. Sesame seeds are flat, pear-shaped, 2–3.5 mg in weight and 2–3 mm in length. Each capsule contains 50–100 seeds (Moazzami & Kamal-Eldin, 2009). Sesame seeds are oval and small, and they come in various colors, such as yellow, dark brown, white, grey, dark grey, black and reddish brown. The number of seeds per capsule, capsule length and seed size significantly vary depending on the cultivar. A total of 1000 sesame seeds weigh approximately 3 grams (Hegde, 2012).

Sesame seeds contain nearly 44%–57% oil, 18%–25% protein and 13%–14% carbohydrates (Borchani, Besbes, Blecker, & Attia, 2010). In other literature, sesame seed contains 37%– 63% oil depending on the variety, growing season and cultivar (Hegde, 2012). The most prominent feature of SSO is its resistance to oxidation rancidity during long exposure to air. The significant resistance to oxidation is due to the naturally occurring endogenous antioxidants in SSO, such as tocopherols and lignins (i.e. sesamin and sesamolin) (Lee, Lee, & Choe, 2008). The remaining part of sesame seeds after

extracting oil (i.e., cake or meal) is rich in protein (45%–50%) and is typically used for animal feed. The cakes of roasted sesame seeds are rich in antioxidant compounds and can therefore be used as a potential source of antioxidants (Moazzami & Kamal-Eldin, 2009).

2.2.2 Sesame seed oil capacity

According to the Food and Agricultural Organization (FAO) statistics, the average global yield of sesame seeds in 2017 was 5.53 million metric tons, harvested on 9.98 million hectares. In 2017, major producers of sesame countries included the United Republic of Tanzania, Burma (Myanmar), India, Nigeria, Sudan, China (Mainland China), Ethiopia, South Sudan, Burkina Faso and Chad, as shown in Figure 2.1. Sesame seed production shares of Africa, Asia, America and Europe in 2017 were 56.9%, 39.7%, 3.4% and 0%, respectively. Africa, Asia and America produced 3.14 million, 2.19 million and 0.189 million tons of sesame seeds, respectively (FAO, 2018). Amongst all oilseed crops, sesame is ranked eighth concerning oil production globally (Mehmood et al., 2018). According to FAO, the average global SSO production in 2014 was 1.63 million tons, and major oil-producing countries were the United Republic of Tanzania, Burma (Myanmar), India, Japan, South Sudan, Sudan, Turkey, Republic of Korea, and Uganda. As a result, sesame seed production shares of Africa, Asia, America, Europe, and Oceania in 2014 were 41.8%, 54.3%, 1.5%, 2.3%, and 0.1%, respectively, as shown in Figure 2.2 (FAO, 2015).

Table 2.1: Production of sesame seed and oil in different regions of the world (FAO, 2018)

Region	Sesame seed (tons)	Sesame oil (tons)
Asia	2,195,089	887,199
Africa	3,146,248	683,027
America	189,974	25,138
Europe	0	36,994
Oceania	0	1,969

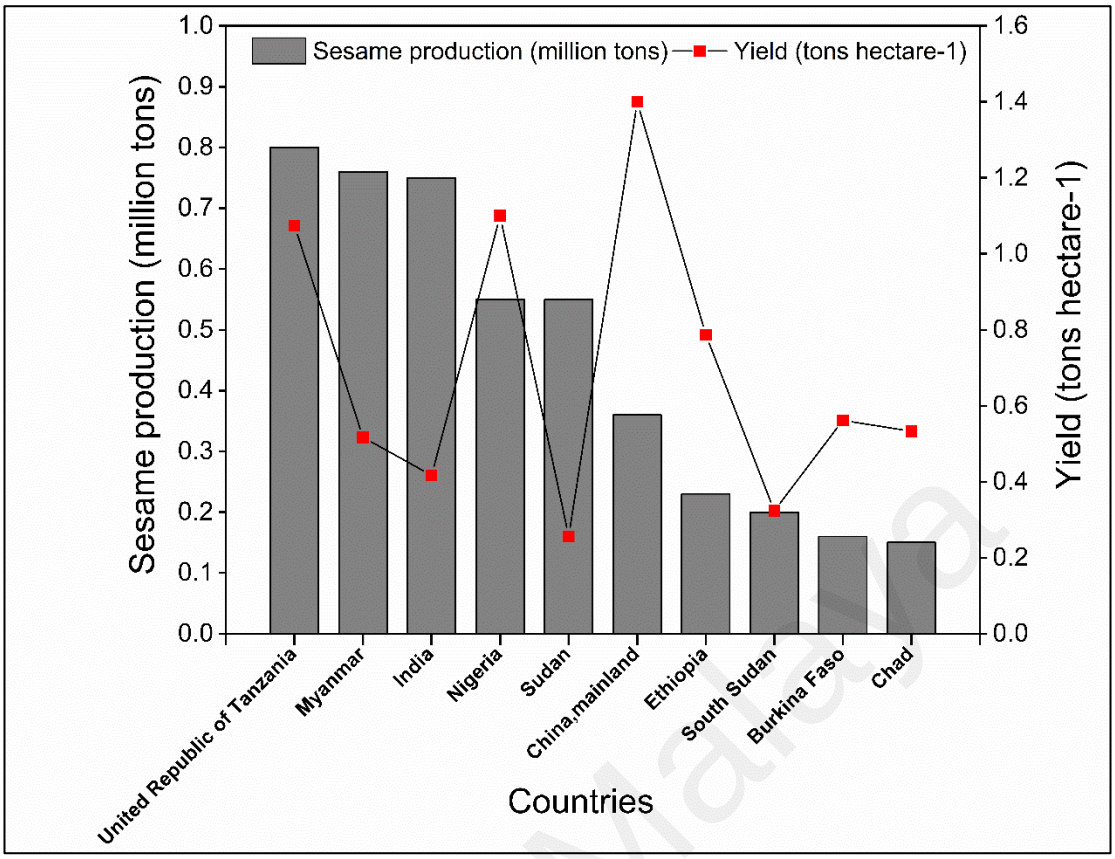

Figure 2.1: Top producers of sesame in the world (FAO, 2018)

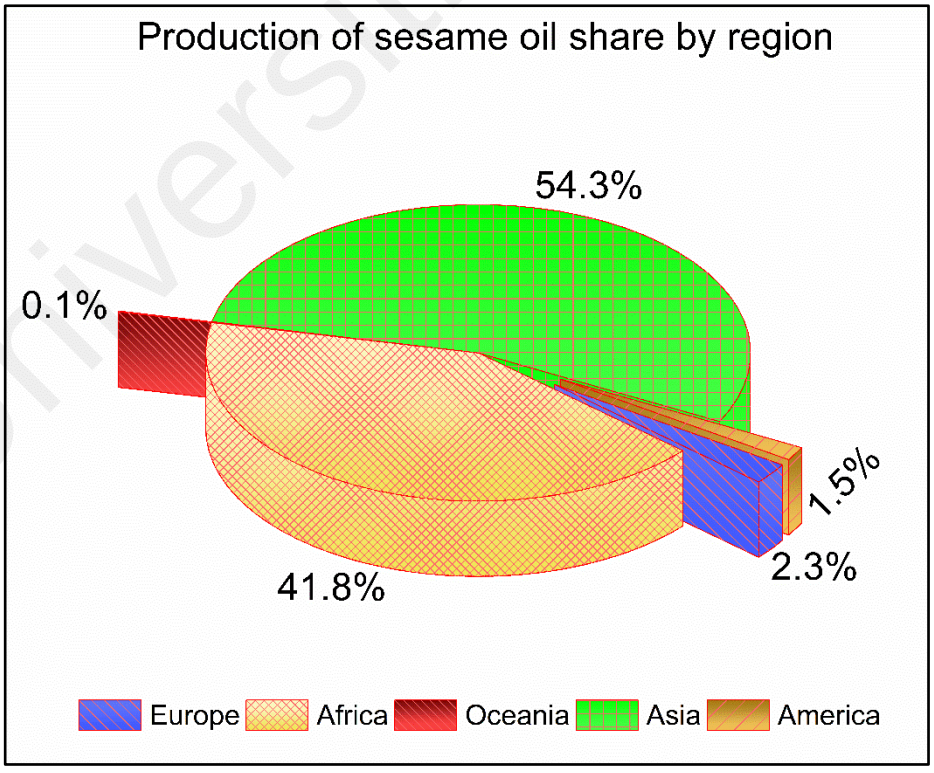

Figure 2.2: Production share of Sesame oil by Region (FAO, 2018)

The average yield of sesame seeds reported in the FAO report (2018) ranged from 256 kg/ha to 1400 kg/ha. The top three countries in the highest yield production were China (Mainland China), Nigeria, and the United Republic of Tanzania with 1400, 1100, and 1074 kg/ha, respectively, as shown in Figure 2.1.

The above-mentioned statistics about sesame seed and oil production should be taken as a rough estimation because most harvested crops are locally consumed and no suitable way to obtain the data for local and domestic production is available. Moreover, only several countries properly record data related to sesame seed and oil production and its part in international trade.

2.2.3 Medicinal, nutritional and industrial applications of SSO

Regarding medical use, sesame seeds oil and paste are applied to the skin for treating wounds and burns. Around the globe, sesame is used for treatment of anaemia, amenorrhea, dysentery, respiratory infections, cholera, scorpion poison, dysmenorrhea, tinnitus, diarrhea, dizziness, memory enhancement and bleeding piles (Hegde, 2012; Khan, Ahmed, Khan, & Khan, 2014). SSO is used to treat coughs, burns, migraines, snake bites, tuberculosis, hair loss, eye diseases and demulcent in addition to being used as an antitussive (Hegde, 2012). Low-quality SSO is also used to produce soap, paints and lubricants (Anilakumar, Pal, Khanum, & Bawa, 2010). In addition, sesame seeds are used in food, such as buns, chips, crackers, salads, cakes, and breads.

SSO has several industrial applications. For instance, sesame is used to prepare perfumes in Africa. Myristic acid made from SSO is used as an ingredient in cosmetics (Anilakumar et al., 2010). Sesamin acts as an antioxidant that can inhibit the absorption of cholesterol and the production of cholesterol in the liver due to its bactericidal and insecticidal effects (Morris, 2002). SSO is used as a solvent for skin softeners and drugs and an ingredient for margarines and soaps.

Some researchers have produced biodiesel from SSO by transesterification using a homogenous and heterogeneous catalyst with methanol. Sarve et al. obtained optimized biodiesel from SSO using a catalyst barium hydroxide ($Ba(OH)_2$) with methanol, which achieved maximum yield at 98.6% at 31.92 °C. The sesame biodiesel properties include flashpoint of 180 °C, cloud point (CP) of −5 °C, pour point (PP) of −9 °C, kinematic viscosity (KV) of 40 °C 4.47 and cetane number (CN) of 56.32 (Sarve, Sonawane, & Varma, 2015).

Various researchers have investigated using sesame biodiesel in existing diesel engines and found lower emissions than crude diesel. B10 sesame biodiesel was tested in a diesel engine compared to other feedstock biodiesels, and the sesame infused biodiesel showed better engine performance than other biodiesels (Naik & Balakrishna, 2018). According to (Altun, Bulut, & Öner, 2008) and (Banapurmath, Tewari, & Hosmath, 2008) sesame biodiesel reduces the CO and NO_x emissions with a slight increase in the brake specific fuel consumption (BSFC). Different researchers have observed that using SSO methyl ester as a fuel reduces exhaust gas emissions, improves BTE and increases BSFC. In accordance with the fuel properties of optimized biodiesel, sesame biodiesel has good cold flow properties and CN, which are favorable for commercializing it for diesel engine fuel blends. Therefore, SSO is a viable source of vegetable oil for biodiesel production to replace fossil fuels.

2.2.4 Chemical composition of sesame oil

The chemical composition of SSO contains oil (44%–58%), protein (18%–25%), carbohydrate (~13.5%) and ash (~5%) (Elleuch, Besbes, Roiseux, Blecker, & Attia, 2007). The fatty acid (FA) composition of SSO varies with geographical region and variety and from feedstock to feedstock. SSO consists of two main FAs: oleic and linoleic acids. The main FAs in SSO are oleic, linoleic, palmitic, stearic and linolenic acids. Table

2.2 summarizes the composition of SSO FAs from different geographical areas (Karmakar, Karmakar, & Mukherjee, 2010), (Hassan, 2012), (Gharby et al., 2017). SSO contains more than 80% of unsaturated FAs, and the major composition belongs to oleic and linoleic acids. The saturated FAs in SSO represent less than 20% of the total chemical composition of SSO. Stearic and palmitic acids are the most critical saturated FAs in SSO.

SSO is considered to be the most resistant towards oxidation rancidity amongst all vegetable oils. The presence of tocopherols (i.e., vitamin E) in SSO exhibits high resistance to autooxidation. SSO contains 0.5%–1.0% sesamin and 0.3%–0.5% sesamolin with few traces of free sesamol. The high resistance of SSO to oxidative rancidity depends on the presence of natural antioxidants (i.e. sesamin, sesamol and sesamolin) and tocopherols (Hegde, 2012).

Table 2.2: Fatty acid composition (%) of Sesame seed oil

	Sudan (El Khier, Ishag, & Yagoub, 2008)	Congo (Nzikou et al., 2009)	Turkey (Ünal & Yalçın, 2008)	Egypt (Hassan, 2012)	Morocco (Gharby et al., 2017)	India (Karmakar et al., 2010)	UK (Pullen & Saeed, 2014)
Myristic acid	-	-	0.02	-	0.1	-	0.1
Palmitic acid	12.9	8.66	8.9	8.47	11.3	7-9	10.1
Stearic acid	3	5.45	5.43	5.53	4.9	4-5	4.0
Oleic acid	47.5	38.86	41.5	41.6	41.9	40-50	37.8
Linoleic acid	36.4	46.2	42.7	42.77	42.1	35-45	45.1
Linolenic acid	-	-	0.3	0.3	0.2	0.4-1	0.7
Saturated fatty acids	15.9 ± 0.2	14.85	14.3 ± 0.2	14	16.3 ± 0.2	12.5	15.8
Unsaturated fatty acids	83.9 ± 0.2	85.15	84.5 ± 0.2	84.37	84.3 ± 0.2	85.7	84.2

2.2.5 Physicochemical properties of sesame seed oil

Various researchers have reported the physicochemical characteristics of SSO in the preceding literature. Typical FAs found in SSO are linoleic (C18:2), oleic (C18:1), palmitic (C16:0), stearic (C18:0) and linolenic (C18:3) acids, as shown in Table 2.2. These properties may vary depending on the extraction method, the geographic location of sesame seeds and analytical methods used for measurement. The physicochemical properties of SSO reported in the literature by various researchers are summarized in Table 2.3.

Table 2.3: Physicochemical properties of Sesame seed oil

Parameters	Units	(Sarve et al., 2015)	(Ferdous, Uddin, Khan, & Islam, 2012)	(Dawodu, Ayodele, & Bolanle-Ojo, 2014)	(Betiku & Adepoju, 2013)	(Younis, Gardy, & Barzinji, 2014)	(Saydut, Duz, Kaya, Kafadar, & Hamamci, 2008)	(S. P. Singh & Singh, 2010)	(Borchani et al., 2010)
Kinematic viscosity at 40 °C	mm^2/s	31.51	52.5	22.63	31.39	33.61	25.78	35.5	-
Density at 15 °C	g/cm^3	0.9	0.88	0.8525	0.833	0.936	0.899	0.913	-
Acid value	mg KOH/g oil	0.42	-	3.15	0.50	0.443	-	-	1.64
Iodine value	g I_2/100 g	-	75.3	86.15	108	-	82.45	-	113
FFA	%	-	6.1	1.58	-	-	-	-	0.82
Moisture content	%	0.03	0.08	-	0.09	0.00	-	-	-
Saponification value	mg KOH/g oil	-	213	142.2	-	-	-	-	186
Cetane No.		48.57	-	-	50.73	-	-	40.2	-
Flashpoint	°C	240	-	-	-	312	245	260	-
Pour point	°C	-6	-	-	-	-3	-10	-9.4	-
Calorific value	MJ/kg	38.9	-	-	40.20		39.5	39.3	-
Cloud point	°C	1	-	-	-	3	1	-3.9	-

2.2.6 Transesterification of SSO

SSO can be used directly or mixed with petroleum diesel in a diesel engine. However, pure SSO and its blends as a fuel in diesel engines are problematic due to its high viscosity, as shown in Table 2.3. The fatty acid content and high viscosity of SSO lead to several problems in diesel engines, such as fuel lines and filter blockage, poor atomization of fuel, injector coking and piston ring sticking, gum formation (due to oxidation) during storage and combustion, severe carbon deposition in the engine due to incomplete combustion and degradation and thickening of lubricating oil (Altun et al., 2008; Cetin & Yüksel, 2007). The solution to these problems caused by the high viscosity of virgin oil can be overcome by converting it to viable biodiesel. Transesterification is the chemical reaction of a triglyceride (fat or oil) with an alcohol to produce esters and glycerol. The production methods cited in the literature for the conversion of SSO to sesame methyl ester are conventional and ultrasonic assisted.

The transesterification of SSO is conducted with homogeneous base catalysts (potassium hydroxide (KOH), sodium hydroxide (NaOH), sodium methoxide (CH_3ONa)) using conventional method (Ahmad, Khan, Zafar, & Sultana, 2009; Betiku & Adepoju, 2013; Dawodu et al., 2014; Pullen & Saeed, 2014; Wakil, Kalam, Masjuki, Fattah, & Masum, 2014; Younis et al., 2014) and has biodiesel yields from 87.80% to 98.36%, as shown in Table 2.4. On the other hand, (Sarve et al., 2015) produced biodiesel from SSO with a heterogeneous catalyst ($Ba(OH)_2$) by using ultrasound-assisted transesterification at a frequency of 20 kHz, which produced a maximum optimized biodiesel yield of 98.6%. Therefore, ultrasound techniques can minimize the time and temperature to obtain the maximum yield.

Table 2.4: Optimum conditions for transesterification of sesame oil

Catalyst Type	Production Technique	Operating Parameters				Biodiesel Yield (%)	References
		Methanol/oil ratio	Catalyst Weight (% wt)	Temp (°C)	Time (mins)		
CH_3ONa	Conventional with CCD	6:1	0.75%	50	30	87.80	(Dawodu et al., 2014)
NaOH	Conventional with RSM	6.24:1	1.04%	-	51.09	98.36	(Betiku & Adepoju, 2013)
KOH	Conventional	6:1	1.5%	60	120	96	(Younis et al., 2014)
NaOH	Conventional	6:1	0.5%	60	120	74	(Saydut et al., 2008)
$Ba(OH)_2$	Ultrasonic with 20 kHz RSM+ANN	6.69:1	1.79%	31.92	40.30	98.6	(Sarve et al., 2015)
CH_3ONa	Conventional	10:1	-	60	-	92	(Ahmad et al., 2009)
KOH	Conventional	25% (V/V)	1%	60	120	-	(Wakil et al., 2014)
NaOH	Conventional	6:1	1%	60	60	96.8	(Pullen & Saeed, 2014)

Table 2.5: Fuel properties of sesame oil methyl ester

Parameters	Units	SME (Younis et al., 2014)	SME (Saydut et al., 2008)	SME (Sarve et al., 2015)	SME (Ahmad et al., 2009)	SME (Wakil et al., 2014)
Density at 15 °C	g/cm^3	0.8972	0.8672	0.867	0.871	0.884
Kinematic viscosity at 40 °C	mm^2/s	4.58	4.2	4.47	5.77	4.3989
Acid value	mg KOH/g oil	0.32	-	0.12	-	-
Iodine value	g I_2/100 g	-	80.32	-	-	-
FFA	%	-	-	-	-	-
Moisture content	%	0	-	0.017	-	-
Saponification value	mg KOH/g oil	-	-	-	-	-
Cetane No.		69.3	50.48	56.32	53	-
Flash point	°C	155	170	180	110	208.5
Pour point	°C	-5	-14	-9	-18	1
Calorific value	MJ/kg	-	40.4	40.1	-	39.996
Cloud point	°C	1	-6	-5	-6.3	1

2.2.7 Optimization of SSO methyl ester

The optimization of the transesterification process is vital to achieve a high yield and ensure the purity of biodiesel. However, determining the optimal values for process variables by conventional methods is time-consuming because the procedure is costly in terms of labor, money, time consumption, and material due to the large number of experiments involved (Ong et al., 2019). Therefore, conventional experiments are usually used to determine the optimum values for process variables by trial and error during the optimization.

RSM software is used for process optimization. It is widely used for optimizing and examining the effect of input variables on output variables (operational variables) (Maran, Sivakumar, Sridhar, & Immanuel, 2013). RSM is typically used to optimize the responses or select the best operating conditions for achieving maximum output results (Maran, Manikandan, Nivetha, & Dinesh, 2017). The central composite design (CCD), which is also called the Box–Wilson design, is an experimental design to obtain maximum information about a process from a small number of experiments (Prakash Maran, Manikandan, Vigna Nivetha, & Dinesh, 2017). In CCD, the experimental design is used to analyze the input variables or parameters on output response. From previous literature or preliminary experiments, process input variables and ranges are normally determined. After the input variables and their ranges are selected, experiments are designed with various factors at three levels, and each input variable is coded between −1,0 and +1 (Prakash Maran, Mekala, & Manikandan, 2013). RSM is used to optimize the response variable (output) depending on various independent variables (input). RSM is the best option with minimal process data; thus, it saves experimental costs and precious time (Shanmugaprakash & Sivakumar, 2013). RSM based on Box Behnken technique has

better optimizing yield capability compared to CCD technique due to a limited number of experiments (Gul et al., 2021).

Artificial neural network (ANN) is a well-known technique for optimizing the process in biodiesel research (Gul et al., 2019) because it can model using the mathematical background of the problem and for studying the linear and nonlinear relationships directly from the set of variables (Sarve et al., 2015). ANN is considered a superior alternative technique to conventional modelling techniques due to its nonlinearity and complexity (Aghbashlo, Hosseinpour, & Mujumdar, 2015). In addition, a well-trained neural network is a fast, reliable and easy to use tool for solving and optimizing engineering problems (Kurtgoz, Karagoz, & Deniz, 2017).

(Sarve et al., 2015) compared both modeling techniques (i.e. ANN and RSM) to predict the yield of SSO methyl ester obtained from ultrasonic-assisted transesterification. ANN is more reliable than RSM in optimizing the biodiesel yield. Ultrasound-assisted transesterification is feasible in producing biodiesel while using heterogenous catalyst (Tan, Lim, Ong, & Pang, 2019).

(Dawodu et al., 2014) used CCD for transesterification of sesame (*Sesamum indicum* L.) oil to optimize the process variables. The maximum yield of SSO methyl ester was predicted to be 87.80% when the reaction temperature, reaction time, CH_3ONa as a catalyst and amount of methanol/oil ratio were 50 °C, 30 min, 0.75% and 6:1, respectively. (Betiku & Adepoju, 2013) used a CCD-based RSM technique to optimize the reaction temperature, the molar ratio (methanol: oil), reaction time and amount of catalyst of the transesterification process to optimize biodiesel yield. The biodiesel yield was optimized at 98.36% under the following conditions: 1) molar ratio (methanol to oil): 6.24:1, 2) reaction time: 2 h, 3) sodium hydroxide (catalyst) concentration: 1.04% and 4) reaction temperature: 63°C.

(Sarve et al., 2015) RSM and ANN to optimize the reaction temperature, catalyst concentration, reaction time and molar ratio of methanol to oil to increase biodiesel yield. The optimized yield conversion was 98.6% under these process conditions: 1) methanol to oil molar ratio: 6.69:1, 2) ($Ba(OH)_2$) heterogeneous catalyst concentration: 1.79%, 3) reaction time: 40.30 min and 4) reaction temperature: 31.92 °C. The sensitivity analysis was used to analyze the effect of each independent variable on the response to the output variables. Sensitivity analysis showed that the catalyst concentration was the main affecting factor of the FA methyl ester content. The results showed that the lower values of correlation of coefficient, root mean square error, standard error of prediction and relative percent deviation for ANN than RSM verified that ANN was a superior prediction model for fatty acid methyl ester (FAME) content.

2.2.8 Physicochemical properties of sesame oil biodiesel

2.2.8.1 Density

The density of biofuel is a key parameter for calculating the precise volume of fuel for adequate combustion (Ramírez Verduzco, 2013). In diesel engines, air to fuel mixing mostly depends on the density of the fuel. The fuel–air mixture is conducted at a pressure range of 15–50 MPa and a temperature range of 300 K–350 K in the combustion chamber (Sajjadi, Raman, & Arandiyan, 2016). Density directly affects the injection process and efficiency of fuel atomization because the quantity of fuel injected through injector nozzle in the combustion chamber is assessed by its volume (Kaya et al., 2009). Density is also considered an important property of biodiesel that links with viscosity, CN and heating value (Hoekman, Broch, Robbins, Ceniceros, & Natarajan, 2012). ASTM D6751 standard does not specify the density of a biofuel. EN 14214 standard specifies that a biodiesel's density should be in the range of 860–900 kg/m^3. Compared with petroleum diesel's density (850 kg/m^3), the density of biodiesel (880 kg/m^3) is slightly higher; such density can be overcome by increasing the percentage of biodiesel in blends (Silitonga et al.,

2013; Wakil, Kalam, et al., 2015). Sesame, palm, coconut and pequi derived FA methyl esters have the lowest density amongst vegetable oil methyl esters (Sajjadi et al., 2016). Biodiesel (higher unsaturated) with more than two double bonds exhibits a relatively high density (Karmakar et al., 2010). According to (Wakil, Kalam, et al., 2015), sesame biodiesel has the trend of increasing density (0.849, 0.853, 0.857 and 0.86 at 50%, 60%, 70% and 80% blend percentage). Figure 2.3 illustrates the densities of all the feedstock are greater than those of petroleum diesel (839 kg/m^3). The density (867 kg/m^3) of sesame biodiesel is within the range of EN 14214 standard.

2.2.8.2 Kinematic viscosity

KV is the measurement of inherent resistance to liquid flow. The thickness of oil is estimated by the time at 40 °C for a volume of liquid to flow through a calibrated liquid in glass in viscometer (Sajjadi et al., 2016; Silitonga et al., 2013). The KV of vegetable oil is usually 10 times higher than that of crude diesel, as shown in Table 2.3 in the case of SSO. According to (Sajjadi et al., 2016), vegetable oils are more viscous at 9 to 17 times and 1.6 times than biodiesel and petroleum diesel, respectively. High viscosity fuels form large droplets during injection and cause problems, such as carbon deposits on engine parts and formation of soot due to poor atomization during combustion (Sajjadi et al., 2016; Silitonga et al., 2013; Wakil, Masjuki, et al., 2015). During the winter season or in cold weather, high viscosity fuel mixes with air slowly, and this condition leads to weak combustion and increased exhaust emissions. Fuel with low viscosity cannot provide sufficient lubrication during fuel injection and thus results in wear and leakage (Freitas, Pratas, Ceriani, Lima, & Coutinho, 2010). According to biodiesel standards EN 14214 and ASTM D6571, the limits of biodiesel viscosity are 3.5–5.0 mm^2/s and 1.9–6.0 mm^2/s, respectively. Engine operation at low speed causes high injection volumes and pressure due to the high viscosity of fuel; as a result, clogging of fuel lines and poor atomization and carbon deposits occur. (Sarve et al., 2015) observed that the viscosity of

SSO was 31.51 mm^2/s. After the transesterification, the high viscosity of SSO is significantly decreased to 4.47 mm^2/s for SSO methyl ester and thus meets the required limits set by biodiesel standards. The transesterification aims to reduce the viscosity of oil for meeting the limits of biodiesel standards. As shown in Figure 2.3, the kinematic viscosity (4.47 mm^2/s) of SME is within the range of EN 14214 standard and is greater than those of crude diesel (2.9 mm^2/s), linseed (3.95 mm^2/s) and corn (4.363 mm^2/s) but is less than those of palm (4.63 mm^2/s), jatropha (4.73 mm^2/s), soybean (5.429 mm^2/s) and sunflower (4.719 mm^2/s).

2.2.8.3 Calorific Value

Calorific value (CV) is also considered the most important parameter in selecting fuel. The amount of heat released during the combustion of a specified amount of fuel produces CO_2 and H_2O at its initial temperature. It has no standard value in American (ASTM D6751) and European (EN 14214) standards, but the minimum value of 35 MJ/kg is given in EN 14213 standard (Silitonga et al., 2013). The calorific value for biodiesel is more influenced by high unsaturation than by the carbon chain length. The calorific value of biodiesel declines up to 0.21 MJ/kg by an increase in each percentage of unsaturation of FA methyl ester (Ramírez-Verduzco, Rodríguez-Rodríguez, & del Rayo Jaramillo-Jacob, 2012). The heating value of biodiesel (39.57–41.33 MJ/ kg) is 12% lower than petroleum diesel (~46 MJ/ kg) due to its higher oxygen content (Sajjadi et al., 2016). As shown in Figure 2.3, SME heating value (40.1 MJ/ kg) is the highest of all feedstocks.

2.2.8.4 Cetane Number

Cetane Number (CN) is a key parameter to evaluate the quality of diesel fuel. CN indicates the ignition delay time within the combustion chamber upon injection. High CN takes short ignition delay time to ignite, and this condition results in low idling noise and good cold startup. By contrast, low CN takes long ignition delay time to ignite, and this

condition results in power output reduction, an increase in engine noise, incomplete combustion and inefficiency in fuel conversion (Mat Yasin et al., 2017). Biodiesel easily fulfills the ASTM D6751 minimum specification of 47 for CN, but European standard EN 14214 is more rigorous and is similar to the minimum specification of 51. As shown in Figure 2.3, palm oil methyl ester exhibits the highest CN (59.5), followed by SSO methyl ester (56.35) and soybean methyl ester (53.8). The CN of biodiesel produced from linseed oil methyl ester (48) is on borderline. According to previous literature, adding alcohol-based additives, such as methanol, diethyl ether and ethanol, in small proportions can improve the CN significantly for biodiesel and blended fuel of diesel (Ali, Mamat, Masjuki, & Abdullah, 2016; Yasin, Yusaf, Mamat, & Yusop, 2014).

2.2.8.5 Cold flow properties

The cold flow properties of biodiesel are considered a significant barrier in widespread utilization (Sajjadi et al., 2016). Cloud point (CP), cold filter plugging point (CFPP), and pour point (PP) is considered the cold flow properties. These properties are crucial in utilizing biodiesel under cold weather conditions (Wakil, Kalam, et al., 2015). CP is the temperature at which cloudy appearance can be visualized due to the wax formation. The fuel filter, injectors and lines of diesel engines are clogged due to wax in biodiesel. PP is the lowest temperature at which biodiesel changes its phase from liquid to semi-solid and loses its flow characteristics. Biodiesel is not pumpable when it reaches a semi-solid phase. A high value of CFPP will clog the diesel engine (Dwivedi & Sharma, 2014), (Sajjadi et al., 2016). The freezing point of biodiesel decreases with double bonds and increases with an increase in carbon atoms in its chemical structure (Atabani et al., 2012a). The low-temperature properties of biodiesel are strongly dependent on its degree of unsaturation FA chains. A high degree of unsaturation leads to an enhanced low-temperature performance of biodiesel (Hoekman et al., 2012). A high percentage of saturated FAs, such as palmitic acid (C16:0) and stearic acid (C18:0), in fuel decreases

the low-temperature performance of fuel and increases the values of cold flow properties; thus, the engine of the vehicle easily clogs (Sajjadi et al., 2016). High-saturated esters have a higher melting point and more insufficient cold flow properties than unsaturated esters. Saturated FA (stearic acid) is solid at 39 °C, whilst unsaturated FAs (methyl oleate) melt at –19 °C and methyl linoleate melts at –35 °C (Lanjekar & Deshmukh, 2016). Ramos et al. (Ramos, Fernández, Casas, Rodríguez, & Pérez, 2009) reported a relationship ($R^2 = 0.96$) of the CFPP with a long chain of saturated FA methyl ester content of different feedstocks. The biodiesel having the highest content of saturation showed the worst CFPP. To overcome this problem in cold countries, various options, such as the following, can be utilized: blending with fossil diesel fuel, blending with different vegetable oil methyl esters with good low-temperature performance, using additives and blending of feedstock oils to obtain good cold flow properties. (Echim, Maes, & Greyt, 2012).

SSO contains (80%–85%) unsaturated FAs. The high degree of unsaturation in SSO methyl ester improves its cold flow characteristics compared with other vegetable oils FA methyl esters. The cold flow properties (i.e., CP and PP) of SSO methyl ester have been studied in various literature. Different researchers have reported values for PP (°C) (−5, −14, −9, −18 and 1) and CP (°C) (1, −6, −5, −6.3 and 1) (Ahmad et al., 2009; Sarve et al., 2015; Saydut et al., 2008; Wakil et al., 2014; Younis et al., 2014). (Wakil et al., 2014) reported the value of CFPP (−1 °C) for SSO methyl ester. SSO methyl ester or SSO can be blended with other methyl esters or feedstocks to improve cold flow properties. SSO methyl ester has more favorable cold flow properties than other feedstock oils, as shown in Table 2.6.

Linseed oil methyl ester has more than 90% unsaturation, favorable for cold flow properties, but has inferior oxidation stability (1.5 h), as shown in Table 2.6. In comparison, SSO methyl ester has good cold flow characteristics and oxidation stability.

Palm oil methyl ester has higher saturation than other feedstock and thus has inferior cold flow properties, namely, CP (10 °C) and PP (11 °C). SSO methyl ester exhibits very the best cold flow properties, namely, CP (−6 °C) and PP (−9 °C), among all feedstock due to its high unsaturation, as shown in Figure 2.3.

2.2.8.6 Oxidation stability

Oxidation stability is an vital biodiesel fuel quality measurement parameter (Sendzikiene, Makareviciene, & Janulis, 2005). Biodiesel is more vulnerable to oxidation than other types of diesels, and its properties deteriorate rapidly during long-term storage due to its chemical composition (presence of double bonds) and high unsaturated FAs (Patel & Sankhavara, 2017). The commercialization of biodiesel is a major problem due to its degradability and susceptibility towards oxidation during storage (N. Kumar, 2017). The major influential factors associated with biodiesel stability are FA composition (presence of double bonds), presence of light, heat, air, a trace of metals, elevated temperature, antioxidants and peroxides (Silitonga et al., 2013; Wakil, Kalam, et al., 2015). These factors act as a catalyst during the start of the oxidation process to remove the hydrogen bond from the backbone of the biodiesel (N. Kumar, 2017). The poor stability of biodiesel is associated with the auto-oxidation rate, which depends on the number and position of the double bond in its chemical composition (Atabani et al., 2012a; Hoekman et al., 2012). The reactivity of biodiesel with oxygen increases in exposure to direct sunlight, air and water due to double bonds in its chemical structure (Wakil, Kalam, et al., 2015). During long-term storage, biodiesel degradation due to oxidation leads to the following: an increase in viscosity, acid value and peroxide value; formation of gums; sedimentation; clogging of the fuel filter; rough engine operation; and fuel thickening (Patel & Sankhavara, 2017). The biodegradability of biodiesel due to oxidation alters its important physicochemical and tribological properties during storage, such as peroxide value, density, polymer content, iodine value, acid value and KV, and

reduces its applicability as an alternative fuel for CI engines (N. Kumar, 2017). Biodiesel oxidation usually occurs in two stages, namely, primary and secondary. In the primary stage of the oxidation process, peroxides and hydroperoxides are formed. In the secondary stage, aldehydes and ketones are formed, and resins, sludges or gums form later on during the polymerization process (Dixit et al., 2012; N. Kumar, 2017). During the primary stage of oxidation, the antioxidants present within fuel deplete, and the quality of fuel remains the same. During the secondary (polymerization) phase, the rapid formation of products, such as acid resins, gums, and sludge, severely deteriorate the fuel quality. These degradable products will create problems, such as the clogging of filters and injectors (Christensen & McCormick, 2014; N. Kumar, 2017; Strömberg, Saramat, & Eriksson, 2013). Biodiesel fuel exposure to a high temperature (250 °C–300 °C or above) can also be the other reason for oxidation (Thermal polymerization) of fuel (Yamane, Kawasaki, Sone, Hara, & Prakoso, 2007). (Moser, 2009) concluded that the oxidation stability of alkyl esters increases with a decrease in double bonds by utilizing pressurized differential scanning calorimetry and rancimat method (EN 14112).

The relative oxidation rates for oleates, linoleates and linolenates are 1, 41 and 98, respectively (Holman & Elmer, 1947). The rate of oxidation depends on number of double bonds and the position of double bond, such as linoleic (with two double bonds and one bis-allylic position at C-11) and linolenic (with three double bonds and two bis-allylic positions at C-11 and C-14); thus, hydrogen radical can be easily extracted from these bis-allylic sites during the initial stage of oxidation; accordingly, linolenic acid is more prone to oxidation than linoleic acid (N. Kumar, 2017). Biodiesel oxidation stability can be improved by transforming cis FA methyl ester to trans FA methyl ester because trans FAs have better oxidation stability and lower reactivity than cis FAs (Liu, Lu, Yang, & Bi, 2019). The contents of unsaturated FAs (e.g. linoleic and linolenic acids) play a significant role in the oxidation stability of biodiesel fuel (Park et al., 2008). Two

important structure indices are allylic position equivalent (APE) and bis-allylic position equivalent (BAPE) related to oxidation stability of biodiesel (Knothe & Dunn, 2003). Oxidation stability can be increased by reducing APE and BAPE (Yang, Hollebone, Wang, Yang, & Landriault, 2013).

Rancimat method is a commonly used accelerated method to determine the oxidation stability of oils and biodiesels. It is mentioned in biodiesel standards EN 14214 and ASTM D6751. As per the biodiesel European standard 14214 and ASTM D6751, the minimum induction periods at 110 °C are 6 and 3 h, respectively, for oxidation stability. In vegetable oils and their FA methyl esters, antioxidants can be present naturally or can be added intentionally to improve the oxidation stability of the fuel. Natural antioxidants, such as tocopherols (i.e. vitamin E), which are present as an additive, ensure the stability of fuels (Pullen & Saeed, 2012). The oxidation stability of methyl ester is improved by adding different synthetic antioxidants, such as propyl gallate, butylated hydroxytoluene, pyrogallol, butylated hydroxy anisole and tert-butyl hydroxyl quinone (Patel & Sankhavara, 2017).

SSO is the least prone to oxidative rancidity amongst all other commonly used vegetable oils (Budowski, 1950). The high stability of SSO is due to the presence of a large proportion of unsaponifiable matters, such as sesamin and γ-tocopherol (i.e. vitamin E), compared with α- and δ-tocopherol, and their concentration is influenced by geographical, genetic and environmental factors (Hegde, 2012). SSO contains 0.5%–1.0% sesamin and 0.3%–0.5% sesamolin with a trace amount of free sesamol (Budowski, 1950). SSO is less susceptible to oxidative rancidity due to natural antioxidants (i.e. sesamin, sesamolin and sesamol) with tocopherols (i.e. vitamin E) present in oil (Gharby et al., 2017). According to (Gharby et al., 2017), SSO contains 446 mg/kg tocopherols. The majority of tocopherol is γ-tocopherol (90.5%), followed by δ-tocopherol (7.3%) and

α-tocopherol (2.2%). (Saloua, Eddine, & Hedi, 2009) concluded that α-tocopherol had lower antioxidant capacity than γ-tocopherol. (Gharby et al., 2017) measured the oxidation stability of SSO at 110 °C with a Rancimat 743 (Metrohm Co., Basel) under an airflow rate of 20 L/h with a sample of 3 g oil. The induction time examined for SSO by Rancimat method was 28.5 ± 1 h at 110 °C. FA composition of SSO revealed high unsaturation (around 86%) and showed 7.32 h induction period due to the presence of natural antioxidants (Conceição et al., 2019).

(Pullen & Saeed, 2014) prepared more than 12 biodiesel samples from different oils (e.g. sesame, olive, sunflower, jatropha, rapeseed, soybean, cold-pressed rapeseed (CPR), corn, palm, used cooking oil, groundnut and grapeseed) and two FAME from animal fats (e.g. tallow and lard). Four commercially prepared FAME samples, namely, jatropha, palm, soybean and coconut, were used for comparison. A total of 18 biodiesel samples were used to measure the oxidation stability using the Rancimat method 873 Biodiesel Rancimat instrument under specific operating conditions. For instance, biodiesel sample (3 g) was heated to 110 °C under a steady flow rate (10 l/h) of air. The Rancimat induction period (RIP) results varied significantly amongst all samples. Only sesame (6.25 h) fulfilled the EN 14214 minimum set requirement (≥ 6 h). Most biodiesel samples showed low RIP (< 1 h). The SSO contained natural antioxidants, such as tocopherol (i.e., vitamin E) and preservatives, sesamin and sesamol. As a result, it is more stable towards oxidative rancidity than other vegetable oil and fats.

Two biodiesel samples, namely, sesame and CPR oil (300 g each), were stored in an airtight glass jar and immersed in a water bath (constant temperature of 40 °C) for 100 days to estimate the storage life. During the storage, KV (at 40 °C) and acid value were measured periodically (after every 10 days) for the prediction of oxidation. In the case of rapeseed, an increase was noticed in KV and acid value around 500 h. However, sesame

showed good resistance towards change in values until 2000 h. In Figure 2.3, SSO methyl ester had 6.25 h oxidation stability instead of having more than 84% unsaturation. The major reason for the high oxidation stability of SSO methyl ester is due to naturally occurring antioxidants and preservatives, such as tocopherol (i.e., vitamin E), sesamol and sesamin.

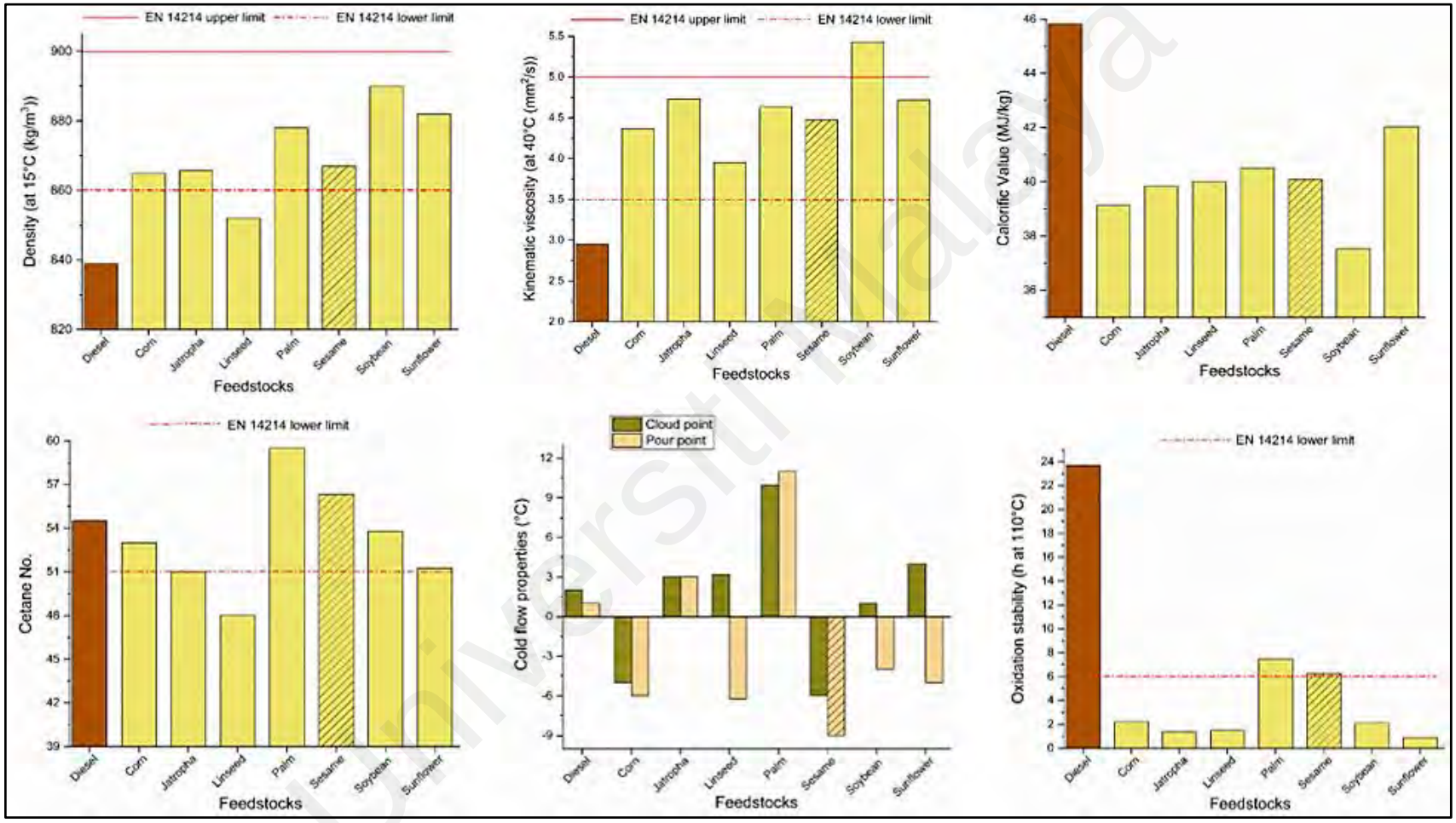

Figure 2.3: Physicochemical properties of various bio-based fatty acid methyl esters (biodiesel)

Table 2.6: Physico-chemical properties of fatty acid methyl esters from various vegetable oils

Vegetable oil Methyl Esters ↓	Fatty acid composition		Cold flow properties		Oxidation stability (OS) (h) at 110 °C	Cetane No.	Density (kg/m^3) at 15°C	Kinematic Viscosity at 40°C (mm^2/s)	Flash Point °C	Heating value (MJ/kg)	References
	Sat %	Un-sat %	CP °C	PP °C							
Palm	44.6	55.4	10	11	7.50	59.5	878	4.63	182.5	40.51	(Rashed et al., 2016)
Linseed	8.3	91.7	3.17	-6.25	1.5	48	852	3.95	151	40	(R. Kumar, Tiwari, & Garg, 2013)
Sesame	16	84	- 6	- 9	6.25	56.32	867	4.47	180	40.1	(Sarve et al., 2015)
Corn	14.4	85.6	- 5	- 6	2.2	53	865	4.363	170	39.12	(Nagaraja, Soorya Prakash, Sudhakaran, & Sathish Kumar, 2016)
Jatropha	22.6	77.4	3	3	1.37	51	865.7	4.73	184.5	39.83	(Rashed et al., 2016)
Sunflower	10.5	89.5	4.0	- 5	0.9	51.25	882	4.719	183	42.02	(A. Saydut et al., 2016)
Soybean	15.6	84.4	1	- 4	2.1	53.80	890	5.429	148	37.52	(Can et al., 2016)
Diesel	-	-	2	1	23.70	54.5	839	2.95	71.5	45.825	(Mat Yasin et al., 2017)

2.2.8.7 Engine performance and emission characteristics of SSO methyl ester and its blends

Most researchers have reported reduction in HC, CO and smoke opacity emissions by substituting diesel fuel with biodiesel, as shown in Table 2.7. Biodiesel contains more than 11% oxygen, which improves the combustion quality (complete combustion) by assisted conversion of CO to CO_2 (Habibullah et al., 2014). Complete combustion of fuel results in low CO and particulate emissions. SSO methyl ester exhibits lower HC, NO_x and smoke emissions and higher CO emissions than crude diesel. The formation of NO_x mainly depends on in-cylinder combustion temperature, residence time of reaction and concentration of oxygen (Sharon, Ram, Fernando, Murali, & Muthusamy, 2013). Sesame biodiesel reduces the NO_x emissions amongst all other biodiesels, as presented in Table 2.7. Low CN of sesame biodiesel reduces the in-cylinder combustion temperature, and this condition results in low NO_x emissions. The BSFC of all biodiesel-diesel blends are higher than that of crude diesel, except linseed and jatropha methyl ester blends. High density and viscosity of biodiesel inject large amount of fuel during combustion, which results in increases in BSFC. BTE is inversely proportional to BSFC. Sesame and corn biodiesel reduce the NO_x amongst the other biodiesel-diesel blends. Engine performance and emission characteristics of sesame biodiesel have been rarely researched (Wakil, Masjuki, et al., 2015) and (Banapurmath et al., 2008). Sesame biodiesel is a potentially viable source to eradicate the NO_x emissions by blending with another potential feedstock.

Table 2.7: Comparison of Engine performance and emission characteristics of various biodiesel-diesel blends with diesel

Biodiesel	Biodiesel blend	References	Engine Performance		Engine Emissions			
			BTE	BSFC	CO	HC	NO_x	Smoke
Linseed	B10	(Akram, Singh, Sharma, & Singh, 2019)	↑	↓	↓	↓	↑	↑
Sesame	B20	(Wakil, Masjuki, et al., 2015)	↓	↑	↑	↓	↓	↓
Palm	B20	(Gad et al., 2018)	↓	↑	↓	↓	↑	-
Soybean	B20	(Özener, Yüksek, Ergenç, & Özkan, 2014)	-	↑	↓	↓	↑	↓
Jatropha	B20	(Ong et al., 2014a)	↑	↓	↓	↓	↑	↓
Sunflower	B10	(Dueso et al., 2018)	↓	↑	↓	↓	↑	↓
Corn	B20	(Balamuruga n, Arun, & Sathishkuma r, 2018)	↓	↑	↑	↑	↓	↑

2.2.8.8 Cost analysis of SSO

Process description of sesame cultivation, harvesting, oil extraction and production of biodiesel, along with cost analysis, is exhibited in Figure 2.4. Sesame crop is mainly cultivated in Africa and Asia. Acid-free, light sandy and medium loam soils are preferable for the cultivation of sesame. Sesame crop is preferably cultivated in July of every year in Asia. The average yield of sesame seeds is 1400 kg/ha in the United Republic of Tanzania (FAO, 2018). Sesame crop matured in 100–120 days, and 75% of the mature crop can also be harvested. Sesame seeds are segregated on seed quality. High-quality seeds are utilized for the food industry, and few seeds are used for SSO production. High-quality SSO is used for salad and meal garnishing. SSO is not recommended for frying the food. The high-quality sesame seed's price in Pakistan is 0.85 $/kg, and that of SSO is 1.7 $/L. Low-quality sesame seeds utilized for extraction of SSO are used for animal

feeding in the winter season. Cake of sesame seeds is also utilized as a food for animals. SSO has the potential to be utilized as an emerging feedstock for biofuel production due to its unique characteristics. The low-quality sesame seed price in Pakistan is 0.64 $/kg, and that of SSO is 1.28 $/L. The production cost of biodiesel is 0.66 $/L. SSO price is relatively expensive due to the weak demand in the market. SSO price will be decreased in the future by increasing the overall production of sesame seeds worldwide. The production rate of sesame seeds can also be increased by suggesting new alternative ways of utilization, such as biodiesel production. SSO can also be blended with other feedstocks to improve their cold flow and oxidation stability characteristics and reduce NO_x emissions. Sesame biodiesel can be used in the future as a viable alternative feedstock for biodiesel production due to its unique physicochemical properties.

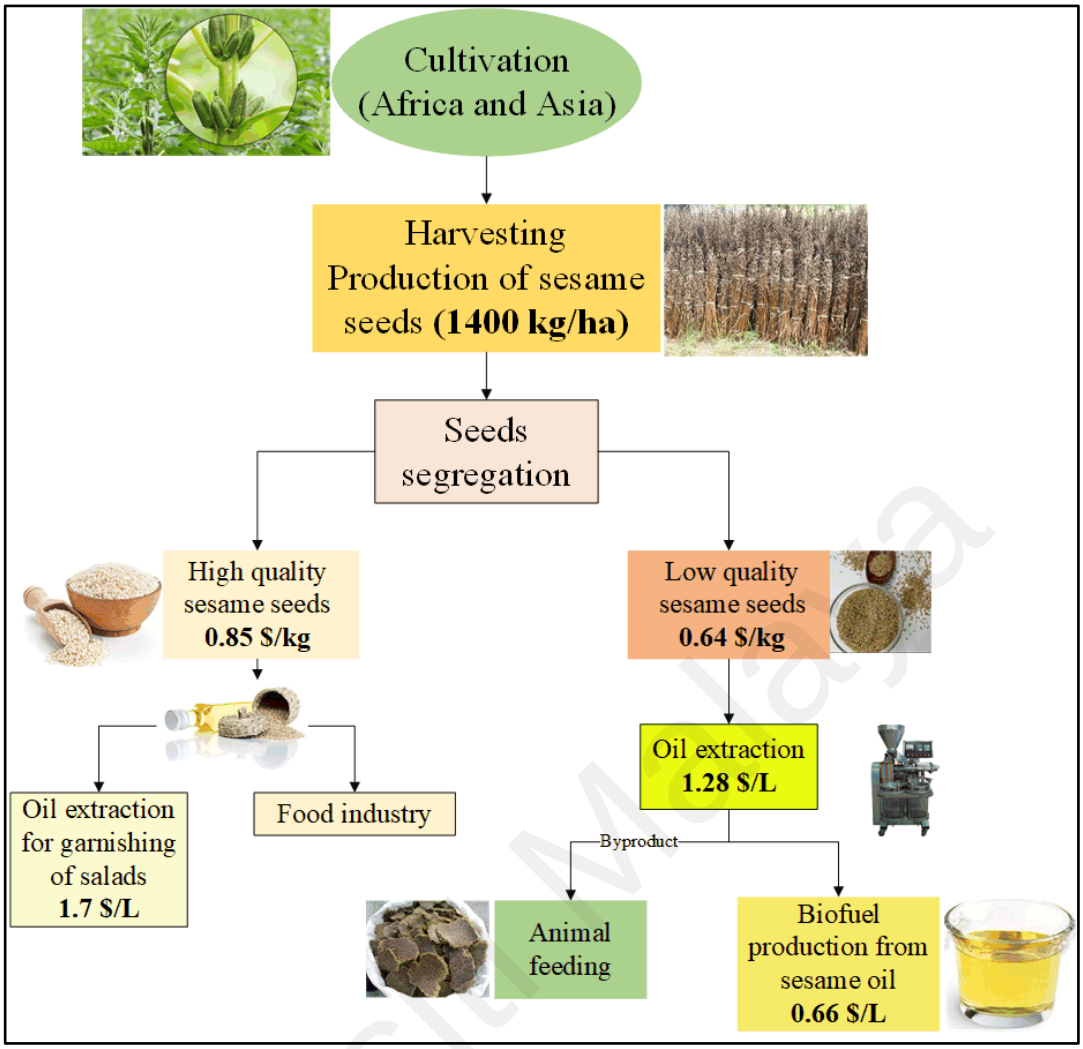

Figure 2.4: Cost analysis of sesame crop to sesame oil for biofuel production

2.3 Production of biodiesel

Vegetable oil can be used directly or mixed with petroleum diesel in a diesel engine. The use of pure vegetable oil and its blends as a fuel in diesel engine had been considered problematic due to its high viscosity. The fatty acid content and high viscosity of sesame oil lead to several problems in diesel engines: fuel lines and filter blockage, poor atomization of fuel, injector coking and piston ring sticking, gum formation (due to oxidation) during storage and combustion, severe carbon deposition in the engine due to incomplete combustion and degradation and thickening of lubricating oil (Altun et al., 2008). The solution to these problems caused by the high viscosity of virgin oil can be overcome by converting it to viable biodiesel.

According to (Ma & Hanna, 1999), there are four possible ways to convert virgin oil to biodiesel as a suitable and viable fuel source for diesel engines: direct use and blends with crude diesel, micro-emulsification, thermal cracking (pyrolysis), supercritical methanol and transesterification. The blending of virgin oil with crude diesel and emulsification of virgin oil with solvents (methanol, ethanol, and 1-butanol) lowers the viscosity of virgin oil, but engine performance is still problematic due to carbon deposition and lubricant oil degradation. Thermal cracking or pyrolysis is normally used for producing bio gasoline instead of biodiesel. Transesterification is the preferred method for the conversion of virgin oil to biodiesel for better engine performance. A comparison between these biodiesel production techniques is discussed in Table 2.8.

Table 2.8: Comparison between biodiesel production techniques

Production techniques	Advantages	Disadvantages
Thermal cracking (pyrolysis)	• No - pollution • Simple process	• Purity is low • High temperature is required • Equipment is expensive
Supercritical methanol	• High conversion rate • Catalyst is not required • Short reaction time	• High energy consumption • Equipment is expensive • High pressure and temperature are required
Direct blending (micro-emulsion)	• Simple process	• Poor volatility • High viscosity • Poor stability
Transesterification	• Fuel properties are comparable to diesel. • Equipment cost is low. • High conversion rate • The process is feasible for commercialized production	• High pollutants are produced. • Separation of products is very difficult. • Side reactions will occur during production. • Low water content and acid value are required for base catalyst

2.3.1 Transesterification

Transesterification is the chemical reaction of a triglyceride (fat or oil) with an alcohol to produce esters and glycerol, as shown in Figure 2.5. The transesterification reaction is the conversion of triglyceride into a fatty acid mono-alkyl ester (biodiesel) in the presence of alcohol (methanol is used generally due to its lower cost and effectiveness (Demirbas, 2005)) using a catalyst and it produces glycerol as a byproduct.

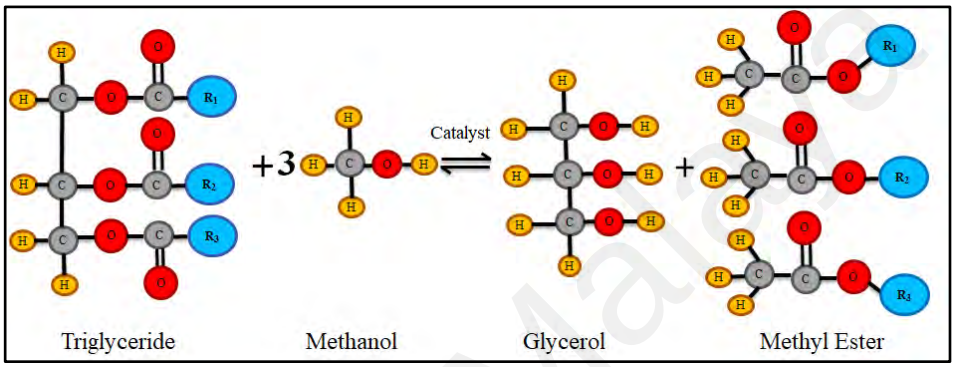

Figure 2.5: Transesterification reaction for biodiesel production

A catalyst is important during the transesterification reaction because it enhances the reaction rate and yield. The selection of a catalyst depends on the free FA content, nature of oil and moisture content (Onoji, Iyuke, Igbafe, & Nkazi, 2016). The alkali-catalyzed transesterification reaction includes NaOH, KOH, carbonates and alkoxides of (Na and K), such as sodium methoxide. Acid catalysts include hydrochloric, sulfuric and sulfonic acids. Lipases can also be used as biocatalysts. The alkaline-catalyzed transesterification is considerably faster than the acid-catalyzed transesterification and is the preferred catalyst in the commercial production of biodiesel (Ma & Hanna, 1999). The conversion of triglycerides into FA mono-alkyl ester and glycerol occurs in three reversible steps (Patel & Sankhavara, 2017), as shown in Figure 2.6.

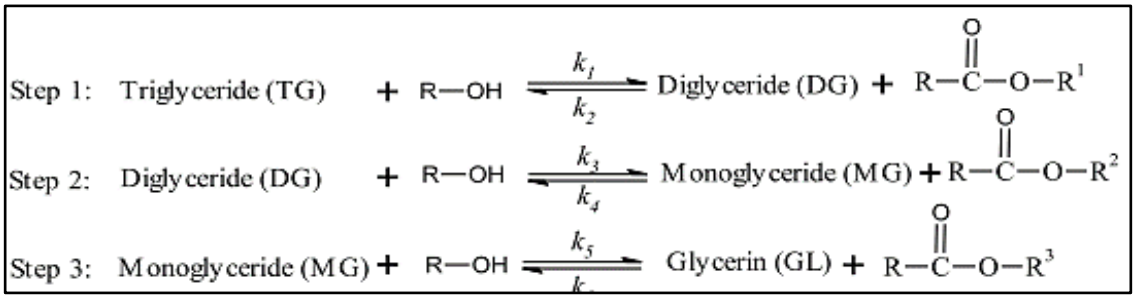

Figure 2.6: Conversion of triglyceride to fatty acid methyl ester step by step transesterification reaction

Homogeneous alkali base catalysts (NaOH, CH_3ONa and KOH) are the most reactive in the transesterification process for oil with a free FA value less than 1%. Acid catalysts (i.e. sulphuric acid (H_2SO_4) and hydrochloric acid (HCl) are used for esterification of oil having a free FA value greater than 1% before transesterification reaction. Esterification is necessary to obtain rid of soap formation and a high yield during the transesterification reaction (Onoji et al., 2016).

Nowadays, the conventional method is used for the transesterification process to convert vegetable oil to biodiesel. Conventional methods encountered mass transfer limitation, higher operating cost, and high energy consumption, resulting in lower biodiesel production yield. Several other methods are used for transesterification like membrane technology, supercritical process (non-catalytic), reactive distillation, microwave, and ultrasonication. Among those techniques, microwave and ultrasonication have the potential to be upgraded to the industrial level for biodiesel production. The microwave process consumed twenty-three times less energy than the conventional method for biodiesel production. The few advantages of microwaves are less energy consumption, higher production yield, less reaction time (10 times shorter), less catalyst required, and uniform heat distribution. It is not advisable to upgrade this microwave technology to the industrial level due to the damage of organic molecules because of high microwave output power. Ultrasonication can be a promising technique among other transesterification methods because it can enhance the mass transfer, heat, and mixing

between reactants of the transesterification process during biodiesel production (Maddikeri, Pandit, & Gogate, 2013).

2.3.1.1 Ultrasound-assisted transesterification method

Ultrasound-assisted transesterification is a very promising technique to produce biodiesel due to its cost-effectiveness and energy-efficiency. Less energy consumed by ultrasound-assisted transesterification as compared to conventional transesterification (Tan et al., 2019). Ultrasound produces cavitation (bubbles formation due to variation in pressure), which enhances the chemical reaction of the transesterification process by providing mechanical and activation energies. (Martinez-Guerra & Gude, 2016) reported that specific ultrasonic energy (pulse sonication or continuous sonication) significantly influenced on the yield of biodiesel. They reported the maximum yield 98% of biodiesel obtained from waste cooking oil for pulse sonication (5s on and 1s off) and 93% of biodiesel yield for continuous sonication. Pulse sonication improves mass transfer and enhances energy efficiency. Pulse sonication can convert any feedstock oil to biodiesel (Martinez-Guerra & Gude, 2014). The duty cycle is generally expressed as a percentage, which corresponds to the ratio of the pulse duration to the total cycle time (Pan, Qu, Ma, Atungulu, & McHugh, 2011). Pulse duration is “On” time and “Off” time of ultrasound sonicator. (Subhedar & Gogate, 2016) revealed that the ultrasonic duty cycle is the most important parameter to be considered when assessing the energy requirements and process economies to obtain maximum yields. An optimum duty cycle is necessary during biodiesel production to ensure that sonicator operates efficiently and protects the ultrasound probe tip from erosion (Martinez-Guerra & Gude, 2016). At an industrial level, ultrasound is the most promising technique in terms of energy-efficient, less catalyst consumption, time-efficient, and cost-effective.

2.3.2 Optimization techniques for the transesterification process

The transesterification process involved many parameters (time, methanol to oil ratio, catalyst concentration, temperature, amplitude, duty cycle, etc.) directly affecting the reaction and biodiesel yield. The response surface methodology (RSM) was utilized to visualize the effect of independent input process parameters on output variables. This tool assists the researchers by designing a fewer number of experiments to get optimum results (Muthukumaran et al., 2017). Various researchers use the RSM tool to optimize biodiesel production process parameters by varying input independent process variables with limited experiments to save cost, effort, material, and time (Milano et al., 2018). (Dwivedi & Sharma, 2015) used RSM based on Box Behnken design to optimize the process parameters for the production of biodiesel from Pongamia oil.. (Niju, Rabia, Devi, Kumar, & Balajii, 2020) optimized the process parameters (heterogeneous catalyst (*Malleus malleus shells*) concentration, methanol-to-oil ratio, and reaction time) to maximize the biodiesel yield from waste cooking oil to 93.81% using RSM based on Box-Behnken design. Box-Behnken design for each process variable restricted to three levels to prevent the extreme values of process parameters that reduce the probability of failure. Box-Behnken based RSM design is most preferable, cost-effective, and efficient than Central Composite based design (Okoye et al., 2020).

The neural network of the ELM is feed-forward with a single hidden layer. In extreme learning machines, the hidden layers do not need tuning, and the hidden layer parameters can be fixed. The parameters of the hidden layer in extreme learning machines are initialized randomly, and the Moore-Penrose generalized inverse is used to determine the output weights analytically with very fast learning speed. Therefore, ELM has superior generalization capability than conventional artificial neural networks (Wang, Wang, & Ji, 2015). (Wong, Wong, Cheung, & Vong, 2013) reported that ELM superior to other modeling in accuracy and time. Cuckoo search with the levy flight is a robust meta-

heuristic optimization that is based on parasitism combining with the Lévy flight algorithm. (Silitonga et al., 2020) used ELM with the cuckoo search algorithm to predict and optimize the process parameters to achieve a maximum yield of 96.19% from *Ceiba pentandra* oil using a microwave-assisted transesterification process. Other researchers explored various techniques to maximize the biodiesel yield are presented in Table 2.9.

Table 2.9: Optimization methods for different feedstocks

Feedstock	Optimization Technique	Biodiesel Yield (%)	References
Pongamia oil	RSM based on Box Behnken	98.4	(Dwivedi & Sharma, 2015)
Terminalia bellerica oil	RSM based on Box Behnken	97.98	(Marwaha, Rosha, Mohapatra, Mahla, & Dhir, 2019)
Neem oil	RSM based on Box Behnken	97.14	(Chhabra, Saini, & Dwivedi, 2020)
Waste cooking oil	RSM based on Box Behnken	93.81	(Niju et al., 2020)
Calophyllum inophyllum-Ceiba pentandra oil mixture	ANN with ant colony	95.87	(Ong et al., 2019)
Ceiba pentandra oil	ELM with Cuckoo search algorithm	96.19	(Silitonga et al., 2020)

This study aimed to optimize the process parameters of ultrasound-assisted transesterification to produce palm-sesame biodiesel using the RSM tool based on the Box-Behnken design and ELM modeling coupled with the cuckoo search algorithm. Palm and sesame oils were blended in appropriate proportion before transesterification to improve the cold flow characteristics of palm biodiesel.

2.4 Lubricity of fuel

Diesel fuel lubricity is crucial for engine components because injection systems and pumps are mainly lubricated by diesel fuel. The lubricity of diesel fuel is reduced due to eliminating polar compounds (polyaromatic and nitrogen) during the desulfurization process. These compounds produce a lubricating film (protective layer) between the metal

mating surface to minimize wear and friction. High-pressure fuel injection systems can also reduce engine emissions, so fuel lubricity is a key parameter to protect the injection system and other different engine components fuel lubricity (Lapuerta et al., 2010). Fuel lubricity is a crucial factor that should be controlled concerning the durability of diesel engine components. Many nations started to use ULSD (Ultra-Low Sulfur Diesel) to fulfill the Kyoto Protocol to minimize greenhouse gas emissions. ULSD has very poor lubricity in comparison to petroleum diesel. Desulfurization process reduced the sulfur content up to the minimum level (15 ppm), polar compounds, and other heteroatoms (oxygen and nitrogen compounds) from crude diesel (Farias, Medeiros, & Alves, 2014). Due to insufficient lubrication provided ULSD fuel during fuel injection and pumping, engine parts become corroded or damaged. The addition of biodiesel in petroleum diesel significantly reduced the wear and friction due to the presence of 98% methyl ester content and other trace elements (monoglycerides, free glycerin, diglycerides, free fatty acids, antioxidants, tocopherols, vitamin E, etc.) (Wadumesthrige, Ara, Salley, & Ng, 2009). By incorporating fuel additives, several experts have researched enhancing engine performance and emissions. It is also necessary that this additive effect on the lubricity of blended fuel or ternary fuel (diesel-biodiesel- additive) should also be evaluated prior to diesel engine testing.

This study evaluates the effect of fuel additives on the lubricity of diesel-biodiesel blends (B30 as a base fuel) that were already proved good for enhancing the performance and emissions of the IC engines. Tribological behavior was observed for ternary blends (diesel-biodiesel-fuel additive) for the durability of diesel engines, pumps, and fuel injectors. According to the procedure described in ASTM, ternary fuel blends' lubricity is evaluated using HFRR (D6079-11). Palm-sesame oil blends were prepared to produce biodiesel. Palm and sesame oil mixed with a ratio of 50:50 to improve cold flow properties and oxidation stability. Sesame oil is mixed with palm oil prior to biodiesel

production to improve palm oil's poor cold flow properties. Sesame oil exhibits excellent cold flow properties as well as oxidation stability, among other feedstocks. Sesame oil contains naturally occurring antioxidants. Sesame crop is cultivated in mostly Africa and Asia region. The United Republic of Tanzania is leading in the cultivation of sesame crops around the globe. The cost of low-quality sesame seeds is 0.64 $/kg, and sesame seed oil is 1.28 $/L.

In diesel engines, pumps and injectors are lubricated by diesel fuel itself during operation. Many researchers used different fuel additives (nanoparticles and oxygenated alcohols) to improve diesel engine performance and emission characteristics (Farias et al., 2014). Few researchers explored the effect of fuel additives on the lubricity of the fuel. The lubricity of fuel is a critical parameter related to the durability of diesel engines. Fuel additive's lubricity should be analyzed prior to engine testing. The lubricity of diesel injectors is crucial during the supply of diesel fuel in the combustion chamber. HFRR test is conducted with a ball-on-plate combination to analyze diesel fuel's lubricity with biodiesel and fuel additives mixture for fuel injector application. For this research work, ethanol and dimethyl carbonate have been chosen as an oxygenated distilled fuel additive and carbon nanotubes and titanium oxide as a nanoparticle additive. A SEM tool was utilized to analyze the plate and ball scars used in HFFR tests.

2.5 Lubricant contamination

Wear and friction contribute approximately 25 percent of the world's total energy loss, Oakridge National Laboratory (USA) states (Taha-Tijerina, Shaji, Sharma Kanakkillam, Mendivil Palma, & Aviña, 2020). Lubricant film reduces friction and wears; consequently, efficiency increases. According to previous literature, the lubricant is contaminated with fuel up to 5% due to crankcase dilution (Arumugam & G. Sriram, 2013). After dilution, lubricant properties will be altered, which directly affects tribological properties. Few researchers investigated the effect of biodiesel dilution with

lubricant on its tribological characteristics (Maleque, Masjuki, & Haseeb, 2000; Sulek, Kulczycki, & Malysa, 2010). (Agarwal, 2003a) reported that lubricating oil with a 20 % biodiesel-fueled system contains less possible contaminants (like soot, wear debris, oxidation products, resins, moisture) and low wear than the diesel-fueled system. This was because of the self-lubricity characteristic of biodiesel. (Arumugam & Sriram, 2012) reported that rapeseed-bio lubricant contaminated with 10 % rapeseed-biodiesel (B20) fuel showed less wear and friction than commercial synthetic lubricant contaminated with 10% diesel fuel tested by pin-on-disc apparatus with engine cylinder liner–piston ring combinations. (Dhar & Agarwal, 2014) investigated the tribology of lubricating oil of diesel engine run on Karanja biodiesel (B20) blend and mineral-based diesel during endurance test of 200 hours. His investigation proved that lubricating oil obtained from the biodiesel fueled engine contained a significantly high amount of wear trace metals, resinous, ash content, and soot than the lubricating oil from the mineral diesel-fueled engine. Hence, 20% Karanja biodiesel (B20) caused more deterioration of lubricating oil than mineral diesel. As the chemical composition of biodiesel fuels (as synthesized from different sources of vegetable oils) and mineral diesel are different so their effects on lubricating oil life and its degradation will also be different as investigated by (Agarwal, 2003b). During engine operation, all the debris resulted from corrosive and metallic wear were added in lubricating oil. Hence, it is necessary to examine the effect of combustible fuels on tribology of lubricant to check their suitability for CI engines.

Few researchers conducted a study on lubricating oil degradation by biodiesel fuels like (Y. Singh, Singla, & Singh, 2017) observed that 5-8% dilution of B100 moringa methyl ester in synthetic lubricant enhances the lubricity of the lubricant, but the further increase in dilution resulted in high wear rate. Similar improvement in tribological characteristics of synthetic lubricant with the dilution of 5% biodiesel reported by other researchers (Maleque et al., 2000; Sulek et al., 2010). A 5% contamination of lubricant

with fuel occurred because of crankcase dilution during engine operation (Arumugam & G. Sriram, 2013). But no-one conducted research on lubricating oil degradation with diesel, diesel-biodiesel, and diesel-biodiesel-fuel additive fuels to study the tribological behavior. Nowadays, everyone is using different fuel additives (oxygenated alcohols and NPs) to enhance the CI engine characteristics (Manzoore Elahi M. Soudagar et al., 2020). However, no one is concerned about lubricating oil degradation during crankcase dilution due to the mixing of combustible fuel with lubricant. This study should be conducted as the engine life will be shortened due to contamination of the lubricant oil with diesel fuel (blended with biodiesel and fuel additive). Many researchers did not give any attention to lubricant degradation due to dilution with diesel-biodiesel-fuel additives. Tribological study of ternary fuel blends should be conducted before engine application to ensure its effect on degradation of the lubricant.

In this current investigation, palm-sesame biodiesel fuels with alcoholic or nano-particle additives diluted up to 5 % (by volume) of commercial lubricant to evaluate their influence on contaminated lubricant tribology. According to our best knowledge, no one researched the influence of different diesel-methyl ester blends with fuel additives on the tribology of contaminated lubricant. Six different types of fuels (including commercial diesel (B10), palm-sesame biodiesel blend (B30), B30 with alcoholic (Ethanol and DMC), and nanoparticle (TiO_2 and CNT additives were selected to investigate their effects on tribological characteristics of lubricating oil by four-ball tribo-tester.

2.6 Engine performance and emission characteristics

The transport sector consumes fossil fuels abruptly to meet energy requirements. Almost 50% of fossil fuels used to meet the energy requirements of the transport sector, due to this factor, fossil fuels are on the verge of exhaustion. Fossil fuel reserves are decreasing rapidly, and the dramatic effect of greenhouse gas (GHG) emissions on

climate change have prompted researchers to explore renewable fuel sources to replace conventional fossil fuels in diesel engines. Many researchers have investigated different renewable biofuels (biodiesel, vegetable oils, alcohol, etc.) (A. Atabani et al., 2019; Milano et al., 2018; Saxena, Kumar, & Saxena, 2019). Biodiesel is best suited alternative fuel in diesel engines due to its better physicochemical properties (biodegradable, high cetane number, non-hazardous, high flash point, low sulfur content, and presence of oxygen content) than diesel (Mahlia et al., 2020). The commercialization of biodiesel in the transport sector is restricted due to poor atomization of fuel, high density, poor cold flow CFPP, PP and CP, higher NO_x emissions, lower brake specific fuel consumption BSFC, poor oxidation stability, sticking the piston ring, and cold start problem (A. Atabani et al., 2013; Ong et al., 2014b; Silitonga et al., 2013). These drawbacks can be resolved by adopting various new methods such as the addition of oxygenated alcohols and nanoparticles as additives which may lead to enhanced diesel engine characteristics (Soudagar et al., 2018).

In Malaysia and Indonesia, biodiesel is basically produced from palm oil. The Malaysian Palm Oil Board (MPOB) aims to introduce B30 palm biodiesel by 2025. The biodiesel blend B10 is currently used in the transport sector in Malaysia; due to highly saturated feedstock, the cold flow properties of palm methyl ester are poor (CP (16 °C) and PP (15 °C)) (Atabani et al., 2012a; Silitonga et al., 2020). These reported poor cold flow properties to result in fuel starvation, incomplete combustion, and fuel filter clogging during cold weather (Nguyen, Pham, & Le Anh, 2020; Ong et al., 2019). Critical review reported that palm oil cold flow properties could be enhanced through blending with high unsaturated fatty acid feedstock such as sesame oil. Sesame oil is ideally suited for mixing with palm oil among the highly unsaturated feedstocks to enhance the cold flow properties and improve the oxidation stability in accordance with ASTM and EN standards.

The addition of various fuel additives, such as liquid (oxygenated alcohols) and solid (nanoparticles), to biodiesel-diesel blends are receiving more attention in diesel engines. The use of alcohol in CI engines as a fuel improver is challenging due to high auto-ignition temperature, weak lubricating properties, and lower cetane number (El-Seesy & Hassan, 2019; Gul et al., 2019). While nanoparticles exhibit an excellent effect in reducing NO_x and carbon emissions and improvement in engine performance such as BP, BSFC, and BTE. Previous studies have reported that the nanoparticles such as Al_2O_3, CuO, ZnO, TiO_2, MnO, CeO_2, Fe_2O_3, CNT, and GO showed excellent results in attaining high BP, high BTE, lower NO_x, and lower carbon emissions among the explored metallic and carbon-based nanoparticles (Nanthagopal, Ashok, Tamilarasu, Johny, & Mohan, 2017; Soudagar et al., 2018; Valihesari, Pirouzfar, Ommi, & Zamankhan, 2019; Z. Zhang et al., 2019). (Ghanbari et al., 2017) used carbon-based multi-wall CNT as a diesel-biodiesel fuel additive which caused lower BSFC and CO emissions but higher HC emissions collated to petroleum diesel. (Raju, Kishore, Nanthagopal, & Ashok, 2018) reported that CNT as a nano fuel additive reduces the BSFC and engine emissions (NO_x, CO, and HC). (Manzoore Elahi M Soudagar et al., 2020; M. E. M. Soudagar et al., 2019) investigated the effect of 20-60 ppm of Al_2O_3 and graphene oxide nanoparticles in Honge and dairy scum biodiesel, respectively. The fuel blends HOME2040 and DSOME2040 enhanced the overall engine characteristics. (Hosseini, Taghizadeh-Alisaraei, Ghobadian, & Abbaszadeh-Mayvan, 2017b) concluded that CNT is a fuel additive in diesel engines improved the BP (3.67%), exhaust gas temperature (5.57%), and BTE (5.57%). Soot, CO, HC, and BSFC decreased while NO_x emission increases. The value of BSFC is also reduced because of the better fuel-air mixture with the use of CNT having a larger surface area. The higher catalytic activity of CNT carbon-based nanoparticles improved the combustion characteristics that reduced engine emissions (Soot, CO, HC, and NO_x). (Gad & Jayaraj, 2020) performed a comparative study on Jatropha biodiesel using different

nanoparticles (AL_2O_3, TiO_2, and CNT). Among these nanoparticles, CNT with 50 ppm concentration reduces the CO emissions by 35% and NO_x emissions by 52%. (El-Seesy & Hassan, 2019) compared different carbon-based nanoparticles (GO, GNPs, and MWCNTs) with Jatropha biodiesel in a diesel engine. MWCNTs exhibited promising results in a reduction of engine emissions the CO, NO_x and HC reduced by 65%, 70% and 50%, respectively, BSFC lowered by 35%) and 25% increase in BTE compared to petroleum diesel. (Mei, Zuo, Adu-Mensah, Li, & Yuan, 2019) compared two nanoparticles (carbon nanotubes and molybdenum trioxide) blended with diesel in the CI engine. CNT fuel blends showed a reduction in BSFC and engine emissions (CO, NO_x and HC). (Saxena et al., 2019) used TiO_2 (150 ppm) as a fuel additive with Acacia Concinna biodiesel in a diesel engine. BSFC and, HC and smoke emissions reduce, BTE increases, while the NO_x emissions slightly increase.

Several studies investigated the influence of oxygenated alcoholic fuel additives in diesel engines. DEE has favorable properties such as high volatility, high oxygen content, less viscosity, non-corrosive, and high cetane number for CI engines collated to diesel (S. Kumar, Dinesha, Ajay, & Kabbur, 2020). Moreover, DEE has a higher heating value in comparison to butanol and ethanol (Rakopoulos, Rakopoulos, Giakoumis, Papagiannakis, & Kyritsis, 2014). DEE as a fuel improver enhanced the engine performance characteristics BTE increases by 7.2% and BSFC reduces by 6.7% compared to diesel (Ibrahim, 2016). (Jayaprabakar, Anish, Beemkumar, Mathew, & Alex George, 2019) blended DEE (10%) with diesel-biodiesel blends in an unmodified engine. Different concentrations (5-12.5% by volume) of DEE as a fuel improver were added to diesel-biodiesel blends. The ternary blends exhibited promising reductions in emissions (NO_x (57%), CO (4.6%) and HC (84%)) at 100% engine load (Nanthagopal, Ashok, Garnepudi, Tarun, & Dhinesh, 2019). DMC contains a high content of oxygen, around 53.3% among other oxygenated fuel alcohols. The process of combustion is enhanced due to the fuel

interaction with oxygen present in the C-C bond to form CO which will further reduce the smoke emissions. DMC is miscible in diesel up to 15 % vol compared to ethanol and methanol which require additional surfactants or solvents to achieve a stable diesel-alcohol blend without phase separation (Rounce, Tsolakis, Leung, & York, 2010). (Pan et al., 2019) examined the influence of DMC (10% and 20% vol.) with petroleum diesel in a CI diesel engine. DMC (10%) showed better BTE than diesel, 80% of soot emissions were minimized when DMC (20%) is blended with diesel.

The literature reviewed shows that both nanoparticles and oxygenated alcohols positively influence performance characteristics and reduce exhaust emission of diesel engines when used as additives with biodiesel-diesel fuel blends. Before the transesterification process, sesame oil can be blended with palm oil (50:50) to enhance the cold flow characteristics. Among many vegetable oils, sesame oil is a promising biodiesel feedstock that can improve the cold flow characteristics of palm oil without modifying the oxidation stability and within the permissible ASTM and EN standards. Therefore, in the current investigation, the drawbacks of palm biodiesel, such as cold weather starting of diesel engines, poor cold flow properties, and higher NO_x emission, can be overcome by using palm-sesame biodiesel with fuel additives nanoparticles and oxygenated alcohols in diesel engines. The literature review suggests that there are no previous studies reported on the application of oxygenated alcohols (DMC and DEE) and nanoparticles (CNT and TiO_2) as fuel additives in diesel-palm and sesame biodiesel in diesel engines. Thus, in the current study, B30 fuel blend is prepared by mixing palm-sesame methyl ester in the 50:50 ratio and blended with CNT (100 ppm), TiO_2 (100 ppm), DMC (10%), and DEE (5%) to form ternary fuel blends for diesel engine application. Then, a comprehensive investigation is carried out on the engine performance (BP, BTE, and BSFC) and emission (CO, NO_x, and HC) characteristics as well as compared with B10 (Commercial Malaysian diesel) and B30 blends without fuel additives. Hence, the

effect of nanoparticles and alcoholic fuel additives with diesel- biodiesel blends on diesel engine performance and emission characteristics are carried out. Finally, palm-sesame biodiesel blended with diesel and fuel additives to evaluate their effect on the diesel engine.

2.7 Biodiesel standards

Most researchers have reported that biodiesel is fire-resistant due to the higher flash point compared to diesel. Amber-yellowish-colored biodiesel has a viscosity comparable to that of crude diesel (Al-Dawody & Bhatti, 2013; Mat Yasin et al., 2017). Biodiesel producers should follow the fuel standard requirements set by two reputable biodiesel standards that are used for testing fuels. The standards used to ensure the biodiesel quality are EN 14214 for European Union (EU) and ASTM D6751 for the American biodiesel standard (Atabani et al., 2012a). The significant factors affecting the quality of biodiesel include the technique used to produce biodiesel, the fatty acid composition of vegetable oil, feedstock quality, animal fats, and waste oil, the refining process and post-production parameters (Gautam & Agarwal, 2015; Mat Yasin et al., 2017). The low fraction variants of biodiesel like B7 or B10 are being utilized in many countries, including Malaysia. In 2019, Malaysia started utilizing B10 biodiesel for the automotive industry, produced from palm oil. Malaysia is the second-largest global producer of palm oil after Indonesia. Malaysia has established its own biodiesel testing standards for palm oil methyl ester. The standard values are mostly taken from ASTM D6751 and EN 14214 standards. According to ASTM D6751 standard, each property of pure biodiesel must be in the range (set by standards) before being utilized neat or blended with diesel in diesel engines. According to EN 14214 European standard, minimum and maximum values of various parameters are defined to ensure the quality of biodiesel. Before the commercialization of biodiesel as a pure biofuel or blending stock for diesel fuel, it should fulfill the minimum or maximum limits set by the standard. The EN 14214 standard specifies the

maximum allowable concentration of different parameters within biodiesel to ensure the quality of biodiesel. To facilitate the local implementation of palm oil methyl ester in Malaysia, MPOB played a key role in the publication of Malaysian biodiesel standard (MS 2008:2008) in October 2008 for Palm oil methyl ester (Lam, Tan, Lee, & Mohamed, 2009).

Table 2.10: Standard physicochemical properties of biodiesel according to ASTM D6751, EN14214 and Malaysian fuel standard MS 2008:2008 (Ahmad et al., 2011; Betiku & Adepoju, 2013; Mat Yasin et al., 2017; Pullen & Saeed, 2012; Sarve et al., 2015)

Properties	Unit	ASTM D6751		EN14214		Malaysian Standard MS 2008:2008	
		Limit	Method	Limit	Method	Limit	Method
Density at 15 °C	kg/m^3	870–890	ASTM D4052–91	860-900	EN ISO 3675	860-900	ASTM D 4052
Kinematic viscosity at 40 °C	mm^2/s	1.9–6.0	D445	3.5-5.0	EN ISO 3104	3.5-5.0	MS 1831
Flash point	°C	130 min	D93	>101	EN CD 3679e	120	ASTM D 5453
Cetane number	-	47 min	D613	51.0	EN ISO 5165	51.0	MS 1895
Acid value	mg KOH/g	< 0.50	D664	0.50	EN 14104	0.50	MS 2011
Oxidation stability	h	> 3	EN 14112	6	EN 14112k	6	EN 14112
FAME content	% (m/m)	-	-	95.5	EN14103	-	-
Water content	mg/kg	500 max	D2709	500 max	EN ISO 12937	500	ASTM E 203
Iodine value	% (m/m)	-	-	120 max	EN 14111	110	EN 14111
Sulfur content	mg/kg	< 15	D5453	10 max	-	10	-
Sulphated ash content	% (m/m)	0.02 max	D874	0.03 max	ISO 3987	0.02	ISO 3987
Methanol content	% (m/m)	-	-	0.2 max	EN 141101	0.2	EN 14110
Monoglyceride content	% (m/m)	-	-	0.8 max	EN14105m	0.8 max	ASTM S 6584
Diglyceride content	% (m/m)	-	-	0.2 max	EN14105m	0.2 max	ASTM S 6584
Triglyceride content	% (m/m)	-	-	0.2 max	EN14105m	0.2 max	ASTM S 6584
Free glycerine	% (m/m)	0.020 max	D6584	0.02 max	EN14105m/EN14106	0.02 max	ASTM S 6584
Total glycerine	% (m/m)	0.240 max	D6594	0.25 max	EN14105m	0.25 max	ASTM S 6584

Table 2.10: Continued

Properties	Unit	ASTM D6751		EN14214		Malaysian Standard MS 2008:2008	
Total contamination	mg/kg	-	-	24 max	EN 12662	24 max	ASTM D 5452
Phosphorus content	mg/kg	10 max	D4951	4 max	EN14107p	10 max	ASTM D 4951
CFPP	°C	-	-	max +5	EN 116	15	EN 116
Pour point	°C	-15 to 16	D 97	-	-	-	-
Group I metal (Na + K)	mg/kg	< 5	EN14538	< 5 max	EN14108	5.0	EN 14108
Group II metal (Ca + Mg)	mg/kg	< 5	EN14538	< 5 max	EN14538	5.0	EN 14109
Carbon residue	% (m/m)	< 0.05	D 4530	< 0.3	EN ISO 10370	-	-

2.8 Summary

According to an extensive literature review, sesame oil has huge potential among other vegetable oil feedstocks for the production of biodiesel. Sesame oil contains naturally occurring antioxidants (i.e. sesamin, sesamol, and sesamolin) and tocopherols. Sesame oil exhibits better oxidation stability due to these antioxidants instead of having high unsaturated fatty acids. Malaysia and Indonesia are a high producers of palm oil in the world. Palm oil has poor cold flow properties which is an important property for cold climate regions. Sesame oil has huge potential to improve the cold flow properties of palm oil with having better oxidation stability. For optimizing the biodiesel yield, RSM based on Box Behnken, and ELM techniques are used. Input parameters are optimized using optimizing tools for saving experimental costs and precious time. Ultrasound-assisted biodiesel production technique is used due to shorter reaction time, simple reaction setup, less energy consumption, enhanced conversion rate, and high-quality glycerol product. No studies have been reported for the tribological study of palm-sesame biodiesel fuel blends with and without fuel additives nanoparticles (CNT, TiO_2) and oxygenated alcohols (DEE and DMC). B20 (80% diesel and 20% biodiesel) fuel can be used in diesel engines for better performance. B30 (70% diesel and 30% biodiesel) palm-sesame biodiesel-diesel fuel blend should be tested on a lab scale to analyze the effect on diesel engine performance and emission characteristics with and without fuel additives.

CHAPTER 3: RESEARCH METHODOLOGY

The methodology for experimental work is discussed in Figure 3.1. The first phase is selecting suitable feedstock for blending with palm oil to improve its cold flow characteristics. The second phase is choosing a suitable blend of two feedstocks based on physicochemical properties for palm-sesame biodiesel production. The third phase is optimizing transesterification process variables to obtain maximum palm-sesame biodiesel yield with ultrasound technique using response surface methodology. The fourth phase is the characterization of produced palm-sesame biodiesel to analyze the physicochemical characteristics. The fifth phase is the tribological study to investigate the effect of fuel additives on fuel lubricity. The sixth phase is to study the effect of fuel additives on diesel engine characteristics using a single-cylinder diesel engine.

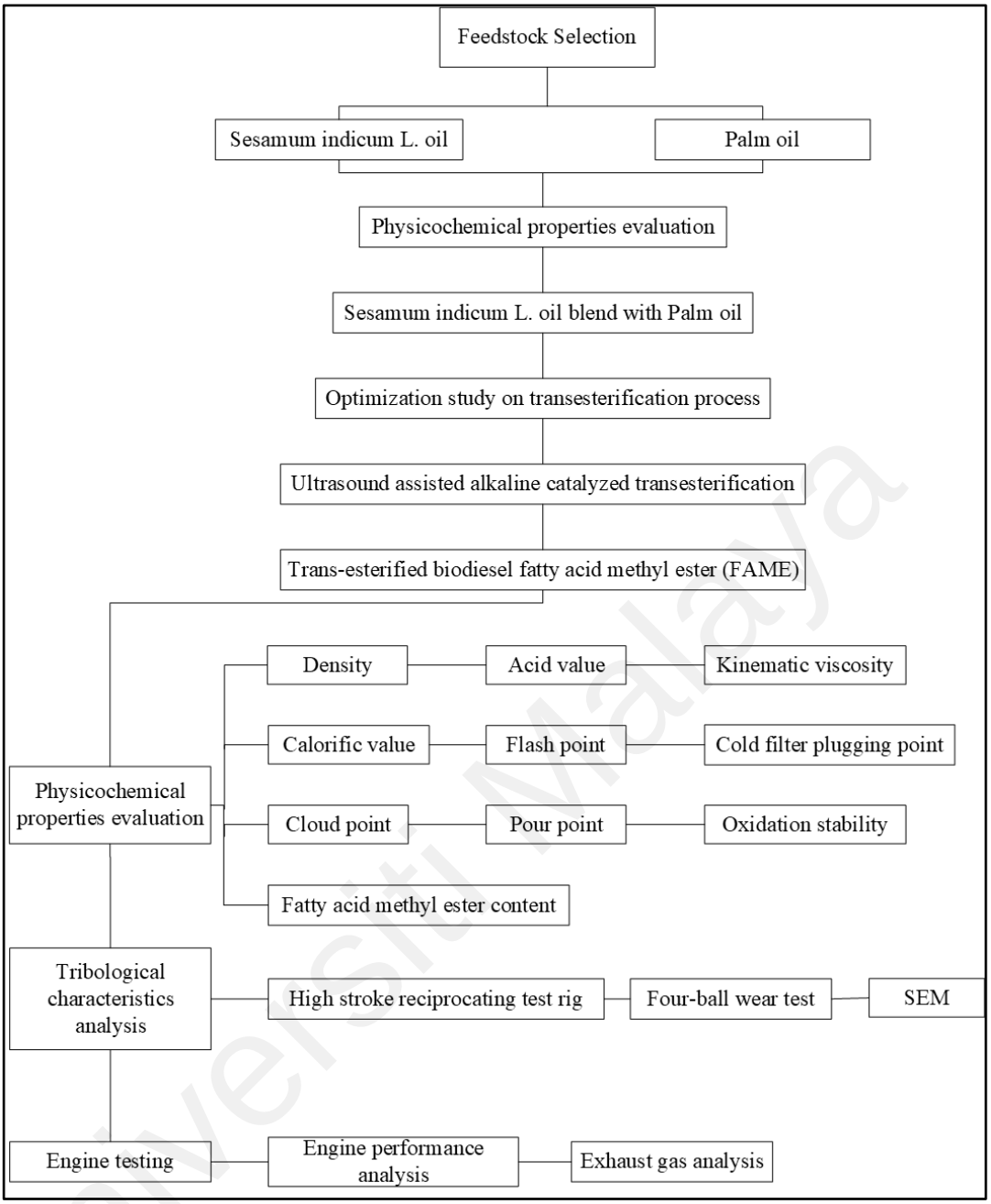

Figure 3.1: Overall flow chart methodology for experimental work

3.1 Materials

Crude palm olein (CPO) was procured from Sime Darby Plantation Berhad (Jomalina Refinery), Malaysia. Crude sesame oil (CSO) was shipped from the local market of Lahore, Pakistan. Methanol with purity 99.9% from Friedemann Schmidt, ACS, KOH pellets of AR grade from Friedemann Schmidt, and Whatman filter papers from Filtres Fioroni). According to ASTM (D6079-11) dimensions, AISI 52100 Chrome hard polished steel balls with a diameter of 6.2 mm, 15 mm SAE-AMS 6440 steel smooth

diamond polish disk, and 12.7mm diameter AISI 52100 steel balls having hardness 64-66 Rc were procured from the local market. DMC Extra Dry (purity: 99+%) from Acros Organics, DEE (purity: 99.5%) from QReC (Asia) Sdn Bhd and Nanoparticles (CNT and TiO_2) were taken from the mechanical engineering department, University of Malaya.

3.1.1 Characterization of nanoparticles

In this section, the morphology, particle size and other parameters of carbon nanotubes and titanium oxide nanoparticles are summarized. Table 3.1 exhibited the specifications and properties of CNT and TiO_2 nanoparticles. Figure 3.2 showed the SEM analysis of TiO_2 and CNT nanoparticles.

Table 3.1: Specifications and properties of TiO_2 and CNT nanoparticles

Description	**Specification**	
Chemical Name	Carbon nanotubes	Titanium dioxide
Appearance	Black	White
Linear Formula	CNT	TiO_2
Nanoparticle avg. size	20-30 nm	30.5 nm
Molecular wt.	146.23	79.87

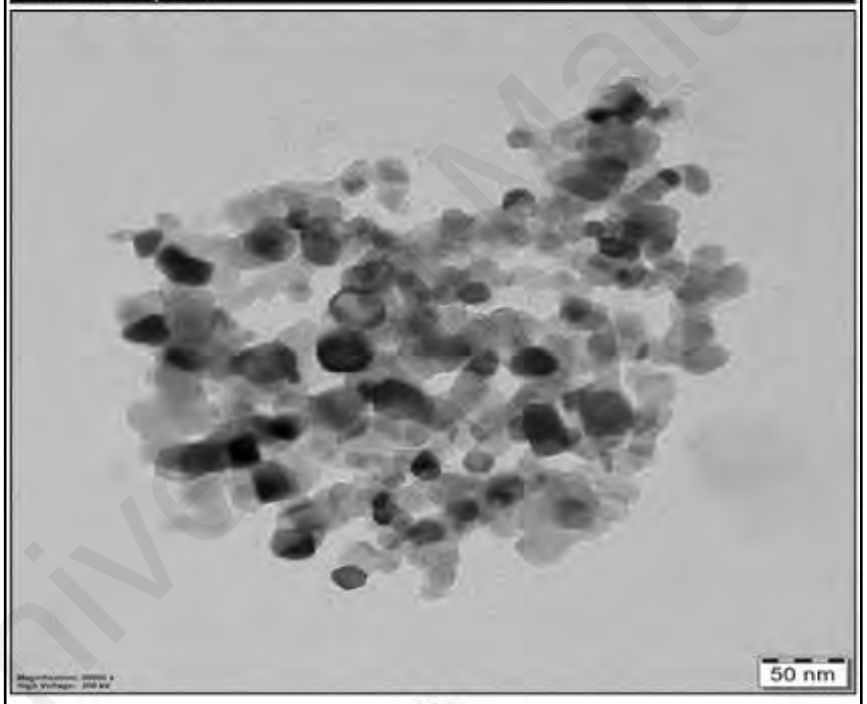

(a)

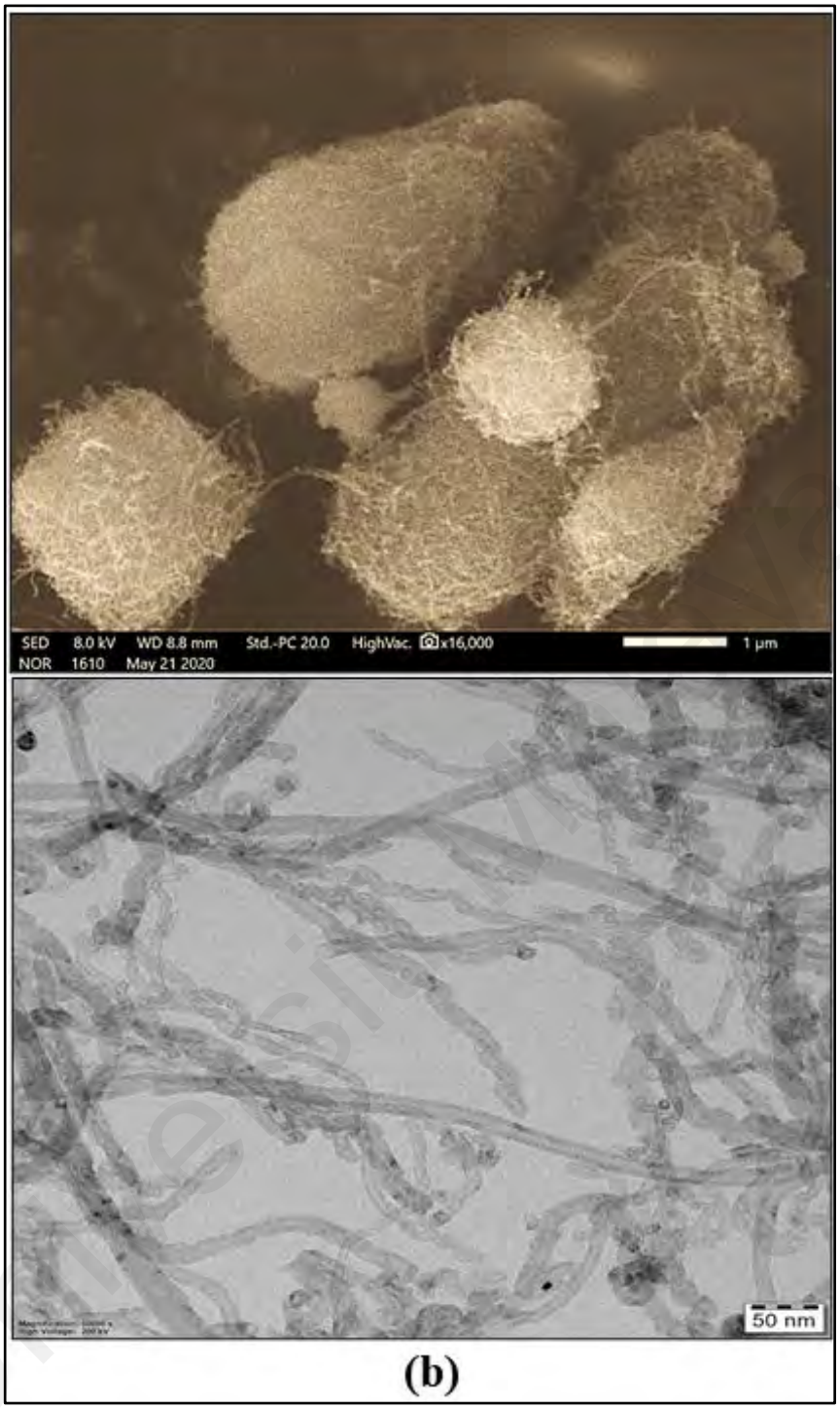

Figure 3.2: SEM and TEM analysis of (a) TiO_2 and (b) CNT

3.1.2 Palm-sesame biodiesel production

3.1.2.1 Palm-sesame oil mixtures and selection of best blend

Five CPCSO (crude palm-crude sesame oil) mixtures were prepared by blending CPO and CSO at different proportions: 1) 90:10 wt.%, 2) 80:20 wt.%, 3) 70:30 wt.%, 4) 60:40 wt.%, 5) 50:50 wt.% and labeled as P90S10, P80S20, P70S30, P60S40, and P50S50,

respectively, whereas P represents Palm Olein, and S represents Sesame. These blends with different proportions were prepared in a double-jacketed reactor at a stirring speed of 1500 rpm and 60 ℃ temperature for 2 hours to get a homogenous mixture.

3.1.2.2 Transesterification process

POME (palm oil methyl ester) and SME (sesame methyl ester) were prepared using the ultrasound-assisted transesterification process with the following operational parameters: methanol to oil ratio (40%), KOH catalyst amount (1 wt.%), time (30 min), amplitude (40%) and duty cycle (70%).

While P50S50 (50% Palm - 50%Sesame blend biodiesel) was also prepared using the ultrasound-assisted transesterification process in a 500 ml batch reactor to get the optimum set of process parameters. For this, the measured amount of homogenized P50S50 oil blend was added to the reactor. The calculated amount of KOH pellets and methanol was mixed until pellets were entirely dissolved in methanol. Then, the blend of methanol and KOH catalyst was charged to the reactor containing the P50S50 oil blend. The ultrasound unit amplitude was fixed to 40% for all batch experiments. The following parameters were varied to analyze their effect on P50S50 biodiesel yield: methanol to oil ratio (30% - 60%), reaction time (10 min – 40 min), KOH catalyst amount (0.5 wt.% - 1.5 wt.%), and duty cycle (50% - 70%). When the transesterification reaction was completed, the reactor mixture was transferred to a funnel to separate biodiesel, glycerin, and other impurities. This mixture was left for eight (8) h settling time in the funnel. The lower layer is separated from the separating funnel by an opening stopcock. The upper layer containing catalyst and methanol content was washed with warm water (40 ℃) until the clear water layer was found. Hot bubble-washed biodiesel was shifted to the round bottom flask (500 ml) to purify biodiesel by removing water and methanol content using rotary evaporator equipment at 70 ℃ with rotational speed 150 rpm for 30 min. Lastly,

evaporated biodiesel was filtered by using the Whatman filter paper to get rid of the remaining trace amount of catalyst and stored in a vacuum chamber. The biodiesel yield was obtained from the transesterification process using Equation 3.1 (Silitonga et al., 2020):

$$\textbf{Biodiesel yield}\ (\%) = \frac{\textbf{weight of (palm}-\textbf{sesame) biodiesel}}{\textbf{weight of palm}-\textbf{sesame oil}} \times \mathbf{100}\% \qquad 3.1$$

(a) ***Experimental setup for the transesterification process***

Ultrasound-assisted transesterification was performed using ultrasound equipment of QSONICA (Q500 Sonicator) as shown in Figure 3.3, which had 20 kHz frequency with a maximum rated power of 500 W. The tapered microtip with a 1/2" (inch) diameter probe was used for this study.

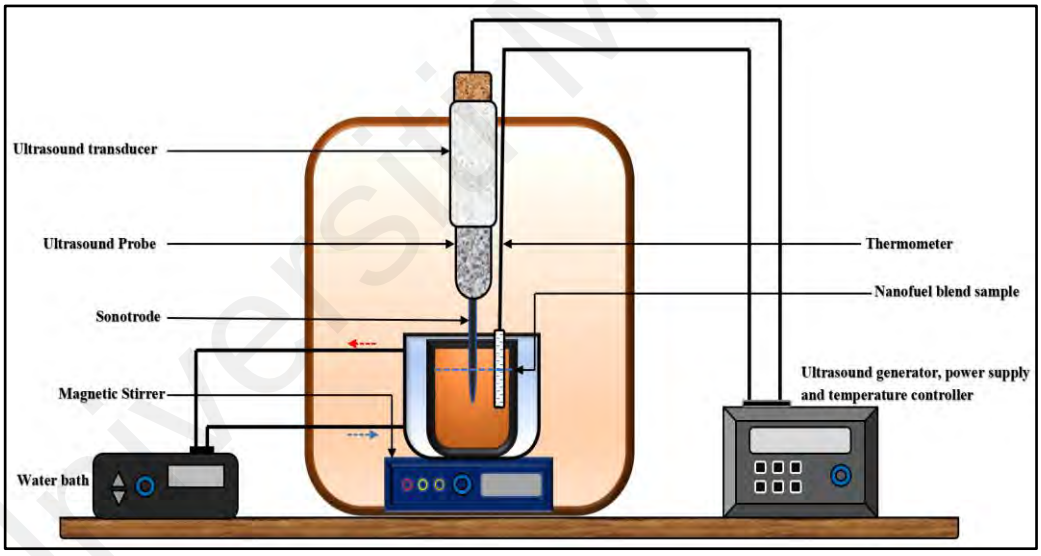

Figure 3.3: Ultrasound setup for biodiesel production and sonication of P50S50 blended oil with nanoparticles

3.1.3 Design of experiment for biodiesel optimization

3.1.3.1 RSM design based on Box-Behnken design

RSM based on the Box-Behnken design in Design-Expert version 10.0 software was used to design the experiments for the transesterification process of the P50S50 oil blend. Design-Expert version 10.0 software was used to design the experiment for optimizing

the P50S50 methyl esters yield. Four input process parameters (time (X_1), catalyst concentration (X_2), methanol to oil ratio (X_3), and duty cycle (X_4) were chosen to study the effect of each parameter (independent input variable) on P50S50 methyl esters yield (output dependent variable). Each input process variable has three coded values included minus 1, center point, and plus 1 are given in Table 3.2 and the total number of experiments is 30. The quadratic polynomial equation was fetched using response surface regression analysis on experimental data in the Box-Behnken experimental design tool. Equation 3.2 co-relates the interaction between response variable (P50S50 yield) and input process variables (time, catalyst concentration, methanol to oil ratio, and duty cycle). This equation was used to predict the response (yield) by varying different input process parameters.

$$Y = C_0 + \sum_{i=1}^{k} C_i\ X_i + \sum_{i=1}^{k} C_{ii}\ X_i^2 + \sum_{j=i+1}^{k} \cdot \sum_{i=1}^{k} C_{ij}\ X_{ij} \qquad 3.2$$

In the above Equation 3.2 Y predicted the yield of P50S50 methyl esters. X_i is the independent input parameter, Co and C_i are the intercept and regression 1st-order coefficients of the RSM model, respectively. C_{ii} is the quadratic regression coefficient of the model for the ith factor. C_{ij} is the regression coefficient among ith and jth input parameters and the number of input parameters represented by k.

Table 3.2: Independent input process variables used for the optimization of P50S50 biodiesel yield

Input process variables	Units	Coded factors	Coded process variables levels		
			-1 Level	Center	+1 Level
Time	min	X_1	10	25	40
Catalyst concentration	Wt.%	X_2	0.5	1	1.5
Methanol to oil ratio	%	X_3	30	45	60
Duty cycle	%	X_4	50	60	70

3.1.3.2 ELM modeling

ELM is a mathematical model with one single hidden layer. In ELM, the parameters of input weights and hidden bias are initialized randomly, while the Moore-Penrose generalized inverse was used to determine the output weights. The generalization of a single hidden layer feed-forward neural networks in ELM using the function as described in Equation 3.3 (Huang, Wang, & Lan, 2011):

$$f_L(x) = \sum_{i=1}^{L} \beta_i G(w_i, b_i, x), \; x \in R^n, a_i \in R^n \qquad 3.3$$

Where w_i and b_i are the hidden notes are learning parameters. ith hidden note and the output node are connected by weight β_i. While $G(w_i,b_i,x)$ gives output value of the ith hidden note for the input x and calculated by Equation 3.4.

$$G(w_i, b_i, x) = g\left(\sum_{j=i}^{n} w_{ij} x_j + b_i\right), \qquad b_i \in R \qquad 3.4$$

Where $w_{ij} = [w_{i1}, w_{i2}, \dots, w_{in}]^T$ is the weight vector which connects the input layer and ith is the hidden node to i with input to j. Also, b_i is the bias of the ith the hidden node $a_i, x = [x_1, x_2, \dots, x_n]^T$ is the inner product of a vector a_i in R^n.

Using Equation 3.4 can find G (w_{ij}, b_i, X) for RBF hidden note with activation function $g(x)$: $R \rightarrow R$ (e.g., Gaussian) in Equation 3.5 as follows:

$$G(w_i, b_i, x) = g\left(b_i \sqrt{\sum_{j=i}^{n} (x_j - w_{ij})^2}\right)^T, \; b \in R^+ \qquad 3.5$$

w_i and b_i represent the center and impact factor of ith RBF node, R^+ represents a set of all positive real values. A particular case of SLFN that has RBF nodes in its hidden layer forms the RBF network. For N, arbitrary distinct samples $(x_i, t_i) \in R^n \; x \; R^m$ where n x 1 input vector is represented by x_i and m x 1 target vector is represented by t_i. If an

SLFN with L hidden nodes approximates N samples with zero error, then it implies there exist $\beta_{i,} w_i$ and b_i such that.

$$f_i\ (x) = \sum_{i=1}^{L} \beta_i G(w_i, b_i, x),\ j = 1, \dots N \qquad 3.6$$

Equation 3.7 may expressed compactly as:

$$H\beta = T \qquad 3.7$$

Where

$$H(\tilde{w}, \tilde{b}, \tilde{x}) = \begin{bmatrix} G(w_1, b_1, x_1) & \dots & G(w_L, b_L, x_1) \\ G(w_1, b_1, x_N) & \dots & G(w_L, b_L, x_N) \end{bmatrix}_{NxL} \qquad 3.8$$

With $\overline{w} = w_1, \dots, w_L;\ \tilde{b} = b_1, \dots, b_L;\ \tilde{x} = x_1, \dots., x_L$

$$\beta = \begin{bmatrix} \beta_1^T \\ \vdots \\ \beta_L^T \end{bmatrix}_{Lxm} \qquad and\ T = \begin{bmatrix} t_1^T \\ \vdots \\ t_L^T \end{bmatrix}_{Nxm} \qquad 3.9$$

H is the hidden layer output matrix of SLFN, with the *i*th column of *H* being the *i*th hidden node's output concerning inputs $x_1, \dots, x_n$ in Equations 3.8 and 3.9.

3.1.3.3 Cuckoo search algorithm

Cuckoo search algorithm is an optimization algorithm that is based on brood parasitism of the cuckoo species by laying their eggs in randomly chosen bird's nest, if the host birds discover the egg (using the probability of pa ∈ [0, 1]), they will either remove the egg or just leave the nest and build a new nest.

For generating the new solutions, a randomization process with Lévy Flights is performed which can be seen as follows:

$$X_i^{(t+1)} = X_i^{(t)} + \alpha \hat{} Levy(\lambda) \qquad 3.10$$

where α > 0 is the step size associated with the level of the problem being worked on. While $Levy(\lambda)$ states the position equation function of Lévy Flights, which form of an equation is as follows.

$$Levy{\sim}u = t^{-\lambda}, where\ 1 < \lambda \leq 3 \quad 3.11$$

3.1.3.4 Random sub-sampling cross-validation

In this study, 30 datasets were used for Random sub-sampling cross-validation. Thus, 24 datasets were selected for training and 6 datasets for testing. The method was run ten times, the mean average percentage error (MAPE) and standard deviation (SD) based on Equation (3.12 and 3.13) were used to analyze the results.

$$MAPE = 100 \times \left| \frac{1}{n} \sum_{i=0}^{n} \frac{(y_e - y_p)}{y_p} \right| \quad 3.12$$

$$SD = \sqrt{\frac{\sum_{i=1}^{n}(x_i - \bar{x})^2}{n-1}} \quad 3.13$$

The number of points is represented by n, and the predicted value is represented by yp, while the predicted value is presented by y_e and y_{avg} , respectively. The mean value of x1;…; xn represent by $\bar{x}$.

3.1.3.5 Statistical analysis

The performance of RSM model and ELM was estimated in terms of coefficient of determination (R^2), mean square error (MSE), the root mean square error (RMSE), and standard error of prediction (SEP) as given in Equations (3.14) - (3.17) according to (Ishola, Okeleye, Osunleke, & Betiku, 2019) and (Ighose et al., 2017).

$$R^2 = 1 - \frac{\sum_{i=1}^{n}(y_e - y_p)^2}{\sum_{i=1}^{n}(y_p - y_{avg})^2} \quad 3.14$$

$$MSE = \frac{\sum_{i=1}^{n}(ye-yp)^2}{n} \quad 3.15$$

$$RMSE = \sqrt{\frac{1}{n}}\sum_{i=1}^{n}(y_e - y_p)^2 \quad 3.16$$

$$\text{SEP} = \frac{RMSE}{y_{avg}} \times 100 \quad 3.17$$

Where, *n* is the number of points, while y_e, y_p and y_{avg} represent actual value, predicted value, and an average of the actual values, respectively.

3.1.4 Determination of fatty acid composition

GC determined the FA composition of P50S50 methyl ester: Agilent 7890, USA using European standard (EN 14103:2011) operating conditions as illustrated in Table 3.3.

Table 3.3: Gas chromatography operating conditions

Operating parameters	Specifications
Column	HP-Innowax (30m x 0.320mm x 0.25mm)
Carrier gas	He
Flow rate	1 ml/min
Split flow	100 ml/min
Injector T	250°C
Flame Ionization detector	250°C
Column T	60°C for 2 min
	10°C/min to 200°C
	5°C/min to 240°C
	Hold 240°C for 7 min

3.1.5 Physicochemical properties of P50S50, palm, and sesame biodiesels

The physicochemical properties of biodiesel samples were measured using different types of equipment such as SVM 3000-automatic (density and viscosity), Automatic NTL Normalab NTE 450 (cloud point, pour point, and cold filter plugging point), C2000 basic calorimeter-automatic (calorific value), Metrohm 873 Rancimat (oxidative stability) and Pensky-martens automatic NPM 440 (flashpoint). The physicochemical properties of palm, sesame, P50S50 methyl esters were compared with standard specifications of

ASTM D-6751 and EN-14214 as shown in Table 4.7. The measured physicochemical properties of biodiesel and biodiesel blends were compared with petroleum diesel.

3.1.6 Tribological study of palm-sesame biodiesel with fuel additives

3.1.6.1 HFRR Tribological Test

(a) ***Fuel sample preparation***

Seven fuel samples were used to study the tribological behavior and lubricity of fuels. B10 was obtained from Shell, Malaysia, which was further used to compare other fuel sample results. B100 (P50S50 biodiesel) is produced at a lab scale. B30 (70% Diesel and 30% biodiesel) fuel sample is prepared by mixing 20% of biodiesel with commercially available diesel. Four fuel additive samples were ready to analyze their effect on the lubricity of fuel during fuel injection. B30 fuel is mixed with DMC 20% by volume. Another alcoholic B30 fuel sample is prepared by mixing 10% Ethanol in volume. Ultrasonicated B30 with CNT fuel sample is produced. Nanoparticle additive B30 with a TiO_2 fuel sample is prepared after ultrasonication. B30 and alcoholic fuel samples were prepared with 900 rpm stirring speed in 20 minutes. Nanoparticle additive fuel samples were prepared by mixing 5 mg of nanoparticle per 50 ml of B30 fuel with 20 mg of sodium dodecyl sulfate as a surfactant. B30 with nanoparticle and surfactant stirred at 900 rpm for 30 minutes and then sonicated for 10 minutes at pulse rate (3 s on and 2 s off) with 30% amplitude. QSONICA (Q500 Sonicate), which had a 20 kHz frequency with a maximum rated power of 500 W, was used for biodiesel production and preparation of nanoparticle fuel samples.

(b) ***Experimental setup of tribological HFRR test***

Seven fuel samples were evaluated using the High-Frequency Reciprocating Rig (HFRR) equipment from DUCOM (Model: TR-281-M8) shown in Figure 3.4. The testing specimen plates were prepared by cutting 15mm x15mm pieces. The specimens were

polished with 600, 800, 1000, 1500, and 2000 silicon carbide papers using the polishing machine. Then, the 3µm and 1µm diamond suspensions were used for further polishing. The specimens' surface roughness was between 0.03 µm (Ra) and 0.04 µm (Ra). The surface roughness of the specimens was measured by a profilometer (Veeco Dektak 150). A ball on a test specimen plate is performed to analyze the tribological behavior of fuel samples. A steel ball slides on a steel specimen plate submerged in 5.0 ± 0.2 ml fuel sample in a reciprocating motion with 2.0 ± 0.02 mm stroke length at a frequency 10.0 ± 1 Hz for 70 minutes with an applied load of 5 ± 0.01 N. Fuel temperature is constant at 60 ± 2ºC during the tribology test. All operating conditions were followed by standard test method ASTM D6079-11 and given in Table 3.4.

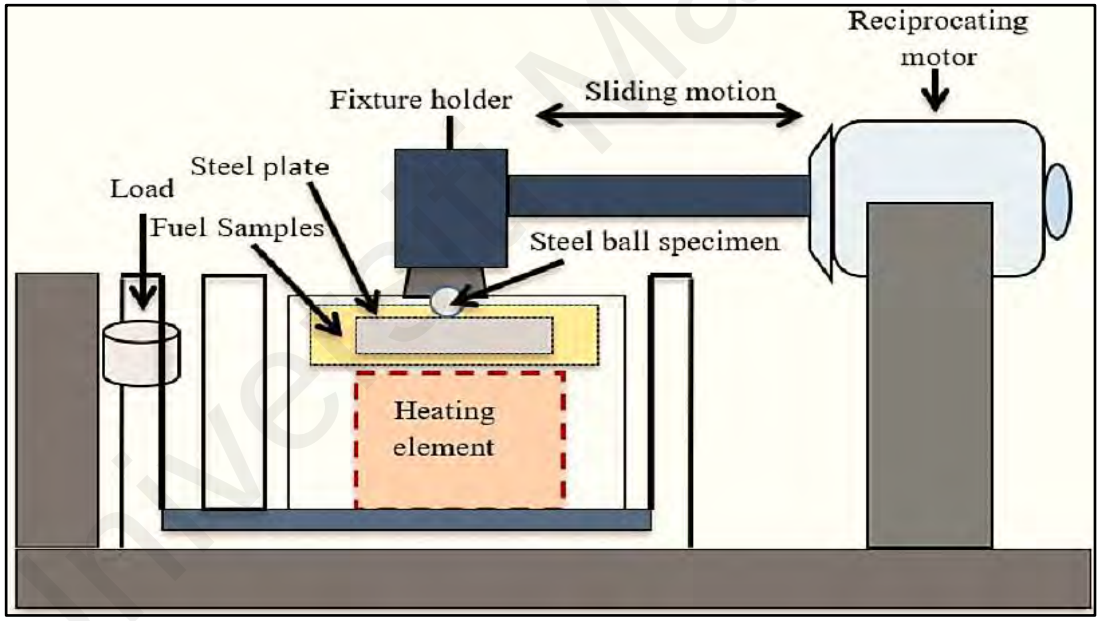

Figure 3.4: Schematic diagram of Reciprocating Friction and Wear Monitor (HFRR) Rig.

After tribological experiments, SEM was utilized to investigate the surface morphology and measure the wear scar diameter (WSD) of worn steel balls and steel plates. SEM images were captured at 2000 x and 3000 x magnification to visualize the nature of wear. The WSD of worn surfaces was calculated using the following equation WSD = (M+N)/2. M represents the major axis in this equation, and N represents the minor

axis (μm) measured through SEM. The coefficient of friction was calculated by using the following Equation 3.18:

$$\text{Coefficient of friction } (\mu) = \text{Actual frictional force (N)}/\text{Applied Load (N)} \quad \textbf{3.18}$$

Table 3.4: HFRR Tribological test operating conditions

Test Parameters	Standard value
Sample temperature	60°C
Sample test duration	70 min
Applied load	500 g
Frequency	10 Hz
Stroke length	2 mm
Sample volume	5 ml

3.1.6.2 Four ball Tribological Test

(a) ***Lubricant sample preparation***

B10 was sourced from a local fuel pump station. B30 fuel sample was prepared by mixing 70% commercial diesel and 30% P50S50 biodiesel, B30 fuel + 20% by volume DMC, and B30 fuel +10% by volume ethanol fuel samples were prepared at 900 rpm stirring speed for 20 minutes. Similarly, B30 +100ppm carbon nanotubes and B30 +100ppm TiO_2 nanoparticle fuel samples were prepared at 800 rpm for 20 minutes on a magnetic stirrer and then sonicated for 30 minutes with 30% amplitude at a pulse rate of 3s on and 2s off.

(b) ***Experimental setup of four-ball tribo-tester***

All the lubricant samples were tested on an automatic 4-ball tribo tester (FBT-3: DUCOM brand) to evaluate the tribological characteristics of lubricant with the dilution of different fuels.

The cup holder with three stationary steel balls containing 10 ml of lubricant samples was attached to a temperature sensor. While the fourth steel ball was fixed in the spindle shaft that rotates on three fixed balls after applying load, as shown in Figure 3.5. New

separate four (4) steel balls have been used for each experiment. Commercial lubricant SAE-40 has also been evaluated for comparison of the results as a reference lubricant. The coefficient of friction was calculated using Equation 3.19.

$$Coefficient\ of\ friction = (T\sqrt{6})/\ 3\ Wr \qquad 3.19$$

Where, T = Frictional torque (kg.mm), W = Applied load (kg) and r = 3.67 mm (perpendicular distance from the rotational axis to the center of the contact surface of balls).

Figure 3.5: Fourball tribo-tester for testing lubricant samples.

According to the ASTM D4172 standard, its working conditions are given below in Table 3.5.

Table 3.5: Four-ball Tribological test operating conditions and specifications of tested ball

Test Parameters	Operating values
Spindle rotational speed	1200 rpm
Load	40 kg
Sample temperature	75°C
Require time	60 min
Specification of tested ball	
Hardness	62
Surface roughness	0.04 µm
Diameter of the ball (size)	12.7 mm
Material	Carbon- chromium steel (SKF)

3.1.7 Diesel engine testing setup and analysis

3.1.7.1 Ternary fuel blends preparation

Five fuel samples were prepared to investigate their effect on CI diesel engine performance and exhaust emission characteristics. B10 obtained from Shell, Malaysia, was further used to compare results among other fuel samples. B100 (P50S50 biodiesel) was produced at a lab scale by ultrasound-assisted transesterification method. B30 (70% Diesel and 30% biodiesel) fuel sample is prepared by mixing 20% of palm-sesame biodiesel with commercially available diesel. Additionally, four fuel additive samples were prepared to analyze their influence on diesel engine characteristics during combustion. The first and second samples were prepared by mixing B30 fuel with 10% DMC and 5% DEE (by volume) at 2000 rpm stirring speed for 30 minutes to fortify a homogeneous blend. Ultrasonication of B30 fuel with CNT and TiO_2 nanoparticles was done to prepare the third and fourth samples, respectively. This has been achieved by doping 5 mg of nanoparticle in 50 ml of B30 fuel with 20 mg of sodium dodecyl sulfate as a surfactant followed by stirring at 2000 rpm for 30 minutes and then sonicated for 30 minutes at pulse rate (3s on and 2s off) with 30% amplitude.

3.1.7.2 Experimental Setup of Diesel engine

Diesel engine test rig (Model: Yanmar (TF 120M)) of the University of Malaya was used to examine the diesel engine characteristics of different fuel samples for this current research work. Figure 3.6 illustrates the schematic view of the experimental diesel engine set-up. In addition, the technical specifications of the diesel engine are presented in Table 3.6.

(a) ***Diesel engine performance***

Initially, B10 was utilized to investigate the CI engine characteristics. A Graduated measuring cylinder was attached to the fuel tank to quantify the fuel flow rate. Three readings were taken during each test and engine speed and averaged for every 10 ml of fuel sample and a stopwatch measured time. Brake torque (BT) and speed were taken from (DASTEP8) software. BP is the power output available at the crankshaft. BP was calculated by using Equation 3.20. BTE is defined as brake power output as a function of heat input from fuel. BTE was calculated by using Equation 3.21.

$$BP = \frac{2\pi N \times T}{60 \times 1000} \text{ (kW)} \quad 3.20$$

$$BTE = \frac{3600}{\frac{\dot{m_f} \times CV}{BP}} = \frac{3600}{BSFC \times CV} \text{ (\%)} \quad 3.21$$

$$BSFC = \frac{Specific\ fuel\ consumption}{BP} = \frac{\dot{m_f}}{BP} \text{ (kg/kWh)} \quad 3.22$$

$$\dot{m_f} = \frac{v\ (L) \times 10^{-3} \times \rho\ (\frac{Kg}{m^3})}{T\ (h)} \text{ (kg/h)} \quad 3.23$$

Where, N = Rotational speed in rev/min (rpm), T = Torque in N.m, BP = Brake power in kW, BTE = Brake thermal efficiency, $\dot{m_f}$ = Specific fuel consumption (mass flow

rate) in kg/h, CV = Calorific value in kJ/kg, BSFC = Brake specific fuel consumption in kg/kWh, v = Volume in liters, ρ = Density in kg/m^3 and T = Time in hours.

(b) ***Diesel engine emission***

BOSCH (BEA-350) exhaust gas analyzer was used to analyze the diesel engine emissions like HC, CO, and NO_x. Measuring accuracy and method were listed in Table **3.7**. Exhaust gas emissions were measured in parts per million (ppm), which should be converted into globally acceptable unit g/kWh according to SAE J177. Equations are given below for conversion of ppm units to g/kWh:

$$HC = \frac{2.87 \times 10^{-2} \times HC\ (ppm) \times \dot{m}_{exhaust}\ (kg/min)}{BP\ (kW)}\ \text{(g/kWh)} \qquad 3.24$$

$$CO = \frac{5.79 \times 10^{-2} \times CO\ (ppm) \times \dot{m}_{exhaust}\ (kg/min)}{BP\ (kW)}\ \text{(g/kWh)} \qquad 3.25$$

$$NO = \frac{6.20 \times 10^{-2} \times NO\ (ppm) \times \dot{m}_{exhaust}\ (kg/min)}{BP\ (kW)}\ \text{(g/kWh)} \qquad 3.26$$

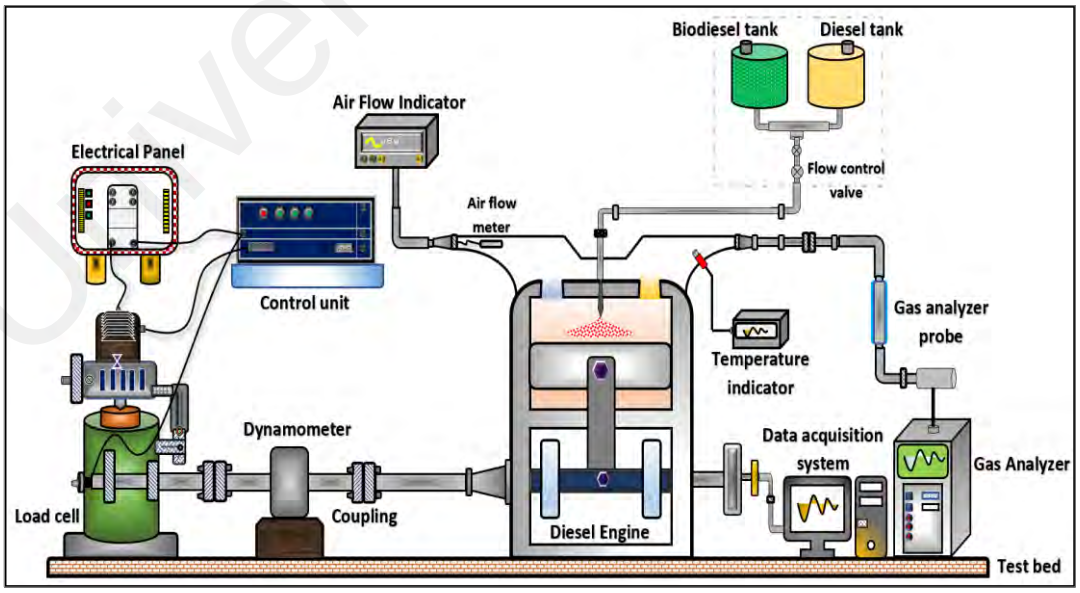

Figure 3.6: Schematic diagram of the engine test set-up

Table 3.6: Engine specifications used for experimental work

Engine specification	Description
No. of cylinders	1
Aspiration	Radiator cooling
Cylinder bore x stroke (mm)	92×96
Displacement (L)	0.638
Compression ratio	17.7
Maximum engine speed (rpm)	2400
Maximum power (kW)	7.7
Injection timing (deg.)	17° BTDC
Injection pressure (kg/cm^2)	200
Power take-off position	Flywheel side
Cooling system	Radiator cooling
Connecting rod length (mm)	149.5

Firstly, B10 was run in a diesel engine to obtain steady operating conditions, and then ternary fuel blends were charged to the diesel engine to investigate engine characteristics. After each ternary fuel blend, the engine was flushed with B10 to empty the tested ternary fuel blend traces. This method is adopted for each ternary fuel blend. The tested fuel samples were B10, B30, B30+CNT, B30+TiO_2, B30+DMC, and B30+DEE.

Table 3.7: Gas analyzer specifications

Equipment	Method	Measurement	Measurement Range	Accuracy	% Uncertainty
BOSCH BEA 350	Flame ionization detector (FID)	HC	0-9999 ppm	±1 ppm	±1 %
	Heated vacuum type chemiluminescence detector (CLD)	NO_x	0-5000 ppm	±1 ppm	±1.30 %
	Non-dispersive infrared	CO	0-10 % vol.	±0.001% vol	±1 %

(c) ***Uncertainty analysis***

Error assessment of the experimental data is analyzed using systematic equations. The uncertainty analysis comprises the mean of repeat measurements to estimate the true

value. The average of three readings of a specific parameter was considered for the error analysis. The error bars are represented all the engine characteristics to indicate the uncertainty in the reported measurement. The percentage of uncertainties of the calculated and measured parameters is demonstrated in Table 3.7. The uncertainty of the measured variable (ΔX_i) is determined by Gaussian distribution as presented in Equation 3.27 within the confidence limits of ±2σ. 2σ is the mean limit on which 95% of measured values rely upon.

$$\Delta X_i = \frac{2\sigma_i}{\overline{X_i}} * 100 \qquad 3.27$$

Where, X_i is the No. of readings, $\overline{X_i}$ implies to the investigational readings and σ_i Signifies the standard deviation. The uncertainties of estimated parameters were evaluated employing the expression given in Equation 3.28:

$$R = f(X_1, X_2, X_3, \ldots\ldots\ldots\ldots X_n) \qquad 3.28$$

$$\Delta R = \sqrt{\left[\left(\frac{\partial R}{\partial X_1}\Delta X_1\right)^2 + \left(\frac{\partial R}{\partial X_2}\Delta X_2\right)^2 + \left(\frac{\partial R}{\partial X_3}\Delta X_3\right)^2 + \ldots\ldots\ldots\ldots\ldots\ldots\left(\frac{\partial R}{\partial X_n}\Delta X_n\right)^2\right]} \qquad 3.29$$

Where R in Equation 3.29 exemplifies the function of $X_1, X_2, \ldots\ldots X_n$ and $X_1, X_2, \ldots\ldots X_n$ signifies the No. of obtained readings. Hence, ΔR is calculated by RMS (root mean square) of errors related to measured parameters. The uncertainty values of each piece of equipment were determined. The overall uncertainty of the current experiment was calculated as ± 2.53%, and it is much lower than the ± 5%. It is well known that the acceptable range for the uncertainty is lower than the above-mentioned value. Therefore, the observed overall uncertainty of the current study was within acceptable limits. By using Equation 3.30, the uncertainties in different measured and individual parameters were calculated and tabulated in Table 3.7.

$$\text{Uncertainty (\%)} = \sqrt{\begin{matrix}\text{Uncertainty (\%) of (sq. BP + sq. BSFC + sq. BTE} \\ \text{+sq. CO + sq. HC + sq. NOx)}\end{matrix}} \quad 3.30$$

The experimental test rig diesel engine was run at six (6) different speeds (1050-2300 rpm) with a step of 250 rpm under full load (100%) conditions. Percentage relative uncertainty for engine parameters (BSFC, BP, BTE, CO, HC, NO_x) was determined through different equipment uncertainties. Sample calculation of BP for B10 with the variable speed at full load condition and uncertainty level of different parameters are presented in Appendix. The overall uncertainty of experiments was predicted by given below Equation 3.31:

$$Overall\ uncertainity = \sqrt{Uncertainity\ \%\ of\ (BP^2 + BSFC^2 + BTE^2 + CO^2 + HC^2 + NOx^2))} \quad 3.31$$

$$= \sqrt{((0.631)^2 + (1.41)^2 + (1.61)^2 + (1)^2 + (1)^2 + (1.3)^2)}$$

$$= \pm\ 2.53\%$$

CHAPTER 4: RESULTS AND DISCUSSION

In this chapter, optimization of palm-sesame biodiesel, tribological and diesel engine study with and without biodiesel-diesel fuel additives have been discussed. In the first stage, palm-sesame biodiesel yield is optimized with the use of RSM based on Box Behnken and ELM techniques. Physicochemical properties of palm-sesame biodiesel are also provided in detail. It is followed by the investigation of tribological study for palm-sesame biodiesel fuel blends with and without fuel additives using HFRR and Four ball tribo tester. Then the effect of lubricant oil degradation was studied due to the mixing of fuel with lubricant oil because of crankcase dilution. In the end effect of palm-sesame biodiesel fuel blends with fuel additives (CNT, TiO_2, DEE, and DMC) was analyzed on diesel engine performance and emission characteristics.

4.1 Selection of feedstock blend for biodiesel production

According to the physicochemical characteristics of different oil blends presented in Table 4.1. P50S50 and P60S40 (60% palm – 40% sesame) oil blends were selected, among other oil blends for biodiesel production. Ultrasound technique is used for biodiesel production from P50S50 and P60S40 oil blends under the following operating conditions: Methanol 40%, catalyst one (1) wt.%, time 30 min, amplitude 40%, and duty cycle 70%. Physicochemical characteristics and fatty acid compositions of P50S50 and P60S40 methyl esters were measured to choose one best oil blend for biodiesel synthesis. Four physicochemical properties were selected and measured for the respective five blends to choose the best one for optimization and presented in Table 4.1.

Table 4.1: Physicochemical characteristics of crude palm, sesame oils, and its oil mixtures

Property	Crude oils				Crude palm and sesame oil blends				
	CPO[a]	CPaO (Yusup & Khan, 2010)	**CSO[a]**	CSO (Sarve et al., 2015)	**P90S10[a]**	**P80S20[a]**	**P70S30[a]**	**P60S40[a]**	**P50S50[a]**
Kinematic viscosity at 40 °C (mm^2/s)	38.82	38.1	33.11	31.51	38.43	38.24	38.16	37.93	37.20
Density at 15 °C (kg/m^3)	914.4	920	922.7	900	915.2	916.0	916.9	917.6	918.4
Acid value (mg KOH /g)	4.16	18.5	1.96	0.42	3.67	3.37	3.07	2.97	2.78
Calorific value (MJ/kg)	38.884	37.5	38.917	38.900	38.086	38.127	38.261	38.558	38.794

CPO: crude Palm olein; CPaO: crude Palm oil; CSO: crude Sesame oil; P90S10: Palm-Sesame oil blend (90:10 wt.%); P80S20: Palm-Sesame oil blend (80:20 wt.%); P70S30: Palm-Sesame oil blend (70:30 wt.%); P60S40: Palm-Sesame oil blend (60:40 wt.%) and P50S50: Palm-Sesame oil blend (50:50 wt.%).

[a] properties measured in this research

Based on the results, the P50S50 oil blend was chosen for this study. It gave us the best substitution in acid value, KV, and CV, among other oil blends. The P50S50 oil blend and P50S50 biodiesel have the lowest kinematic viscosities at 40 ℃ and acid values. The P50S50 oil blend and P50S50 biodiesel have higher densities at 15 ℃ and calorific values. Moreover, the P50S50 oil blend has a lower saturated fatty acid composition among other oils, as shown in Table 4.2. Lower saturated fatty acid composition leads towards double and triple bonds, which results in poor oxidative stability and more prone to rancidity of oil. Regardless of having high unsaturation, crude sesame oil exhibits very good oxidative stability because of naturally existing antioxidants and tocopherols. Due to this unique property, the P50S50 oil blend will produce biodiesel with better oxidative stability and lower cold flow characteristics.

Table 4.2: Fatty acid compositions of palm, sesame, and palm-sesame blends biodiesels

Chemical name	Carbon structure	Palm-sesame blend biodiesel		Palm biodiesel	Sesame biodiesel
		P60S40[a]	P50S50[a]	POME[a]	SME[a]
Myristic acid	C14:0	0.64	0.48	0.92	-
Palmitic acid	C16:0	29.85	24.59	38.96	9.71
Stearic acid	C18:0	4.31	4.45	4.05	4.90
Oleic acid	C18:1	43.42	42.48	44.95	39.88
Linoleic acid	C18:2	20.87	26.92	10.54	43.63
Linolenic acid	C18:3	0.43	0.49	0.37	0.56
Arachidic acid	C20:0	0.47	0.57	-	0.89
Total saturated fatty acids		35.27	30.09	43.94	15.5
Total unsaturated fatty acids		64.62	69.89	55.86	84.07

P60S40: Palm-Sesame oil blend (60:40 wt.%), P50S50: Palm-Sesame oil blend (50:50 wt.%), POME: palm oil methyl esters and SME: sesame methyl esters

[a] Fatty acids composition measured by GC equipment (Model: Agilent 7890A, USA) with the operating condition as described by (Milano et al., 2018)

4.2 Optimization of process parameters of ultrasound-assisted transesterification by RSM

In this study, the P50S50ME yield was maximized by optimizing the independent process variables, time, catalyst concentration, methanol to oil ratio, and duty cycle. The quadratic regression model was suggested after a regression analysis performed on Box-Behnken experimental design results. The P50S50ME yield results for 30 experimental runs, obtained by using the quadratic regression model equation, are shown in Table 4.3.

Table 4.3: Experimental design for optimization of ultrasound-assisted transesterification process parameters of the P50S50 oil blend

No	Time, X_1 (min)	Catalyst concentration, X_2 ((w/w) %)	Methanol to oil ratio, X_3 ((v/v) %)	Duty cycle, X_4 (%)	Experimental P50S50 biodiesel yield (%)	RSM Predicted P50S50 biodiesel yield (%)	ELM Predicted P50S50 biodiesel yield (%)
1	40	0.5	45	60	92.74	92.92	92.71
2	10	0.5	45	60	88.04	87.86	88.04
3	25	1	60	50	94.47	94.48	94.47
4	10	1	30	60	89.94	89.85	89.57
5	40	1.5	45	60	90.71	90.9	90.71
6	25	1	45	60	93.47	93.67	93.77
7	25	1.5	60	60	89.44	89.47	89.44
8	10	1	45	70	91.14	91.31	91.14
9	25	0.5	45	70	90.17	90.33	90.17
10	25	1	60	70	90.97	90.81	90.97
11	40	1	45	70	94.17	94.06	94.16
12	25	1	45	60	93.94	93.67	93.77
13	10	1	45	50	91.91	92.01	91.91
14	25	1.5	30	60	90.82	90.98	90.82
15	25	0.5	45	50	90.8	90.86	90.80
16	40	1	60	60	93.51	93.61	93.51
17	25	1	45	60	93.61	93.67	93.77
18	40	1	30	60	92.31	92.13	92.31

Table 4.3: Continued

No	Time, X_1 (min)	Catalyst concentration, X_2 ((w/w) %)	Methanol to oil ratio, X_3 ((v/v) %)	Duty cycle, X_4 (%)	Experimental P50S50 biodiesel yield (%)	RSM Predicted P50S50 biodiesel yield (%)	ELM Predicted P50S50 biodiesel yield (%)
19	25	0.5	30	60	87.35	87.3	87.35
20	25	1	30	50	89.46	89.63	89.46
21	25	1	45	60	93.51	93.67	93.77
22	10	1	60	60	91.08	91.27	91.08
23	25	1	45	60	93.57	93.67	93.77
24	25	1.5	45	70	91.38	91.33	91.38
25	10	1.5	45	60	91.51	91.33	91.51
26	25	1	30	70	92.77	92.77	92.77
27	25	0.5	60	60	91.87	91.7	91.87
28	25	1	45	60	93.91	93.67	93.77
29	25	1.5	45	50	91.47	91.32	91.47
30	40	1	45	50	94.07	93.89	94.07

The P50S50 methyl esters yield is calculated by the quadratic model Equation 4.1 as given below.

$$Y_{P50S50} = 93.67 + 1.16X_1 + 0.36X_2 + 0.72X_3 - 0.13X_4 - 1.37X_1X_2 + 0.015X_1X_3 + 0.22X_1X_4 - 1.48X_2X_3 + 0.13X_2X_4 - 1.70X_3X_4 - 0.53{X_1}^2 - 2.38{X_2}^2 - 1.42{X_3}^2 - 0.32{X_4}^2 \quad 4.1$$

Here, Y_{P50S50} shows the P50S50 biodiesel yield, and X_1, X_2, X_3, and X_4 exhibit the time, catalyst amount, methanol to oil ratio, and duty cycle. The relationship between the predicted yield of P50S50 methyl esters and the experimental yield of P50S50ME is expressed in Figure 4.1.

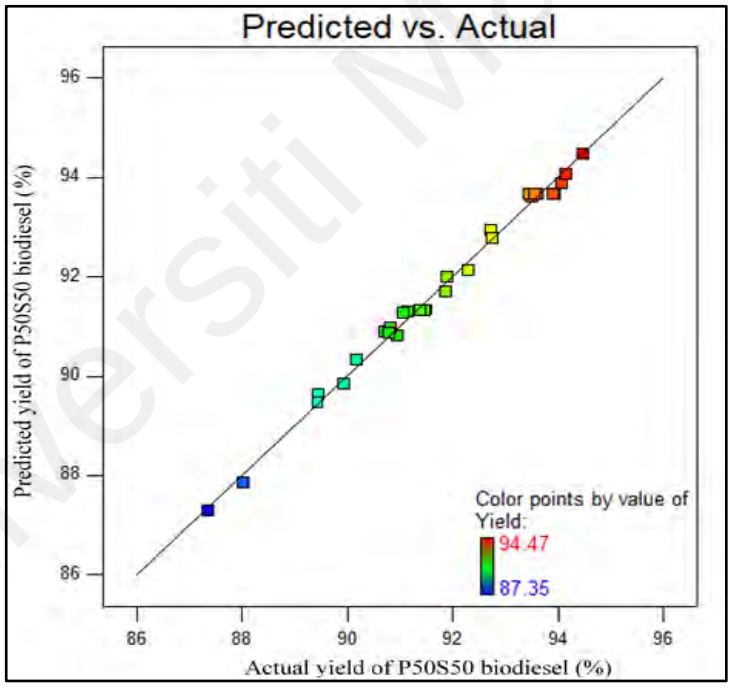

Figure 4.1: Actual yield vs. predicted yield of P50S50 methyl esters

A statistical tool ANOVA (analysis of variance) is used to investigate the importance of the RSM (quadratic) model to optimize the P50S50 biodiesel's yield. ANOVA results described in Table 4.4.

Table 4.4: ANOVA results for a quadratic regression model

Source	Sum of Squares	Degree of freedom	Mean Square	F value	P-value Prob > F	
Model	99.66	14	7.12	157.64	< 0.0001	Significant
X_1-Time	16.08	1	16.08	356.04	< 0.0001	
X_2-Catalyst	1.58	1	1.58	35.08	< 0.0001	
X_3-Methanol	6.29	1	6.29	139.36	< 0.0001	
X_4-Duty cycle	0.21	1	0.21	4.61	0.0486	
X_1X_2	7.56	1	7.56	167.47	< 0.0001	
X_1X_3	0.164	1	0.164	0.020	0.8896	
X_1X_4	0.19	1	0.19	4.19	0.0586	
X_2X_3	8.70	1	8.70	192.72	< 0.0001	
X_2X_4	0.073	1	0.073	1.61	0.2232	
X_3X_4	11.59	1	11.59	256.75	< 0.0001	
X_1^2	1.93	1	1.93	42.72	< 0.0001	
X_2^2	38.98	1	38.98	863.16	< 0.0001	
X_3^2	13.88	1	13.88	307.45	< 0.0001	
X_4^2	0.72	1	0.72	15.96	0.0012	
Residual	0.68	15	0.045			
Lack of Fit	0.47	10	0.047	1.12	0.4810	Not Significant
Pure Error	0.21	5	0.042			
Corrected Total	100.34	29				
Std. Dev.	0.21		R^2	0.9932		
C.V. %	0.23		Adj R^2	0.9869		
Mean	91.80		Pred R^2	0.9701		
			Adeq Precision	47.789		

The quadratic model F value was 157.64, and the p-value was also (< 0.0001), which specified that the quadratic regression model was "significant." Less than 0.0500 values of "Prob > F" indicates that model terms are significant and but if "Prob > F" is greater than 0.10, then model terms will be insignificant. Table 4.4 showed the ANOVA of the quadratic regression model that was developed for maximizing the biodiesel yield. This model X_1, X_2, X_3, X_4, X_1X_2, X_2X_3, X_3X_4, X_1^2, X_2^2, X_3^2, X_4^2 model terms are the most significant parameters that affect the yield of biodiesel. The lack of fit "F value" is 1.12, indicating that lack of fit is insignificant relative to the pure error. The value R^2 is 0.9932, which indicates that 99.32% deviation in P50S50 methyl esters yield was due to independent input process variables chosen for this model. A high R^2 value ensures a better estimation between experimental data and the quadratic model.

4.2.1 Combined effect and interaction between process variables on P50S50 biodiesel yield

4.2.1.1 Effect of each parameter on P50S50 biodiesel yield

According to ANOVA results presented in Table 4.4, the most critical parameters were time and methanol to oil ratio, followed by catalyst concentration and duty cycle. An increment in reaction time helps in diffusion between oil, catalyst KOH, and methanol and results in higher reaction rate and methyl esters yield (Gunawan et al., 2014; Milano et al., 2018).

The P50S50 methyl esters yield is slightly increased with the increase of KOH concentration from 0.5 to 0.8 (wt.%), and then further increase in concentration from 0.8 to 1.5 (wt.%) results in the reduction of biodiesel yield. The excess amount of catalyst KOH increased the viscosity of biodiesel due to emulsification and leads to the formation of gels (Patil & Deng, 2009).

The duty cycle has significantly less impact on biodiesel yield. The biodiesel yield was gradually decreased with an increase in duty cycle % due to a reduction in reaction rate caused by improper mixing of the reaction mixture and lower cavitation phenomena. A similar trend was reported by different researchers (Joshi, Gogate, & Kumar, 2018; Maddikeri et al., 2013). 3-D response surface graphs were also plotted to analyze the combined effect of process variables on P50S50 methyl esters yield.

4.2.1.2 Interaction between two process variables on P50S50 biodiesel yield

3-D surface graphs are plotted and presented in Figure 4.2 to investigate the combined interaction effect of process variables on P50S50 methyl esters yield.

The combined effect of reaction time (10 to 40 min) and catalyst amount (0.5 to 1.5 (wt. %)) on P50S50 methyl esters yield is visualized from Figure 4.2 (a). The maximum 94.54% biodiesel yield was achieved at time 40 min and catalyst amount 0.874 (wt.%). In the case of catalyst concentration, biodiesel yield increased up to 0.87 (wt.%) concentration, but further increase in catalyst amount causes a decrease in biodiesel yield from 94.54% to 90.84%. A higher dosage of KOH concentration reversed the transesterification process, which decreased the conversion of oil to biodiesel and assisted in forming soap. The purification process of biodiesel becomes very complicated due to the presence of soap with glycerol and biodiesel. The lowest yield (89%) at the highest concentration of catalyst (KOH) and the lowest reaction time indicate that the reaction time is insufficient to attain optimum biodiesel yield. It can be observed that adequate reaction time is required to obtain a homogeneous mixture of catalyst (KOH), methanol, and palm-sesame oil to form products and achieve optimum yield (Ishola et al., 2019).

The combined effect of reaction time (10 to 40 min) and methanol to oil ratio (30 to 60 (V/V) %) on biodiesel yield are presented in Figure 4.2 (b). The maximum output yield of P50S50 biodiesel (94.65%) was obtained at a reaction time of 40 (min) with a methanol

to oil ratio of 53.108 (V/V) %. The biodiesel's yield increases with an increase in reaction time up to 40 min because adequate time is supplied for completing the transesterification reaction. In the case of methanol to oil molar ratio, P50S50 biodiesel's yield increased up to 53 (V/V) %, then further increase in methanol resulted in a slight reduction of biodiesel yield from 94.65 % to 94.22%. Excess dosage of methanol will dilute the reaction mixture and reduce catalyst effectiveness during the transesterification process (Ighose et al., 2017). If the methanol-to-oil molar ratio exceeds the optimum limit, biodiesel separation becomes difficult due to emulsion formation, and the overall cost will be increased (Goff, Bauer, Lopes, Sutterlin, & Suppes, 2004; Hamze, Akia, & Yazdani, 2015; Milano et al., 2018).

The combined effect of reaction time (10 to 40 min) and duty cycle (50 to 70 %) on P50S50 biodiesel yield is shown in Figure 4.2 (c). Biodiesel's yield is increasing gradually with an increase in reaction time. The duty cycle is a significant parameter to optimize the energy consumption during the ultrasound-assisted transesterification process (Martinez-Guerra & Gude, 2016). The duty cycle is varied from 50 to 70 %; biodiesel yield is increased up to 57.44 % then further increase in duty cycle resulted in the reduction of biodiesel yield from 94.52 to 94.01%. The higher the duty cycle, the longer the cavitation effect arises in fixed reaction time. It was observed from the 3D graph, increasing the duty cycle increases reaction progress due to increased cavitation activity until optimum value (Kashyap, Gogate, & Joshi, 2019). Further increase in duty cycle beyond optimum value resulted in lower biodiesel yield. A similar trend was reported by (Maddikeri et al., 2013) and (Joshi et al., 2018) with optimum values of duty cycles 60% and 70%, respectively.

The combined effect of catalyst amount and methanol to oil ratio is presented in Figure 4.2 (d). Maximum biodiesel yield of 94.75% P50S50 was obtained at catalyst

concentration 0.80 (wt. %) and methanol to oil ratio 53.46 (V/V) %. Biodiesel yield enhanced with an increase in the methanol to oil ratio up to 53.46 (V/V) % beyond this limit yield will decrease. The high percentage of methanol to oil ratio leads to the emulsification of biodiesel and glycerol. Less amount of catalyst and methanol leads to lower biodiesel yield due to the possibility of reversible reaction and incomplete conversion of feedstock oil to biodiesel. Beyond the optimal concentration of catalyst, the biodiesel yield decreased significantly due to saturation of catalyst particles in the reaction mixture, formation of soap (saponification process), and increased reaction mixture viscosity (Nayak & Vyas, 2019). A similar trend was reported by (Ong et al., 2019) and (Dharma et al., 2016).

The combined effect of catalyst concentration and the duty cycle is shown in Figure 4.2 (e). The maximum 94.55% biodiesel yield was attained at a concentration of KOH 0.86 (wt.%) and duty cycle 57.15 %. There is a slight reduction in yield by increasing the duty cycle % beyond the optimum limits. A higher duty cycle produces too many consecutive cavitation activities, which leads to cushioning effect resulting in less cavitation activity which decreases the yield of biodiesel with an even higher catalyst dose. A similar result was reported by other researchers (Joshi et al., 2018; Kashyap et al., 2019; Maddikeri et al., 2013). Biodiesel yield is decreased by up to 90.78%, with a further increase in the concentration of catalyst from 0.86 to 1.5%. Excess dosage of the KOH catalyst helped in gel-forming due to emulsification resulting in a reduced amount of methyl ester content in the final product (Kashyap et al., 2019). The duty cycle effect is very less in the reduction of yield as compared to catalyst concentration. The duty cycle is a more important parameter in the optimization of energy consumption of ultrasound-assisted transesterification. Catalyst is the most important variable, which should be optimized to obtain the maximum yield.

The combined effect of methanol to oil molar ratio and duty cycle have been plotted in Figure 4.2 (f). There is an inverse relationship between the duty cycle and methanol to oil ratio. Biodiesel yield was enhanced by increasing the methanol to oil ratio up to 59%, but further increase resulted in a small decrease of biodiesel's yield. Biodiesel yield decreased from 95.27 to 92.23% gradually with an increase in duty cycle from 50 to 70%. Biodiesel yield decreased, due to poor cavitation activity, beyond the optimal value of the duty cycle. The duty cycle is an important parameter that should be optimized for maximum biodiesel yield and energy savings. (Maddikeri et al., 2013) obtained a maximum yield of Karanja methyl esters with a 60% duty cycle. The optimum value of the duty cycle varied according to feedstock, catalyst, and alcohol used for obtaining the maximum yield.

It can be observed from the Appendix that maximum energy output of 50% is saved with a 50% duty cycle. Maximum energy 625 kJ is consumed with pulse sonication (5s on and 1s on). For this study, a 50% to 70% duty cycle was selected to produce biodiesel. Under same operating conditions: reaction time (25 min), methanol to oil ratio (60%) and catalyst concentration (1 Wt%), maximum energy savings of 50% are possible while maintaining a maximum biodiesel yield of 94.47% with a 50% duty cycle (5,5). Using a 70% duty cycle (5,2), the maximum biodiesel yield of 90.97% was obtained under the same operating conditions with maximum energy savings of 28.5%.

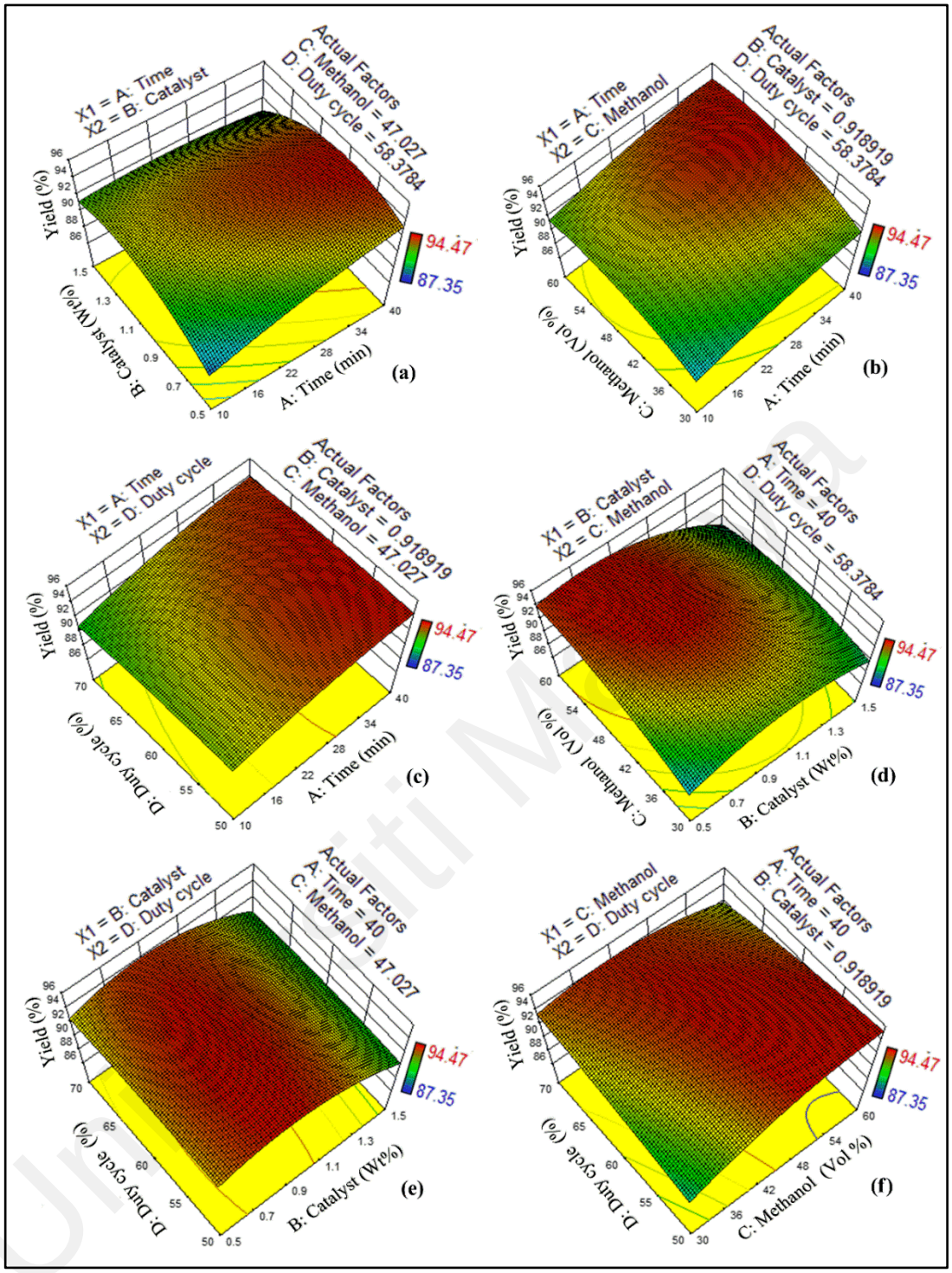

Figure 4.2: 3-D graphs from RSM representing interaction effects between process variables: a) time and catalyst concentration, b) time and methanol, c) time and duty cycle, d) catalyst and methanol, e) catalyst and duty cycle and f) methanol and duty cycle on P50S50 biodiesel yield

4.2.2 ELM modeling

Figure 4.3 shows the values of the correlation coefficient (R) determined by the ELM. From Figure 4.3, it is shown that the R values for the training (R=0.99972), testing (R=0.99357), and overall datasets (R=0.99815) are close to 1. These values indicated a good correlation developed between the experimental values and the predicted values generated by ELM.

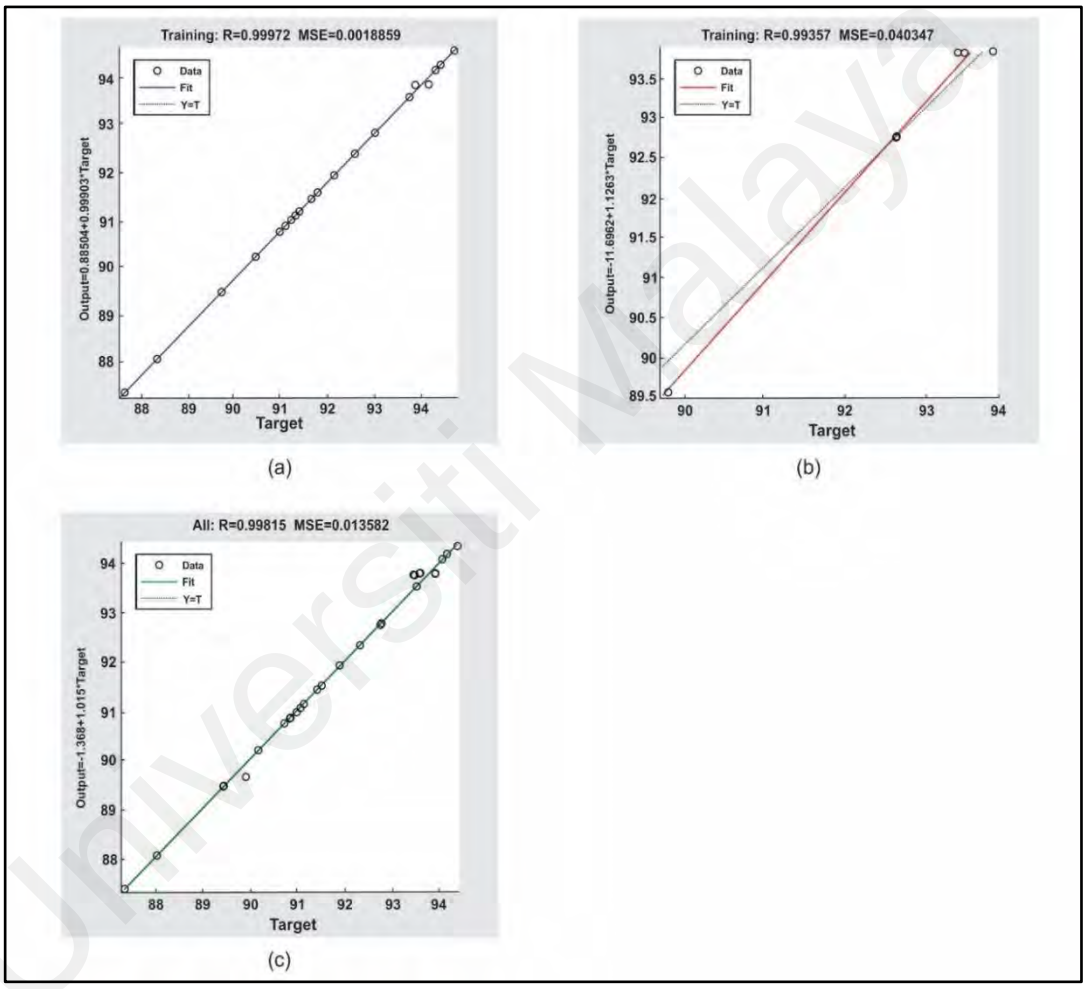

Figure 4.3: The value of coefficient determination (R) for ELM

4.2.2.1 Random sub-sampling cross-validation for the ELM model

24 datasets were imported for training and 6 datasets for testing out of 30 datasets. The procedure was used in this study is the data running ten times, as shown in Table 4.5. The values of MAPE and SD are < 0.5 (i.e., 0.101315 and 0.02179, respectively); these results prove that the ELM model will predict the yield of P50S50ME more accurately.

Table 4.5: Results of the random sub-sampling cross-validation

Repetition	MAPE
R-1	0.065651
R- 2	0.119798
R- 3	0.109659
R- 4	0.129578
R- 5	0.059996
R- 6	0.095333
R- 7	0.106328
R- 8	0.094248
R- 9	0.116168
R- 10	0.116391
Average	0.101315
SD	0.02179

4.2.3 Statistical analysis

The statistical analysis of the performances between RSM and ELM is mentioned in Table 4.6. From Table 4.6, it is shown that both ELM and RSM models have R^2 values that are close to 1, indicating a good fit of the models. The MSE, RMSE, and MAPE value was found greater for RSM (0.022657, 0.1505, 0.146952) compared to ELM (0.013582, 0.1168, 0.059996), respectively. The SEP for RSM and ELM was found to be 0.1639 and 0.1272, respectively. Based on the statistical analysis results, it is concluded that ELM has better performance in terms of prediction accuracy as compared to RSM.

Table 4.6: Statistical analysis

Statistical analysis	RSM	ELM
R^2	0.9935	0.9963
MSE	0.022657	0.013582
RMSE	0.1505	0.1168
MAPE	0.146952	0.059996
SEP	0.1639	0.1272

4.2.4 Optimization of transesterification process parameters using Cuckoo search optimization algorithm

The optimum of P50S50 biodiesel yield determined from the ELM coupling with cuckoo search algorithm via levy flight model is 96.6138%, under the condition as follows: (1) Time: 38.96 (min), (2) KOH catalyst concentration: 0.70 %(w/w), (3) Methanol to Oil ratio: 60 %, and (4) duty cycle: 59.52 %. The experiments were conducted in triplicate using optimum ultrasound-assisted transesterification input process variables to validate the optimum predicted P50S50 yield. ELM coupled with the cuckoo search algorithm predicted a higher yield of 96.6138%. The average experimental yield of P50S50 biodiesel is 95.89%, with a standard deviation of 0.0026, which depicts a good agreement between observed yield and predicts yield by ELM coupled with the cuckoo search algorithm.

4.3 Physicochemical characteristics of P50S50, POME, and SME methyl esters

The physicochemical properties of palm methyl esters, sesame methyl esters, and palm-sesame blend (50:50) methyl esters were estimated in accordance with biodiesel standard methods ASTM D6751, EN 14214, and MS 2008:2008 presented in Table 4.7.

In this study, sesame oil was blended with palm oil to enhance its cold flow properties and lubricity characteristics. The high percentage of unsaturation causes improvement in cold flow properties, like sesame oil methyl esters, have 84% (unsaturated fatty acids), and palm oil biodiesel has 55% (unsaturated fatty acids). P50S50 biodiesel has very good cold flow characteristics like pour point (3.80 ℃), cloud point (7.94 ℃), and cold filter plugging point (−1.77 ℃). P50S50 biodiesel is more viable as biodiesel in comparison to palm-biodiesel due to its better cold flow properties.

According to ASTM and EN biodiesel standards, the oxidative stability of biodiesel should be 3 h and 6 h, respectively. Sesame oil is a viable feedstock to blend with palm

oil to get better cold flow characteristics and maintain its oxidative stability within a range of biodiesel standards. P50S50 biodiesel had 6.89 h oxidative stability, which fulfilled both standard biodiesel limits. P50S50 biodiesel had 30 % saturated fatty acids, which is better to achieve high oxidative stability.

Other physicochemical properties of P50S50 methyl esters are also better than POME and SME, like lower acid value, lower kinematic viscosity, higher calorific value, and better cold flow properties. FAME content of P50S50 methyl esters is more than 98 (wt.%), which is above the value specified by EN 14214 (96.5 wt.%). Physicochemical properties of P50S50 methyl esters meet the minimum criteria set by biodiesel standards ASTM D6751 and EN14214, so it is concluded that P50S50 biodiesel is a potential fuel in the replacement of crude diesel.

Table 4.7: Physicochemical properties of POME, SME, and P50S50 biodiesels (Continued).

Property	Unit	Test Method	Diesel	Biodiesel standard specifications		Biodiesel and biodiesel blends				
			(Ong et al., 2019)	ASTM D6751	EN 14214	POME	POME (Atabani et al., 2012a)	SME	SME (Sarve et al., 2015)	P50S50
Kinematic viscosity at 40 ℃	(mm^2/s)	ASTM D445	2.87	1.9-6.0	3.5-5.0	4.48	4.5	4.37	4.47	4.42
Density at 15 ℃	(kg/m^3)	ASTM D4052	839.4	870-890	860-900	876.1	864.4	884.7	867	880
Acid value	(mg KOH /g)	ASTM D664	0.15	< 0.50	0.50	0.40	0.24	0.35	0.12	0.37
Calorific value	(MJ/kg)	ASTM D240	45.67	-	35	39.56	38.5	39.71	40.1	41.24
Flashpoint	℃	ASTM D93	78.50	130	> 101	>120	135	>150	180	>150
Cloud point	℃	ASTM D2500	2.0	-	-	15.50	16	0.12	- 5	7.94
Pour point	℃	ASTM D97	2.0	-	-	12	15	-4.69	- 9	3.80

Table 4.7: Continued

Property	Unit	Test Method	Diesel	Biodiesel standard specifications		Biodiesel and biodiesel blends				
Cold filter plugging point	°C	ASTM D6371	0.0	-	-	2.12	12	-5.73	-	-1.77
Oxidative stability	h	EN 14112	13.20	3 h	6 h	13.40	10.3	6.32	> 6	6.89
Copper strip corrosion	-	ASTM D130	1a	3 max	-	1a	1a	1a	-	1a
Cetane number	-	ASTM D4737	48.50	47	51	59.15	54.6	47.65	56.32	53.37
FAME content [a]	wt.%	-	-	-	96.5	> 98	-	> 98	> 98	> 98
Linolenic acid methyl ester content [a]	wt.%	-	-	-	1-15	0.37	-	0.56	-	0.49
	POME: Palm olein methyl esters, SME: Sesame methyl esters, P50S50: Palm-Sesame blend methyl esters (50:50 wt.%) [a]FAME content and Linolenic acid content of methyl esters were calculated using gas chromatography									

4.4 Lubricity and wear characteristics of P50S50 biodiesel

Friction and wear behavior of B10 (Diesel), B100 (Palm biodiesel), and B100 (P50S50 biodiesel) were estimated according to ASTM D4172 standard. The experimental conditions were speed 1200 rpm, temperature 75 ℃, load 40 kg, and duration of experiment 600 s. Figure 4.4 (a) represents the coefficient of friction of tested fuels with respect to time variation at 1200 rpm. In the early stage of the experiment, instability of the coefficient of friction (COF) can be seen up to 90 s that is named as run-in period; after that, a steady-state condition is achieved, as shown in Figure 4.4 (a), which is due to the presence of ester content (Konishi, Klaus, & Duda, 1996). During the start of the experiment, the COF was very high due to the absence of a lubricating film between metallic contact, and later on, the steady-state friction trend starts to stabilize after the formation of the lubricating film between mating surface (Habibullah et al., 2015). The run-in period for pure P50S50 biodiesel is the lowest due to the absorption of ester molecules existing in the biodiesel sample. P50S50 biodiesel has high unsaturation (presence of double bonds) compared to palm biodiesel. The presence of ester content in the fuel sample leads to the conversion of run in the period to steady-state condition quickly (Konishi et al., 1996). B10 has a higher COF among tested fuels due to high Sulphur content. Fuel lubricity is a very critical parameter related to the durability of diesel engine components. Most diesel engine components are self-lubricated with diesel fuel, such as (fuel injectors, fuel pumps, etc.).

Wear scar diameter (WSD) of tested fuels that are measured by SEM micrographs of metal balls. Figure 4.4 (b) exhibits the WSD and average COF of B10 (Diesel), B100 (Palm biodiesel), and B100 (P50S50 biodiesel). B10 (diesel) had high value of WSD 0.948 mm than B100 (Palm biodiesel) 0.869 mm WSD and B100 (P50S50 biodiesel) 0.746 mm. Biodiesel P50S50 exhibited less WSD value than other test fuels due to high unsaturated fatty acids that formed the lubricating film between metal contact surfaces.

The average COF of P50S50 biodiesel 0.085 is the lowest, followed by B100 (Palm biodiesel) 0.087 and B10 (diesel) 0.097. The higher percentage of oxygen content, high percentage of unsaturation in fatty acids, and long carbon chain of fatty acids in biodiesel enhanced the fuel's lubricity. It reduced the wear and friction between metallic contact surfaces.

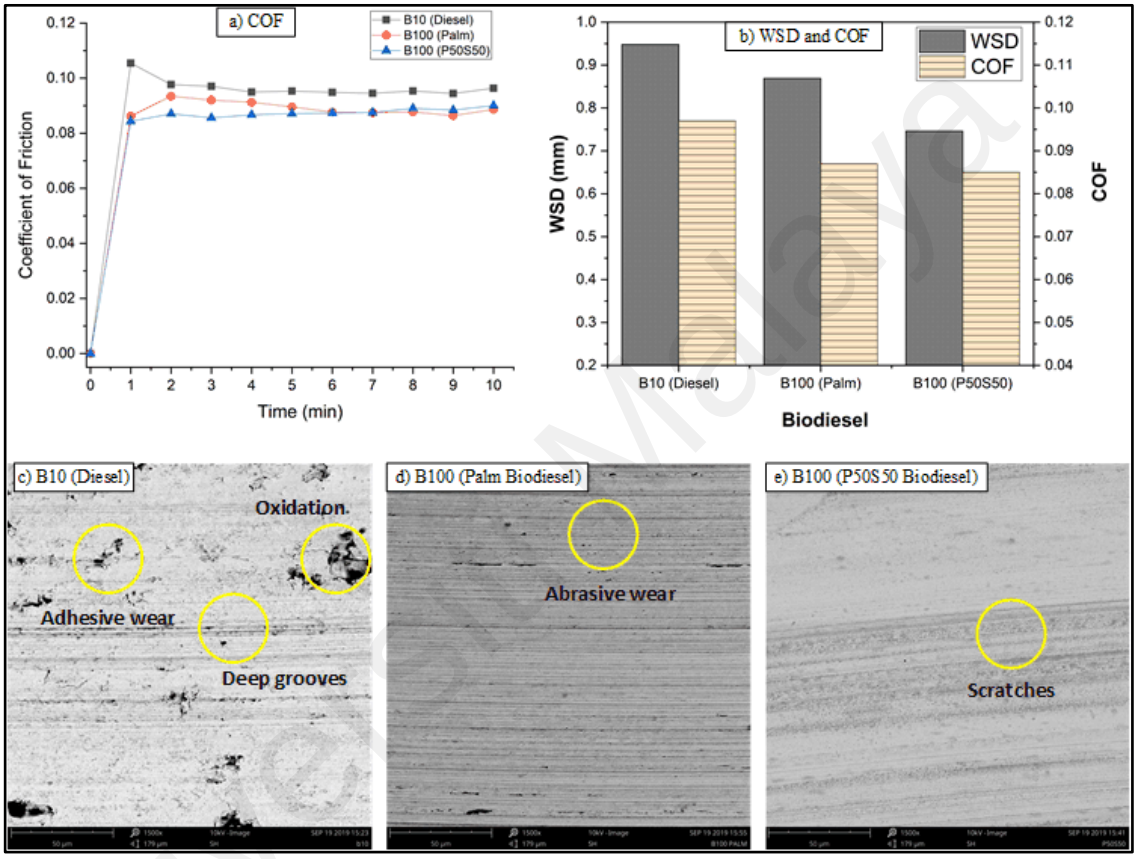

Figure 4.4: a) Coefficient of friction of B10 (Diesel), B100 (Palm biodiesel), and B100 (P50S50 biodiesel) at 1200 rpm, temperature 75 °C, time for test 600 seconds and load 40 kg. b) wear scar diameter (WSD) and the average coefficient of friction (COF) of B10 (Diesel), B100 (Palm biodiesel), and B100 (P50S50 biodiesel) at 1200 rpm. c), d) and e) SEM micrographs (worn surfaces) of stationary steel balls for B10 (Diesel), B100 (Palm biodiesel), and B100 (P50S50 biodiesel) at 1200 rpm

SEM micrographs of worn surface of stationary steel balls under 40 kg load of B10 (Diesel), B100 (Palm biodiesel) and B100 (P50S50 biodiesel) tested fuels presented in Figure 4.4 (c), (d), and (e), respectively. Abrasive wear can be seen in the form of scratches, and extrusion of small metal can be visualized in the form of adhesive wear. Adhesive wear can be seen in the case of B10 due to the detachment of particles from the

worn surface. Deep grooves and scratches can be seen in the case of B10 due to a lack of lubricating film between rubbing surfaces. The removal of material in B10 is more than biodiesel-tested fuel specimens. Pure biodiesel tested fuels showed less wear compared to B10 due to a high concentration of oleic and linoleic acids that acts as a lubricity enhancer (Geller & Goodrum, 2004).

4.5 Tribological analysis of ternary fuel blends

4.5.1 Tribological study (HFRR)

The density and viscosity of different fuel samples with and without fuel additives are presented in Figure 4.5. The lubricity of diesel fuel is evaluated by a very common standard test method (ASTM D6079-11) using the HFRR. Before tribological studies, seven fuel samples' physicochemical properties were measured like viscosity, viscosity index, and density (SVM 3000), and calorific value (C2000 basic calorimeter) in Table 4.8.

Table 4.8: Physicochemical properties of tested fuel samples

Fuel samples	Physicochemical properties of fuel and its blends			
	Density	**Viscosity**	**Viscosity Index**	**Calorific Value**
	kg/m^3	**mm^2/s**	**-**	**MJ/kg**
Standard specifications for pure biodiesel				
ASTM D6751 (Standard specifications)	870-890	1.9-6.0	-	-
EN 14214 (Standard specifications)	860-890	3.5-5.0	-	-
Tested fuel samples				
B10 (commercial diesel)	855.9	3.1507	81.2	44.1927
B100 (P50S50 biodiesel)	880.4	4.2110	186.2	40.2151
B30 (70% Diesel and 30% Biodiesel)	852.6	3.3189	164.2	43.4013
B30 + 20% (V/V) Dimethyl carbonate	878.0	2.0149	-	40.4611
B30 + 10% (V/V) Ethanol	847.0	3.0025	-	41.7887
B30 + Carbon Nano Tubes (100 ppm)	853.1	3.8064	176.8	43.075
B30 + TiO_2 (100 ppm)	853.0	3.8606	208.3	44.006

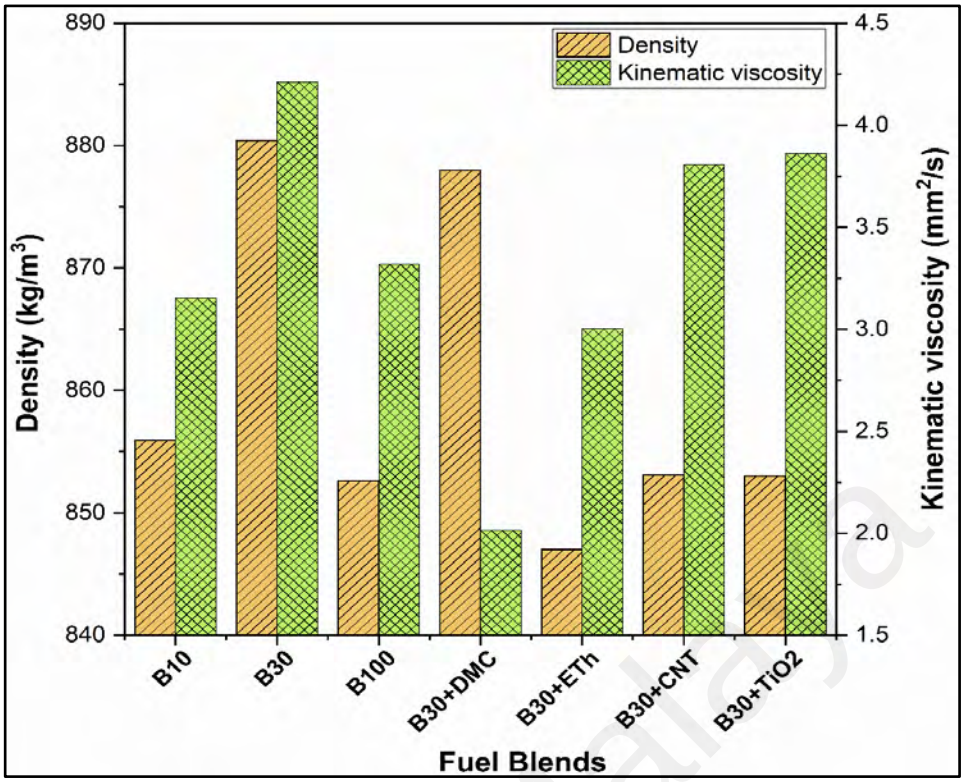

Figure 4.5: Density and viscosity trend with and without fuel additives

4.5.1.1 Tribological behavior: Coefficient of friction and Wear scar diameter

The coefficient of friction trend for seven fuel samples is illustrated in Figure 4.6. The lubricity of diesel fuel is evaluated using a common standard test method (ASTM D6079-11) using the High-Frequency Reciprocating Rig (HFRR). The maximum allowable wear scar diameter measured by the standard test method at 60 °C is 520 µm (ASTM D 975-10) and 460 µm (EN 590-10), according to American and European standards, respectively (Farias et al., 2014). At the start of each experiment, the friction trend is unstable with respect to time, known as the run-in period. After a few minutes, this friction trend starts to stabilize, known as the steady-state condition (Habibullah et al., 2015). It is seen from the friction trend that the unsteady state of B10 increases with time in comparison to other B30 fuel samples with additives. The presence of more percentage of ester content in biodiesel fuel samples provides a better protection layer as compared to B10 and B30 fuel samples. The presence of ester content in the fuel sample leads to the conversion of run in the period to steady-state conditions quickly (Konishi et al.,

1996). The run-in period for pure P50S50 biodiesel is the lowest due to ester molecules' adsorption existing in the biodiesel sample. In the case of B100 biodiesel, ester molecules of biodiesel stick to the metallic contact surface. Fatty acids methyl ester reacts with metallic surfaces and forms a protective layer between them, which decreased the 'run-in period' for pure biodiesel. A similar trend can be seen in nanoparticle fuel samples; the presence of nanoparticles in fuel samples acts as a surfactant for two metallic contact surfaces. Ester molecules and nanoparticles' presence in fuel samples act as a surfactant for contact surfaces (Fazal, Haseeb, & Masjuki, 2013). It can be deduced from Figure 4.6; the friction coefficient decreases gradually with respect to time for all fuel samples except B100 and B30+Eth fuel samples. The coefficient of friction for B100 and B30+Eth increases up to 10 minutes and then a sudden reduction in value with time. This phenomenon occurred due to the fatty acid composition of biodiesel like after the run-in period, fatty acids of B100 and B30+Eth fuel samples were not involved in lubricant film formation until the period of 10 minutes after the development of a thin film layer resulting in a rapid reduction of the friction coefficient for B30 and B100 respectively (Zulkifli, Kalam, Masjuki, Shahabuddin, & Yunus, 2013).

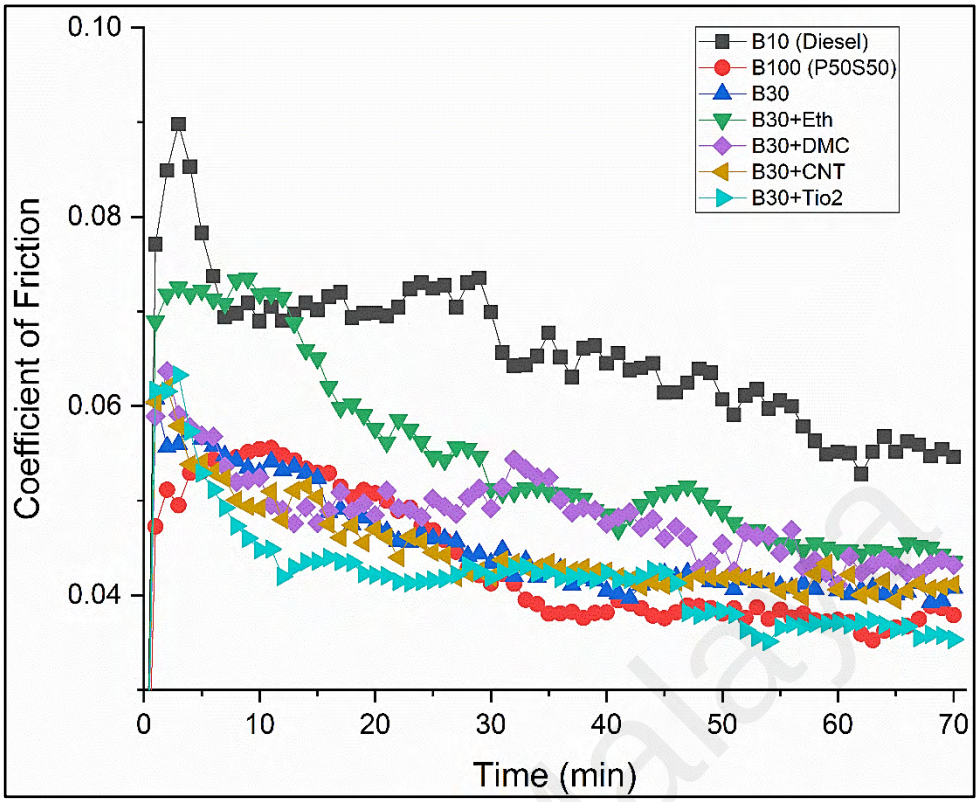

Figure 4.6: Coefficient of friction trend with respect to time (min).

B10 has a higher average coefficient of friction (0.0676) and lower lubricity among other fuel samples due to the presence of higher Sulphur content. In diesel engines, fuel lubricity is important because it provides lubrication during rotating pumps and fuel injection (Barbour, Rickeard, & Elliott, 2000). B100 biodiesel and B30 fuel sample showed good lubricity and low coefficient of friction compared to alcoholic additives (B30+DMC and B30+Eth) and B10. The higher percentage of unsaturated fatty acids and long carbon chain fatty acids in biodiesel enhanced the lubricity of fuel and reduced the wear and friction between metallic contact surfaces. Another reason is that heteroatom lubricating film's uniform availability between mating surfaces also reduces the friction because heteroatom includes oxygen and Sulphur content. The kinematic viscosity of the B30+Eth fuel sample is 3.0025 mm^2/s, as shown in Table 4.8. The B30+Eth sample's lubricity is significantly affected due to lower density, which further hinders the formation of the lubricating thin film between ball-plate metallic contact. B30 fuel sample contains a low percentage of oxygen content, but the B30+Eth fuel sample contains a high oxygen

content rate due to high oxygenated alcohol (ethanol). The higher percentage of oxygen resulting in increased wear and friction coefficient due to oxidation of metallic surface can be seen from Figure 4.7. A similar trend is reported by various researchers (Kuszewski, Jaworski, & Ustrzycki, 2017; Lapuerta et al., 2010). The lower lubricity of ethanol B30 blend is mainly affected by the following properties like volatility, temperature-sensitive, tribological behavior, and blending stability. The addition of ethanol up to 10% by volume resulted in a higher coefficient of friction, and wear scar diameter can be seen from Figure 4.6 and Figure 4.7. These results attributed that higher COF and WSD in the case of B30+Eth was due to the high evaporation rate of ethanol from the lubricating film.

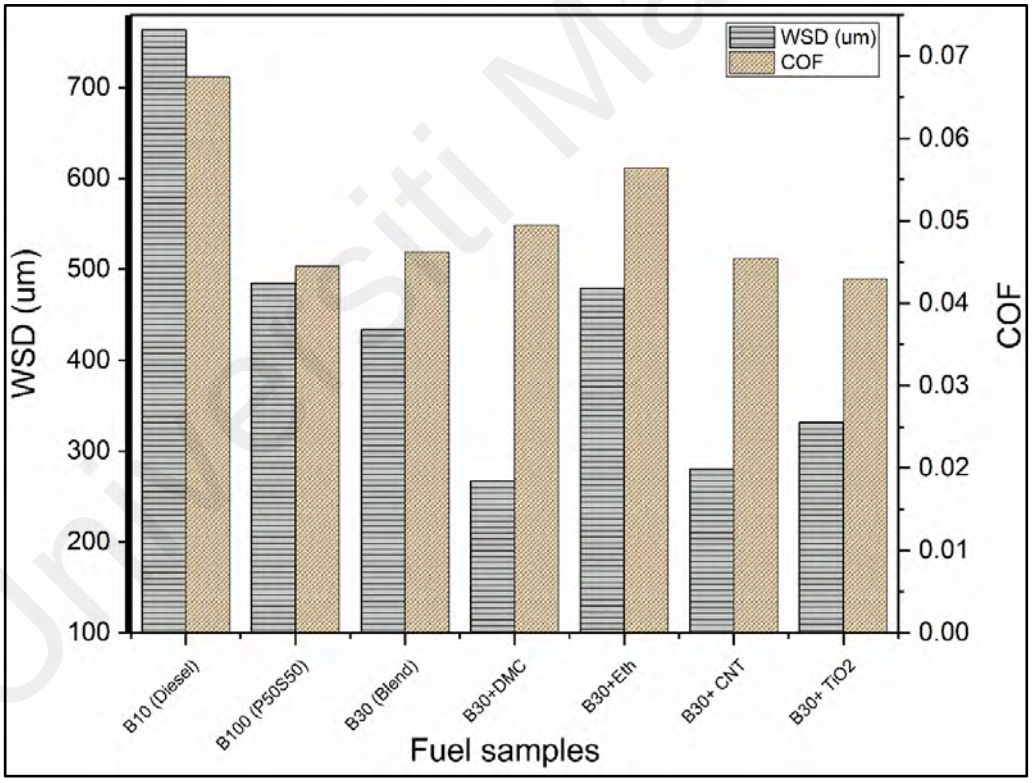

Figure 4.7: Wear scar diameter and coefficient of friction of tested fuel samples

B30 fuel blended with ethanol-fueled in compression ignition engine, which produced oxidation products during continuous flow through the injection system. These products removed the oxide layers from the injection system's moving components, and

consequently, the anti-wear effects weaken. Similar increases in wear for diesel-ethanol blends were reported by other researchers (Corkwell & Jackson, 2002). DMC as an oxygenated fuel additive blended with B30 showed promising WSD and COF results compared to B30 blended with ethanol. DMC contains a higher amount of oxygen content among all fuel samples. From Figure 4.7, the WSD value for B30+DMC is the lowest among all fuel samples. The result can be attributed that at the start of the experiment, the anti-adhesive oxide layer is formed between metallic contact surfaces, which resulted in less wear and less WSD.

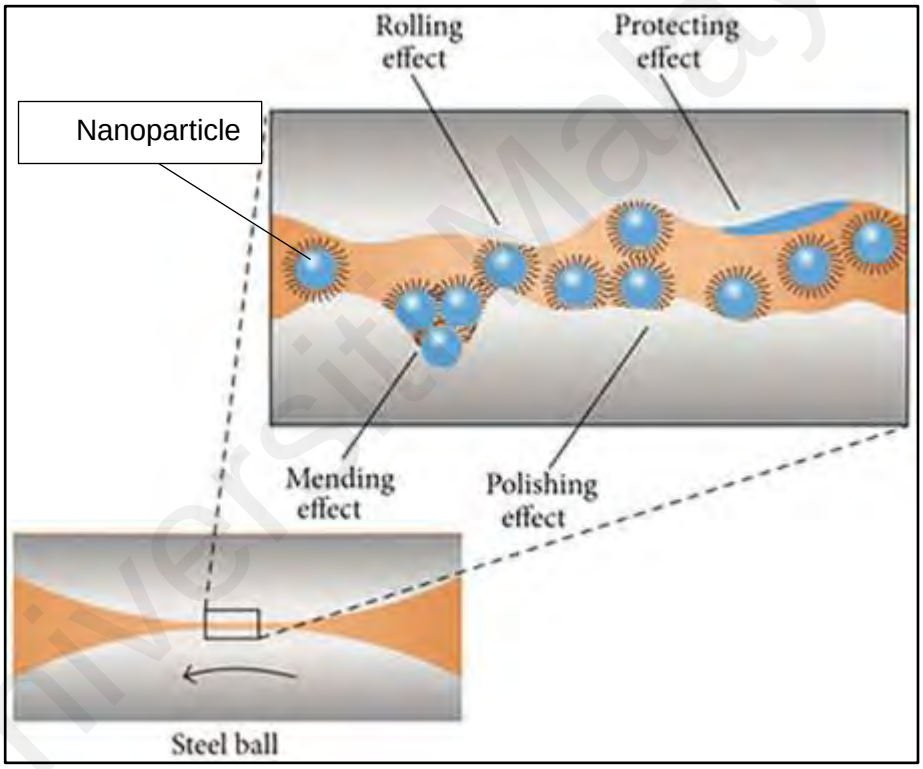

Figure 4.8: Schematic diagram of the lubrication mechanism during the HFRR test with Nanoparticles (Gulzar, 2018)

Nanoparticles combined with lubricants to improve their lubricity, wear, and friction. During this HFRR test, nanoparticles make a lubricating film between the metallic contacts. There are four different types of phenomena in the lubrication mechanism, like ball-bearing effect, protecting film formation, polishing, and mending impact, as shown in Figure 4.8.

In this research work, TiO_2 and CNTs were combined with a B30 fuel sample to investigate its effect on the lubricity of fuel for injection system application. B30+TiO_2 fuel sample showed the least friction coefficient (0.0430) among all other fuel samples, followed by B100. From Figure 4.7, B30+TiO_2 exhibited better anti-wear behavior and reduced coefficient of friction. This result attributed the formation of effective and uniform lubricating thin TiO_2 film between metallic surface contact (ball to plate). Other researchers also reported the significance of nano-TiO_2 in reducing the friction coefficient of mineral lubricant (Arumugam & G. Sriram, 2013; Ingole et al., 2013; Shahnazar, Bagheri, & Abd Hamid, 2016; Wu, Tsui, & Liu, 2007). Similarly, the above-mentioned experimental results support the addition of TiO_2 in fuels to enhance its lubricity for fuel injectors.

B30+CNT fuel samples showed better tribological properties (WSD and COF) among all other fuel samples instead of B30+TiO_2. B30+CNT fuel sample exhibited the lowest WSD due to the formation of lubricating thin CNT anti-adhesive film between contact surfaces. COF of the B30+CNT fuel sample is higher than B30+TiO_2 due to particles' agglomeration in the fuel sample. The dispersion of CNT's in the fuel sample is quite challenging due to CNT's chemical inert behavior (Shahnazar et al., 2016).

Lubricating thin films' stability between metallic mating surfaces depends on the fuel's fatty acid composition, fluid viscosity, temperature, dispersion of Nano-additives in fuel, applied load, and speed (Maleque et al., 2000). The oxidation phenomenon transforms ester into different fatty acids (propionic acid, formic acid, acetic acid, etc.) that increase fuel lubricity. Still, sometimes it becomes corrosive for diesel engine components (pump and injection system) (Anastopoulos et al., 2001; Maleque et al., 2000; Sulek et al., 2010). Length of carbon chain molecules, degree of unsaturation (presence of double and triple bonds), oxygen content in biodiesel, nanoparticle additives, and oxygenated alcoholic additives play an important role in enhancing the lubricity of the fuel. In the form of

monoglycerides, diglycerides, and free fatty acids in biodiesel, impurities also contributed to the lubricity improvement (Hu, Du, Li, & Min, 2005).

4.5.1.2 Morphological study of worn steel ball and plate

*(a) **Morphological study of worn steel plate***

Figure 4.9 shows the micrographs of worn steel balls used for various fuel samples during the HFRR test to visualize wear behavior. Major surface deformation can be visualized from micrographs of B10, B30, B30+Eth, and B30+CNT. It is observed that particles detached from the cavities of worn steel balls of B10, B30, B30+Eth, B30+CNT, and B30+TiO_2 are much bigger than 20 µm, which is attributed to adhesive wear. The particles detached from the surface of B100 and B30+DMC worn steel balls are lower than 20 µm (abrasive wear). The removal of larger particles of more than 20 µm from surface cavities is known as adhesive wear (Rabinowicz, 1984). The small particles detached from worn surfaces lower than 20 µm reflecting abrasive wear (Sperring & Nowell, 2005). Figure 4.9 (1) B100 shows that Black spots can be seen, predicting the oxidation phenomena. It will demonstrate oxygen content, which will help form a lubricating film between mating surfaces due to the conversion of Fe_3O_4 and Fe_2O_3 inorganic oxides (Zulkifli et al., 2013). In B10, severe adhesive wear can be seen due to large particles' detachment from the worn surface.

Abrasive wear can also be visualized in the form of scratches. From Figure 4.9 (3,5,6,7), the extrusion of small metal can be seen in the form of adhesive wear. Micro pits and corrosion activity can be visualized in the case of B30+DMC and B30. As a result, oxidative corrosion is occurred in the form of corrosive wear due to the formation of different peroxides and acids during oxidation.

(b) ***Morphological study of worn steel plate***

Figure 4.10 showed the surface morphology of worn surface plates. The micrograph of B100 depicts the oxidation process, which provides a lubricating film between rubbing surfaces. This result is attributed to oxygen content, double bonds, and a long chain of carbon atoms in biodiesel. This oxidative layer formed and removed continuously due to sliding motion, therefore giving a smooth surface. But with time, these removed unreactive detergents cause an increase in wear.

Deep grooves and scratches were observed in the case of B10. These results are attributed to the erratic friction coefficient behavior and lack of lubricating thin film between rubbing metallic surfaces, small sliding grooves, micro pitting due to corrosion activity in the case of B30+Eth fuel sample. The B30+DMC surface's micrograph shows a corrosive surface due to a chemical attack on the plate's surface. These results are attributed to oxidative wear and metallic soap formation due to metallic surface reaction with the chemical. Oxidation can be seen in B30+TiO_2, which provides lubricating film between mating surfaces and reduces the overall coefficient of friction. Few deep grooves were also observed due to the rubbing of debris which leads to adhesive wear.

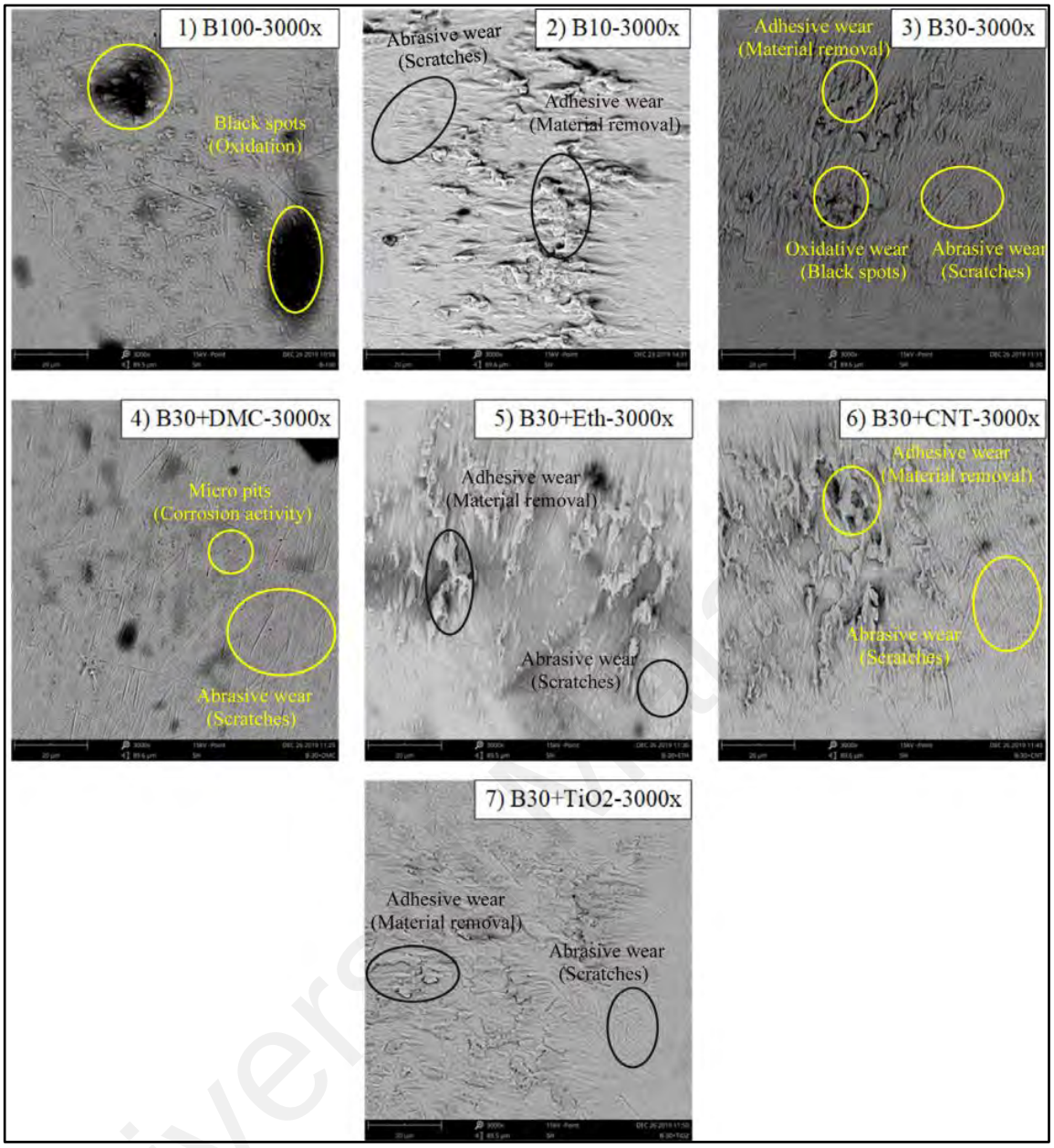

Figure 4.9: SEM micrographs of worn steel ball used in HFRR test magnified at 3000x

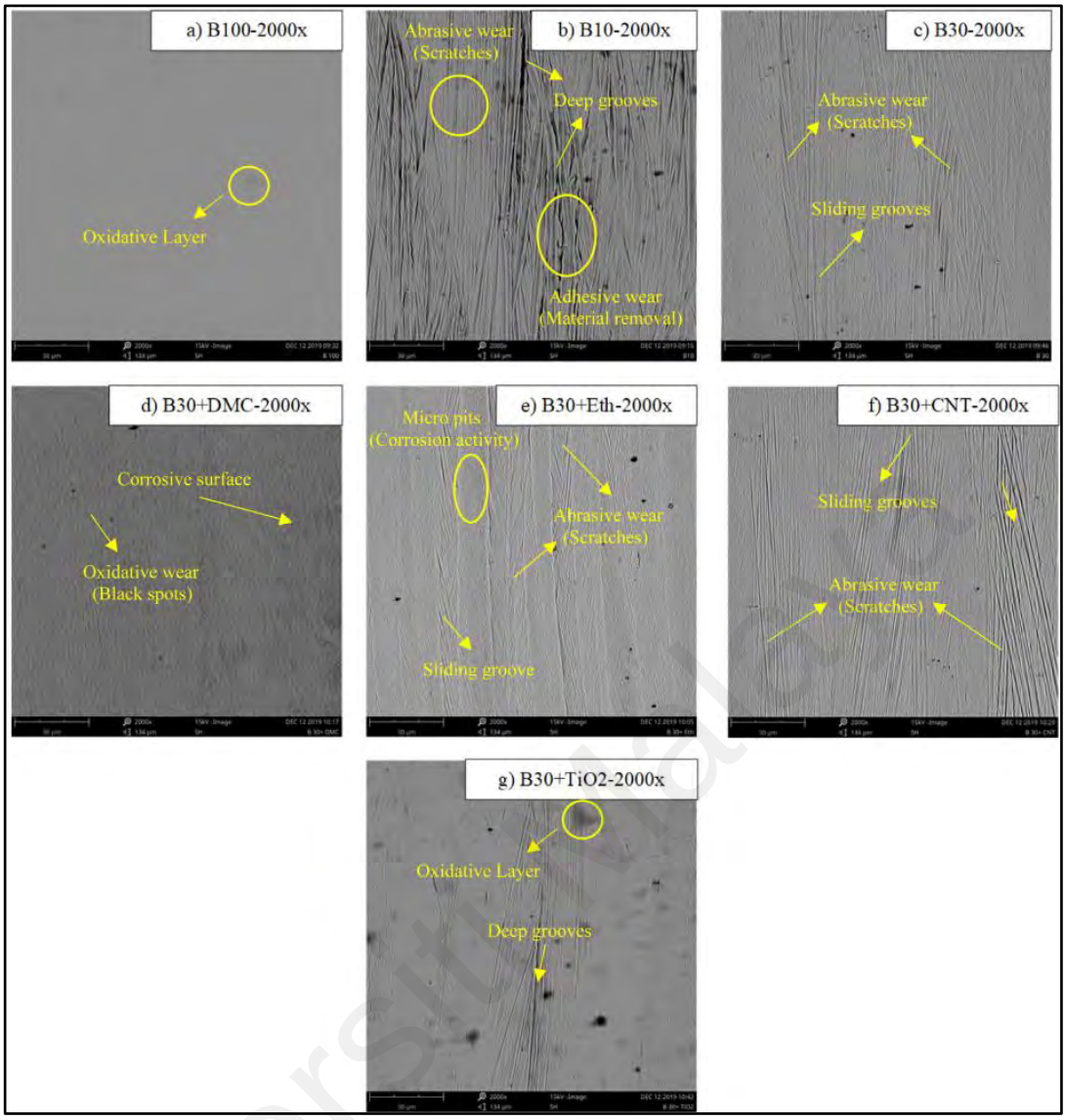

Figure 4.10: SEM micrographs of worn steel plate used in HFRR test magnified at 2000x

4.5.2 Tribological study (Fourball tribo tester)

As 5% contamination of lubricant with fuel occurred because of crankcase dilution (Arumugam & G. Sriram, 2013). Thus, 5% of each above-mentioned fuel was blended with the SAE-40 (a commercial lubricant). Viscometer (Make: Anton Paar: SVM 3000) was used to measure the physio-chemical properties of SAE-40 and all other contaminated lubricant samples, as shown in Table 4.9. Contamination of the fuel in the lubricating oil caused its dilution, which decreased its viscosity and lubricity. Density and viscosity trends for lubricant samples clean and diluted are presented in Figure 4.11.

Table 4.9: Lubricant samples physicochemical characteristics with the addition of 5% fuel blends

Lubricant samples	Physicochemical properties of lubricant samples		
	Density (Kg/m^3)	Viscosity @ 40 °C (mm^2/s)	Viscosity Index
100% Lubricant (SAE 40)	873.7	87.022	201.3
Lubricant + 5% B10 (commercial diesel)	872.0	71.072	205.3
Lubricant + 5% B30 (70% Diesel and 30% Biodiesel)	873.3	76.652	221.6
Lubricant + 5% (B30 + 20% (V/V) Dimethyl carbonate)	872.0	64.509	-
Lubricant + 5% (B30+ 10% (V/V) Ethanol)	871.0	69.316	-
Lubricant + 5% (B30+ 100 ppm Carbon Nano Tubes)	872.7	69.606	230.6
Lubricant + 5% (B30+ 100 ppm TiO_2)	872.1	69.311	205.4

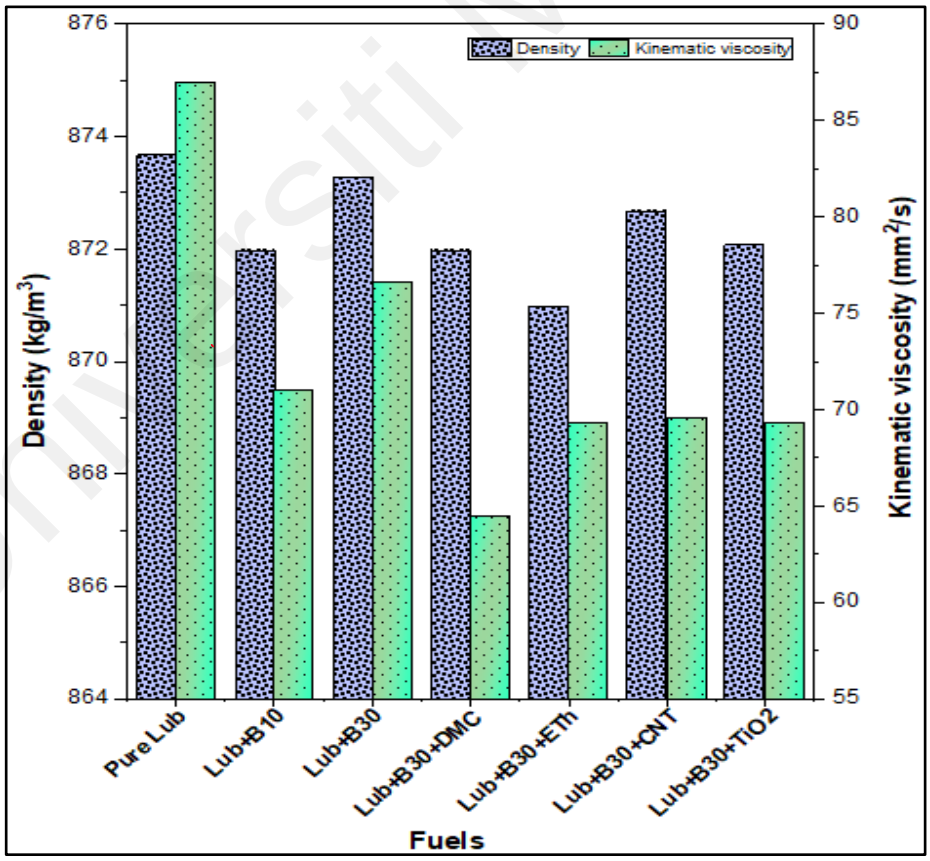

Figure 4.11: Density and viscosity trend for lubricant with and without fuel dilution

4.5.2.1 The tribological characteristics of lubricant samples: COF and WSD

COF of all lubricant samples during running-in state and steady-state are presented in Figure 4.12. There is a sharp spike in the COF value of all measured samples at the beginning of the run, known as the run-in period, which can be visualized from Figure 4.12. COF is very high because of the lack of lubricating film between these metallic contact during this run-in period.

After a few minutes, the friction trend stabilizes because of the protective lubricating film formation among rubbing surfaces, known as steady-state condition (Habibullah et al., 2015). Lubricant with biodiesel fuel dilution showed less frictional force and almost 7.7 % lower COF than lubricant contaminated by commercial diesel. Biodiesel fuel dilution in lubricating oil causes less degradation, as described by earlier research (Arumugam & G. Sriram, 2013; Y. Singh, Singla, Kumar, & Kumar, 2016).

Also, the addition of NPs in methyl esters enhanced the lubricity of lubricant as compared to diesel contaminated lubricant and showed the least COF. B30 + TiO_2 and B30 + DMC fuels caused the least lubricant degradation among all other lubricant samples. The reason for the least degradation of lubricant is the presence of oxygenated moieties, and the excess amount of oxygen in the chemical composition of DMC and TiO_2 led to an additional improvement in the overall lubricity of B30+ fuel additives-contaminated lubrication oil (Arumugam & Sriram, 2012).

Figure 4.13 showed the average COF between stationary balls and rotating balls and the WSD of tested steel balls. 100% pure reference lubricant (SAE-40) showed minimum COF. But dilution of lubricant by fuels caused an increase in COF because of the decrease in viscosity. Lubricant contaminated with B10 showed the highest (0.1053) COF than all other lubricant samples. B30+DMC, B30+nanoparticles contaminated lubricant showed considerably low COF than diesel, biodiesel, and biodiesel + ethanol fuel contaminated lubricants. On average, all contaminated lubricant fuel samples Lub+B10,

Lub+B30+Ethanol, Lub+B30, Lub+B30+CNT, Lub+B30+DMC and Lub+B30+TiO_2 exhibited higher COF 42.295%, 35.81%, 31.355%, 27.56%, 27.02% and 13.78% respectively than 100% lubricant sample. Lub+B30+TiO_2 sample showed the least friction coefficient among all tested fuels under similar operating conditions. Lub+B30+TiO_2 lubricant sample showed 13.4 % lower COF than biodiesel (B30) contaminated lubricant and 20.04% lower COF than diesel contaminated lubricant. B30+TiO_2 acts as a friction-reducing agent in the lubricant sample. It produces a protective coating between the metallic contact because of ester molecules in biodiesel and the spherical shape of TiO_2 NPs acting as a ball bearing between rubbing surfaces (Fazal et al., 2013). Similar results were obtained by various researchers (S. Arumugam & G. Sriram, 2013; Ingole et al., 2013). Lub+B10 showed a high average COF value and lowered lubricity among all analyzed samples because of a high percentage of Sulphur content in B10 fuel. B30+Eth fuel sample contains a large quantity of oxygen content, resulting in high wear and COF due to oxidation of the metallic surface. Many researchers have reported a similar result (Kuszewski et al., 2017; Lapuerta et al., 2010). Lubricating film stability between rubbing surfaces is mainly affected by speed, applied load, fluid viscosity, dispersion of nanoparticles, the fatty acid composition of fuel, and temperature (Maleque et al., 2000).

The WSD of reference commercial lubricant (SAE-40) was significantly high while dilution of lubricant with biodiesel fuels decreased WSD because of polarity-imparting oxygen atoms present in the methyl esters group of biodiesel fuel that improves the lubricity. The same reasons were described by other researchers (Farias et al., 2014; Knothe & Steidley, 2005). B30 with the addition of fuel additives exhibited less WSD values because of ester molecule as well as nanoparticles that act as a tiny ball bearing that roll between rubbing surfaces and resulting in lower wear compare to pure 100% lubricant and Lub+B10 (Gulzar, 2018). Lub+B30+Eth showed maximum WSD value

among fuel additive blends due to oxidation products which will remove the oxides layers between metallic contact surface like piston and cylinder, which resulted in high wear and coefficient of friction. Similar behavior was reported by other researcher (Corkwell & Jackson, 2002).

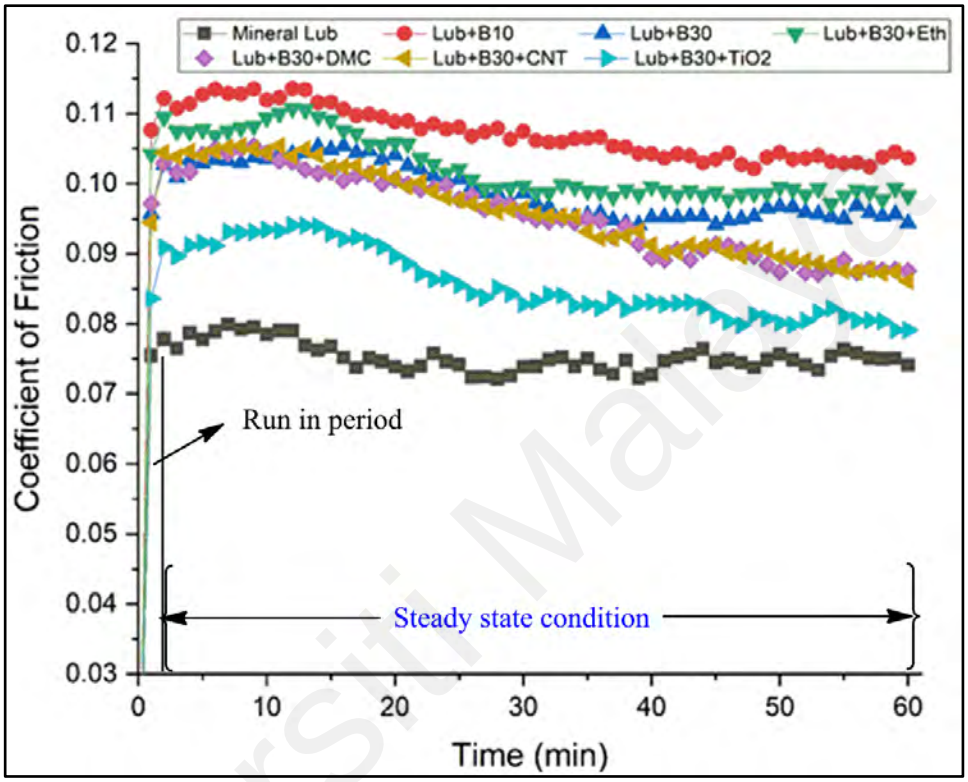

Figure 4.12: Coefficient of friction trend for all tested samples with respect to time

All contaminated lubricant fuels exhibited a decreasing trend in WSD values due to the ester molecule in a B30 biodiesel sample. Lub+B30+Eth tested sample showed maximum COF and WSD among all contaminated lubricants with different fuel additives. Lub+B30+Eth sample's poor lubricity is due to its lower kinematic viscosity that creates difficulty in the forming of a protective layer between metallic surfaces. Formation of anti-adhesive layer among metallic contact in case of Lub+B30+DMC sample exhibited better lubricity compared to ethanol diluted lubricant sample. Lubricant diluted with B30+ nanoparticles exhibited less coefficient friction and wear compared to other samples.

Lub+B30+CNT showed the lowest value of WSD among all fuel additive contaminated lubricant samples. The COF value of Lub+B30+CNT is high compared to Lub+B30+TiO_2 due to the clustering of NPs in fuel samples because of the poor dispersion stability of CNT nanoparticles. Few studies reported that the dispersion of CNT in the fuel sample is very difficult due to the inert chemical behavior of CNT nanoparticles (Shahnazar et al., 2016). However, the use of surfactant in the current study stably blends the CNT in the fuel samples, which avoids the agglomeration, settling and clustering of nanoparticles in the fuel blends. Also, to stably mix the CNT nanoparticles in the fuel blends, initially, it is mixed using the magnetic stirrer, followed by bath sonication for a period of 60 mins and probe sonicated at 25 Hz ultrasonic waves at 3 seconds ON/OFF, which enables the mixture to stably blend. Lubricant contaminated with B30 fuel showed the least WSD value due to the long carbon chain fatty acids and the high percentage of unsaturated fatty acids in biodiesel. On average, there is reduction in WSD values 31.7%, 29.8%, 26%, 25.2%, 22.4% and 16.7% compared to pure lubricant for B30+CNT+Lub, B30+Lub, B30+DMC+Lub, B30+TiO_2+Lub, B30+Eth+Lub and B10+Lub respectively. The reduction in the WSD values is due to the presence of ester molecules in biodiesel and the presence of oxygen content contributing to better wear properties.

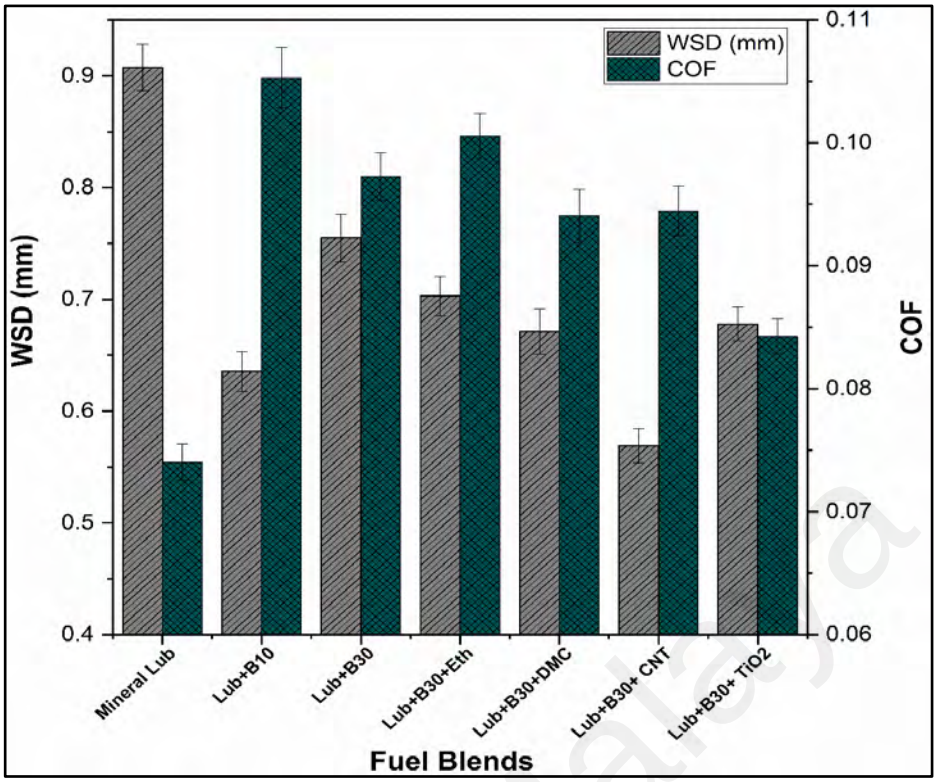

Figure 4.13: Avg. COF and Avg. WSD of lubricant samples

4.5.2.2 Worn ball surface analysis by SEM

Morphological images of worn steel balls used in testing the lubricant samples are shown in Figure 4.14. Contamination of commercial diesel (B10) in lubricant increased its wear as abrasive and adhesive wear is observed. Material detached from the worn steel ball cavity of lubricant contaminated with B10 is bigger than 20µm, which is named adhesive wear. The particles in all tested samples removed from the worn steel ball cavities are smaller than 20µm, which is known as abrasive wear (Sperring & Nowell, 2005). Abrasive wear in the form of scratches can be seen. Scratches and deep grooves can be observed in the case of B10 contaminated lubricant. This result is attributed to the unsteady friction coefficient behavior and absence of lubricating thin film between mating metallic surfaces. B30 biodiesel fuel in lubricating oil caused less wear than diesel fuel and can be seen as light and deep grooves (abrasive wear) on the worn surface. Biodiesel blend B30 showed less wear than B10 because P50S50 biodiesel has a high

concentration of linoleic and oleic acids that acts as lubricity enhancer (Geller & Goodrum, 2004).

Alcoholic-based B30 fuel in lubricant showed the polishing wear as a result of the chemical reaction of fuel on the steel ball surface to protect rubbing surfaces. It means ethanol and dimethyl carbonate are chemically active additives in the fuel that gave comparatively smooth surfaces. Dimethyl carbonate gave less wear debris in lubricating oil due to chemically active film formation between rubbing surfaces. Lubricant samples contaminated with B30+DMC fuel showed the least degradation of lubricant, as presented in Figure 4.14.

Similarly, nanoparticle based B30 fuel in lubricant showed less wear than the commercial diesel contaminated lubricant. B30+ CNT showed less abrasive wear than B30+ TiO_2 fuel.

The wear and overall coefficient of friction of lubricating oil decrease with the addition of nanoparticles in biodiesel blend (B30) because of lubricating film generation between rubbing surface and nanoparticles serve as a ball bearing between these surfaces. Tribofilm formation is caused by the reaction between the additives and tested samples in the given atmosphere. Tribofilm is also named protective film on the tested surfaces (Chou et al., 2010; Viesca, Hernández Battez, González, Chou, & Cabello, 2011). Various researchers reported filling deep groves with nanoparticles, known as the mending process in the previous study, enhancing wear-protection capability (Gulzar, 2018). Nanoparticles stability and dispersion are major parameters that lead to better tribological characteristics than nanoparticles' structure, size, and shape. Lubricant samples contaminated with B30+ TiO_2 exhibited better tribological behavior (less wear and COF) than B30+ CNT due to better stability and dispersion of TiO_2 in the fuel sample. The ball-bearing effect can be another reason for better tribological characteristics in B30+ TiO_2 due to the spherical shape of TiO_2 nanoparticles. In many recent studies on nanoparticle-

based lubrication systems, the idea of active lubrication mechanisms remains a matter of discussion. Various researchers have suggested different phenomena, including the ball-bearing effect, protective film formation, mending effect, and polishing effect (Mubashir, 2017). These phenomena are divided into two major categories. The first one is the creation of protective/tribofilm and the effect of ball bearings. The second one is to improve the surface by the remediation/repairing effect and the polishing/smoothing effect. In the current investigation, Lubricant with TiO_2 nanoparticles exhibited better tribological characteristics compared to other fuel additives. Spherical-shaped TiO_2 nanoparticles act as a ball bearing between metallic contact. In previous research articles, different lubrication mechanisms of various nanoparticles were reported like, ball-bearing effect, mending effect, and tribo film formation using XPS rubbing surface characterization technique (Laad & Jatti, 2018).

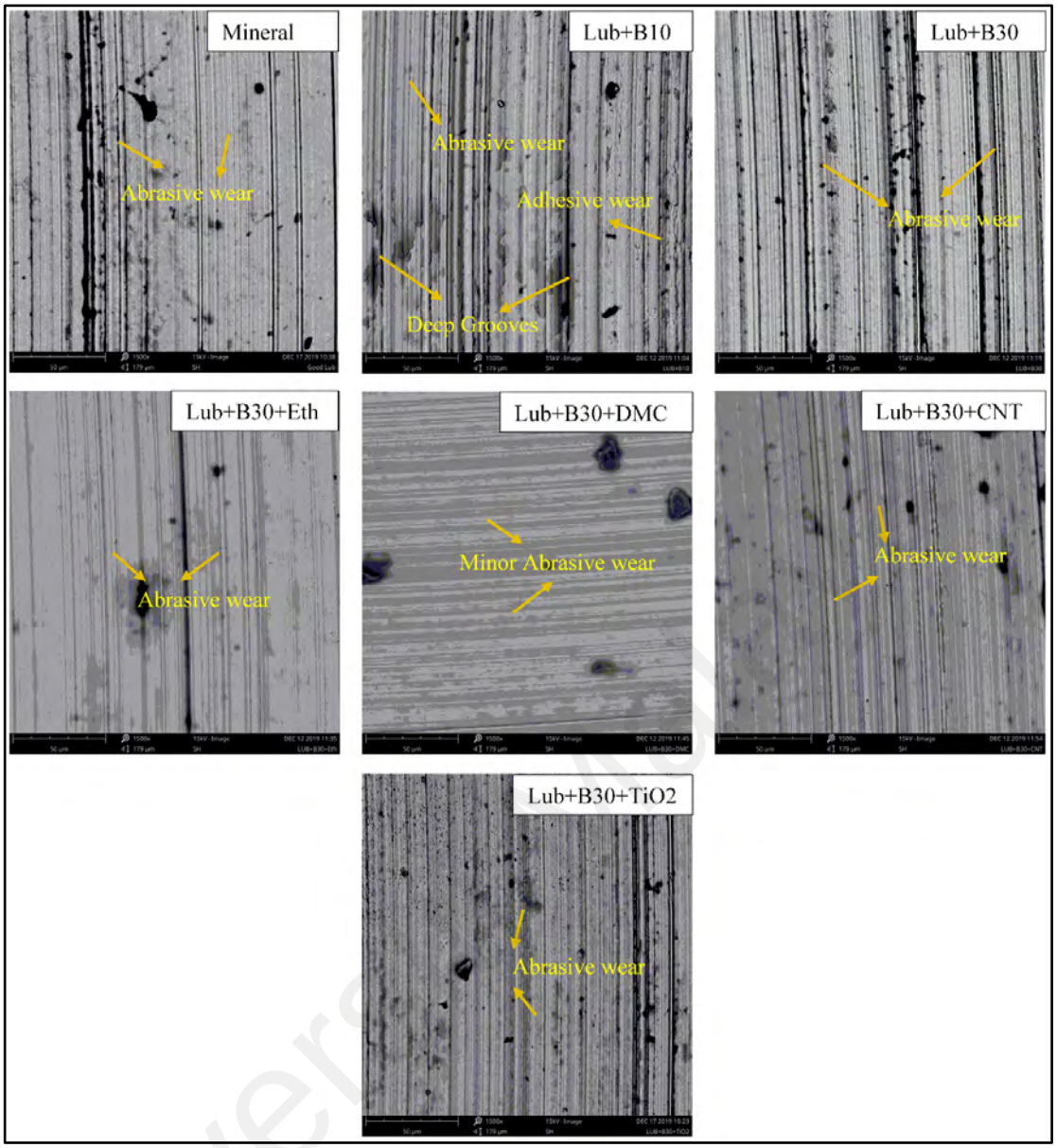

Figure 4.14: Morphological images of worn steel ball by SEM

4.6 Diesel engine testing and analysis

Three key fuel properties of the five fuel samples before being diesel engine tested were measured, including kinematic viscosity and density and the Calorific value shown in Table 4.10. Density and kinematic viscosity are key parameters of fuel properties. Engine performance and emission characteristics depend on these fuel properties. The addition of different fuel additives (nanoparticles and oxygenated alcohols) varies the key fuel properties.

Table 4.10: Physicochemical properties of fuel and its blend

Fuel Samples	Density at 40 °C	Kinematic Viscosity at 40 °C	Calorific Value
	kg/m^3	mm^2/s	MJ/kg
B10 (commercial diesel)	826.8	3.1526	43.9194
B30 (70% Diesel and 30% Biodiesel)	830.0	3.3475	43.1398
B30 + 10% (V/V) Dimethyl carbonate	849.2	2.4573	39.7779
B30+ 5% (V/V) Diethyl Ether	827.4	2.9572	42.3006
B30+ (100 ppm) Carbon Nano Tubes	831.1	3.3723	42.8598
B30+ (100ppm) TiO_2	831.4	3.3643	42.9261

4.6.1 Diesel engine performance analysis

4.6.1.1 Brake engine power (BP) and torque (BT)

The brake engine power and torque results obtained for all fuel samples with variable engine speeds at 100% engine load are presented in Figure 4.15 and Figure 4.16, respectively. For all tested fuels, an increase in BT values was observed at low speeds then decreased from medium to high speeds. The maximum torque values for all tested fuels of 34.81 Nm, 34.59 Nm, 34.54 Nm, 34.40 Nm, 34.32 Nm, and 34.21 Nm were obtained at 1300 rpm for B30+DEE, B30+DMC, B30, B30+CNT, B30+TiO_2, and B10 Diesel tested fuels, respectively. Compared to B30, both B30+DMC and B30+DEE (alcohol fuel additives) showed an increase in average BT values of 0.22% and 0.04%, respectively, while B30+TiO_2 and B30+CNT (nanoparticle fuel additives) showed a slight decrease in average BT values of 1.28% and 0.88% respectively. The value of BT is increased for ternary fuel blends compared to B30 fuel due to phenomena of complete combustion as a result, more energy is generated, and average pressure will be more in the engine cylinder, which resulted in an increase of BT and piston force (Hosseini, Taghizadeh-Alisaraei, Ghobadian, & Abbaszadeh-Mayvan, 2017a). Nanoparticle blended fuels exhibited lower brake torque values compared to B30 due to an increase in viscosity and density values. The average BT values decreased by 10.11% for all measured fuels as engine speed rises from 1300 rpm to 2300 rpm. This is due to the

inadequate filling of the combustion chamber during the intake stroke with completely opened vales resulting in a reduction in volumetric efficiency, as there is not enough time for a sufficient air intake phase resulting in a reduction in the combustion chamber pressure (Heydari-Maleney, Taghizadeh-Alisaraei, Ghobadian, & Abbaszadeh-Mayvan, 2017; Hosseini et al., 2017b).

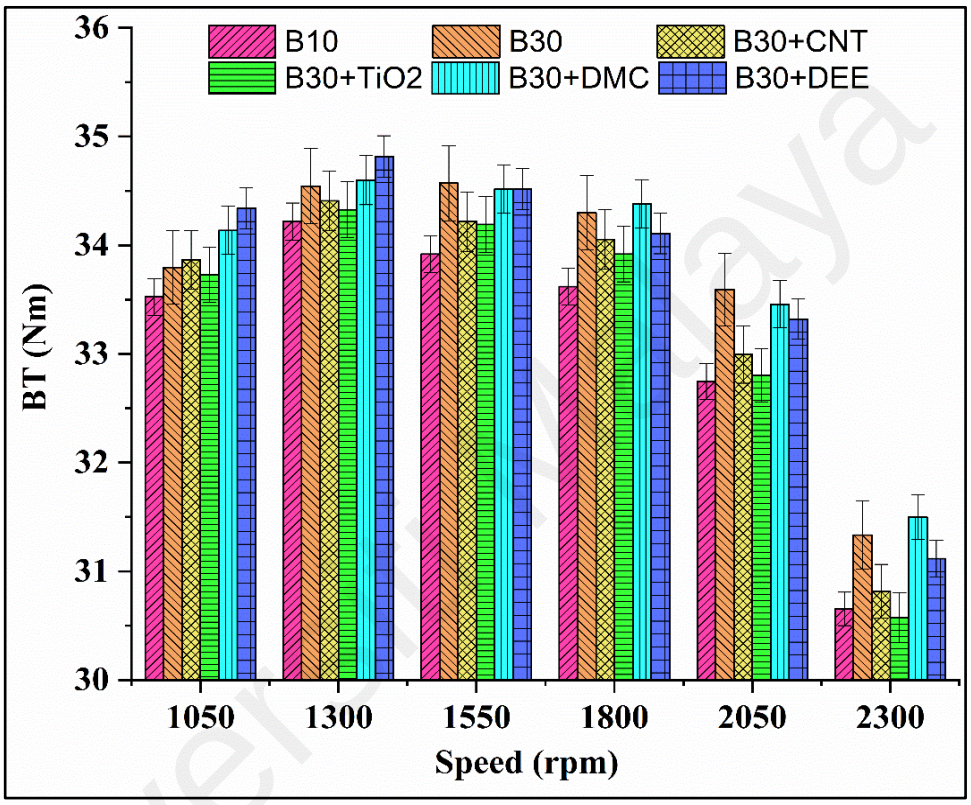

Figure 4.15: Variation of BT for all tested fuels according to engine speed at full load condition

The BP results of each CI diesel engine have a direct relation with BT. Figure 4.16 showed the BP of different tested fuels. The BP is gradually increased with an increase in the engine speed. The maximum BP of 7.56, 7.52, 7.47, 7.40, 7.36, and 7.33 kW were recorded at 2300 rpm for all tested fuels B30+DMC, B30, B30+DEE, B30+CNT, B10 (commercial diesel), and B30+TiO_2, respectively. The average BP values of B30+DMC, B30+DEE, B30, B30+CNT, B30+TiO_2, B10 (commercial diesel) for all engine speed range (1050 to 2300 rpm) were 5.88, 5.87, 5.86, 5.80, 5.77, and 5.75 kW, respectively. The average BP increased for the ternary fuel blends collated to B10 (commercial diesel).

The oxygenated ternary fuel blends (B30+DMC and B30+DEE) showed a slight increase in the average BP of 0.33% and 0.15% compared to B30 fuel, respectively, while other ternary blends (nanoparticle additive fuels) showed a slight decrease of 1.04%, 1.47% for B30+CNT and B30+TiO_2, respectively. The relatively higher BP of oxygenated alcoholic ternary fuel blends can be linked to the high percentage of oxygen content in ternary fuel blends in comparison to other ternary blends. The ignition delay time is increased in the case of oxygenated ternary fuel blends, which resulted in a better combustion performance because of the lower cetane number of ternary oxygenated fuel blends and higher latent heat of vaporization. The ignition delay time is dependent on the combination of cetane number, autoignition temperature, and latent heat of vaporization of the fuel (J. Zhang et al., 2013). Similar results were reported with the use of oxygenated alcoholic fuel additives (Chen et al., 2013; Pan et al., 2019). Moreover, B30 fuel has higher density and viscosity in comparison to oxygenated ternary fuel blends (B30+DMC and B30+DEE), which resulted in poor atomization at high speed. However, the evaporative nature of oxygenated ternary blends provided better atomization at a higher speed (Sayeed Imtenan et al., 2014).

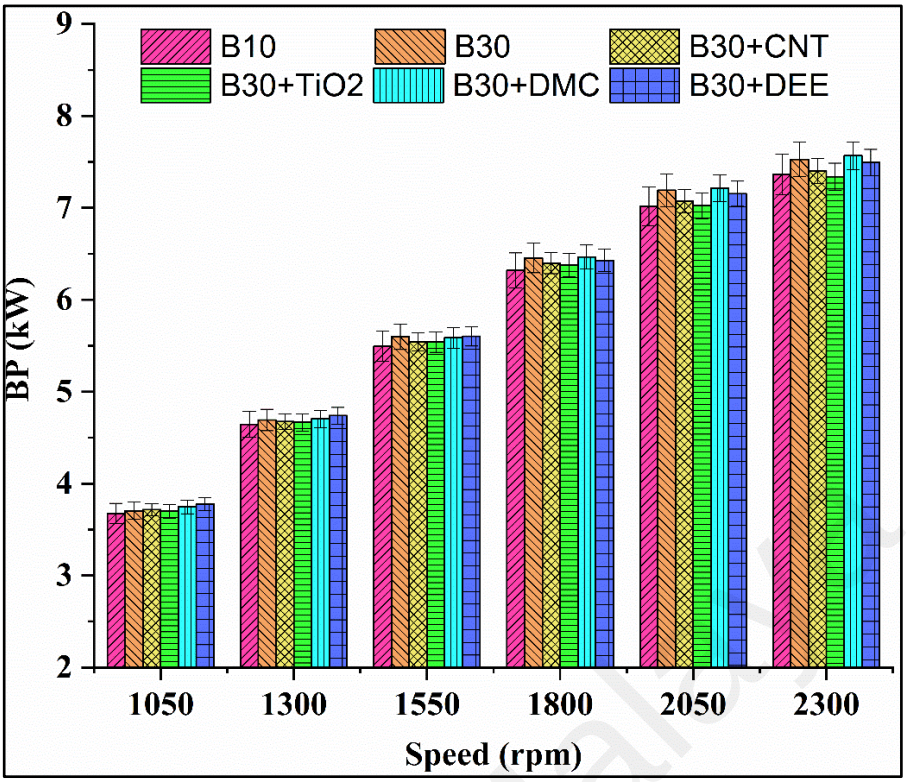

Figure 4.16: Variation of BP for all tested fuels according to engine speed at full load condition

4.6.1.2 Brake specific fuel consumption (BSFC)

Figure 4.17 illustrated the BSFC results for all fuels tested at 100% load condition with variable engine speed. BSFC for all tested fuels decreased with an increase in rpm up to 2050 rpm and then slightly showed a reduction at 2300 rpm. The minimum value of BSFC 0.377, 0.383, 0.386, 0.389, 0.393 and 0.404 kg/kWh were recorded at 2050 rpm for B30+TiO_2, B30+CNT, B30+DEE, B10, B30 and B30+DMC, respectively. The average BSFC values for all tested fuels from were 0.418 (B30+TiO_2), 0.421 (B30+CNT), 0.426 (B30+DEE), 0.4302 (B10 commercial diesel), 0.432 (B30+DMC) and 0.436 (B30) kg/kWh. Compared to B10 (commercial diesel), B30 and B30 DMC fuels showed higher BSFC due to their lower heating values, the performance of injector, high viscosity, and oxygenated nature of ternary fuel blends (Chauhan, Kumar, & Cho, 2012), while other ternary blends exhibited a reduction in the average BSFC. Compared to B30, all ternary fuel blends (B30+TiO_2, B30+CNT, B30+DEE and B30+DMC) showed a reduction in average BSFC value of 4.1%, 3.5%, 2.22%, and 0.87% respectively. Oxygenated ternary

fuel blends showed less BSFC because of lower viscosity and density, which resulted in the improved air-fuel mixture and better atomization. An increase in volumetric efficiency decreased the work needed during the compression stroke, which resulted in the improvement of BSFC values for oxygenated fuel blends (Khalife, Tabatabaei, Demirbas, & Aghbashlo, 2017b; Murcak, Haşimoğlu, Çevik, Karabektaş, & Ergen, 2013). High volatility of oxygenated alcohols may be the reason for the better air-fuel mixture, which leads to a better combustion process and results in high combustion efficiency (Qi, Chen, Geng, & Bian, 2011). The cetane index of DEE is better than DMC, thus B30+DEE showed more reduction in BSFC compared to B30+DMC. Tiny fuel droplets of B30+fuel additives enhance the air-fuel mixing due to the high evaporation rate which resulted in improved combustion characteristics.

It has been observed that nanoparticle fuel blends exhibited a promising reduction in BSFC. B30+TiO_2 showed the least BSFC value, followed by B30+CNT collated to all other fuels. The combustion process can be improved by better atomization, higher calorific value, shorter ignition delay, decreased burn times, high evaporation rate, and more reactive surface area with air (Khalife, Tabatabaei, Demirbas, & Aghbashlo, 2017a). Nanoparticles serve as a potential catalyst during the burning of fuel, which resulted in high in-cylinder pressure and a high heat release rate (Saxena, Kumar, & Saxena, 2017). The reduction in ignition delay encouraged reduced burning off excess fuel during the premixed phase, resulting in a reduction of BSFC (Nadeem et al., 2006). Nanoparticle ternary blends led to a micro explosion of fuel droplets in the engine cylinder and enhanced the combustion reaction resulting in enhancement of engine performance (BSFC) (Najafi, 2018).

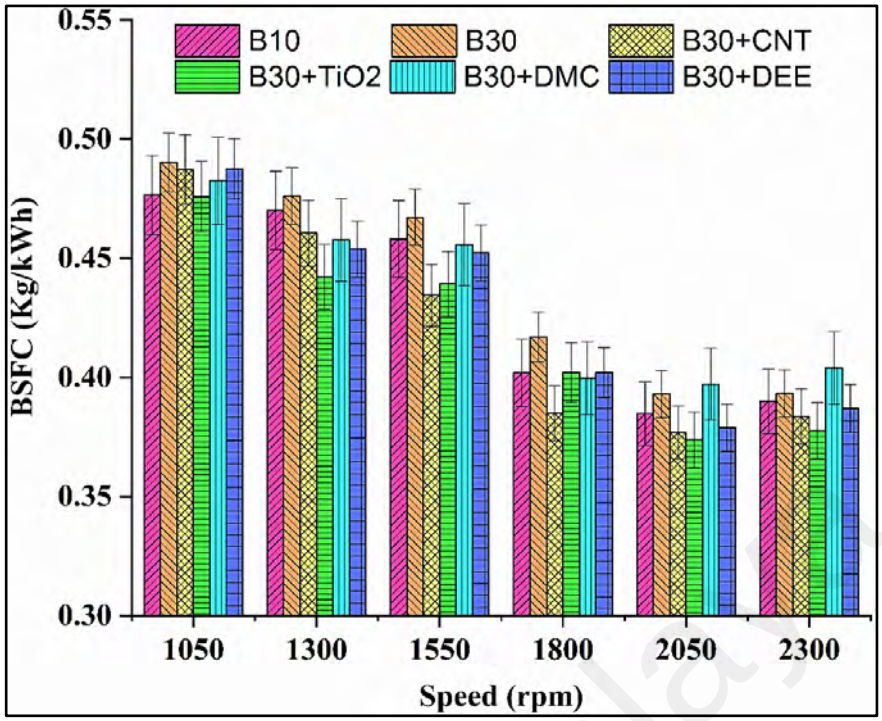

Figure 4.17: Variation of BSFC for all tested fuels according to engine speed at full load condition

4.6.1.3 Brake thermal efficiency (BTE)

The variation of BTE for all tested fuels at 100% engine load with variable engine speeds (1050-2300 rpm) is illustrated in Figure 4.18. BTE for all tested fuels showed an increase up to 2050 rpm and then a slight reduction at 2300 rpm due to the bad air-fuel mixture and poor spray characteristics at high engine rpm. The maximum BTE values of 22.78%, 22.46%, 22.43%, 22.28%, 21.30%, and 21.23% were obtained at 2050 rpm for B30+DMC, B30+DEE, B30+TiO_2, B30+CNT, B10 (commercial diesel) and B30 respectively. The average values of BTE at different engine speeds (1050-2300 rpm) is 21.03%, 20.19%, 20.13%, 20.11%, 19.20% and 19.14% for B30+DMC, B30+TiO_2, B30+CNT, B30+DEE, B10 (commercial diesel) and B30 respectively. All ternary fuel blends showed an increase in BTE compared to B10 (commercial diesel) and B30. The high viscosity of B30 fueled poor atomization and resulted in less power and BTE. On average, all ternary blends showed improvement in BTE 9.88%, 5.49%, 5.17%, and 5.03% for B30+DMC, B30+TiO_2, B30+CNT, and B30+DEE, respectively compared to B30. The longer ignition delay time of the B30+ DMC ternary fuel blend resulted in

higher BTE among all other ternary fuel blends. Oxygenated alcohols increased the BTE because of shorter combustion time and improved combustion process (Khalife et al., 2017a). Oxidizing agents improve the combustion in the diesel engine cylinder due to the introduction of oxygen into a fuel-rich zone which improves thermal efficiency for oxygenated ternary fuel blends. (Pan et al., 2019) reported a similar increase in BTE with the use of DMC (10%) as a fuel additive collated with petroleum diesel. The authors argued that the possible reason for BTE improvement is due to the complete combustion process as DMC has high oxygen content which improves the fuel-air ratio in the fuel-rich area during diffusive combustion. (Sayeed Imtenan et al., 2014) were compared three different alcohols (DEE, n-butanol, and ethanol) as fuel improvers with biodiesel-diesel fuel blends in a CI engine. DEE (5%) with biodiesel-diesel fuel blends exhibited the best BTE among all other tested fuels.

Among nanoparticle additives, metal-based nanoparticles (TiO_2) showed a higher increase in BTE compared to carbon-based nanoparticles (CNT). CNT as a fuel additive in ternary blends showed slightly less BTE compared to TiO_2 diesel-biodiesel fuel blends. B30+CNT has a low calorific value and high viscosity compared to B30+TiO_2. The high value of BTE for B30+CNT in comparison to other fuel blends is due to its high chemically reactive surface, which acts as a suitable combustion catalyst during the burning of fuel. Najafi (Najafi, 2018) investigated different concentrations of CNT as a fuel additive with diesel. CNT (120 ppm) exhibited the highest BTE due to high in-cylinder pressure, high heat release rate, high cetane number, and lowest ignition delay.

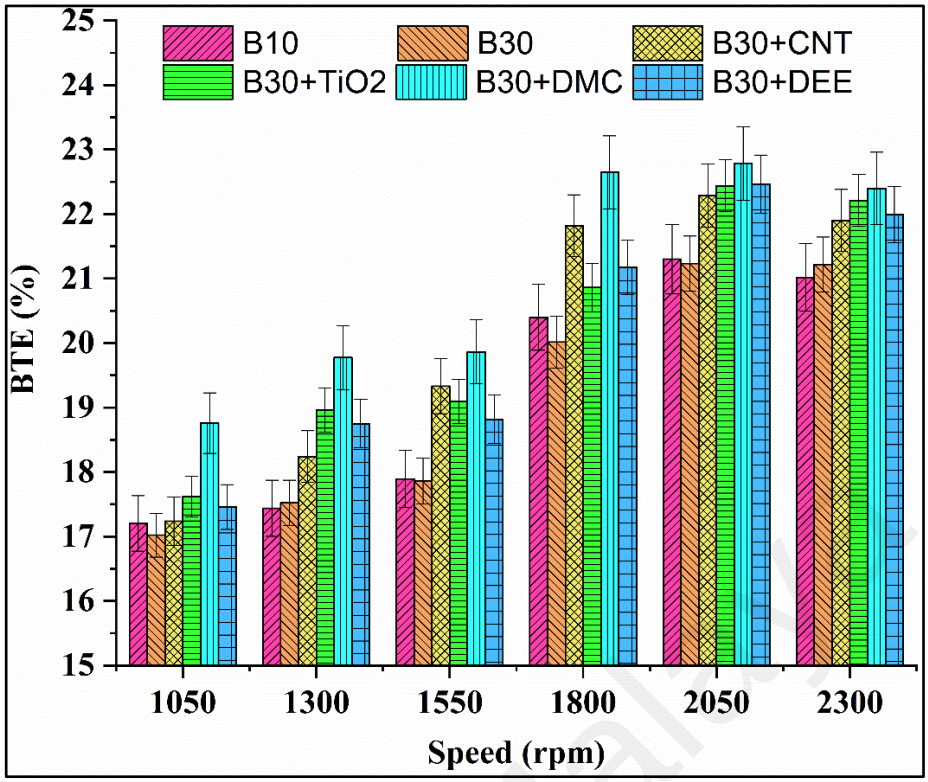

Figure 4.18: Variation of BTE for all tested fuels according to engine speed at full load condition

4.6.2 Diesel engine emission analysis

4.6.2.1 CO emissions

The effect of CO emissions with an engine speed for tested fuels is presented in Figure 4.19. The maximum CO emissions for all tested fuels were recorded at 1050 rpm. CO emission is produced due to partial combustion and partial oxidation of carbon atoms in fuel. CO emissions are altered according to the fuel-air ratio in the engine cylinder (M. Habibullah et al., 2014). CO emissions exhibited reduction with the increase in engine speeds. The conversion rate of CO to CO_2 increased because of a high fuel-air ratio and high temperature at the maximum engine speed, resulting in lower CO emissions, as shown in Figure 4.19. All tested fuel samples exhibited a significant reduction in CO emission collated to B10 (commercial diesel) due to complete combustion during the combustion process in diesel engines. The average CO emissions for B30+DMC, B30+DEE, B30+TiO_2, B30+CNT, B30 and B10 (commercial diesel) between (1050-

2300 rpm) were 45.24, 50.41, 56.49, 59.01, 64.54 and 69.08 g/kWh respectively. On average, all ternary fuel blends showed a remarkable reduction in CO emissions of 29.90%, 21.9%, 12.46%, and 8.5% for B30+DMC, B30+DEE, B30+TiO_2, and B30+CNT, respectively compared to the B30 fuel blend. Because of the high oxygen content in its molecular structure, oxygenated alcohol ternary fuel blends displayed a substantial reduction among all the tested fuels. Lower viscosity and density of oxygenated ternary fuel blends enhanced the atomization of fuel. The high content of oxygen assisted in the complete burning of fuel, leading to lower CO emissions. (S Imtenan et al., 2015) reported a similar reduction in CO emissions using oxygenated alcohol as a fuel additive. The extra oxygen content value in ternary fuel blends ensures the oxidation of CO in fuel-rich areas inside the cylinder, which leads to a reduction in CO emissions (Sayeed Imtenan et al., 2014).

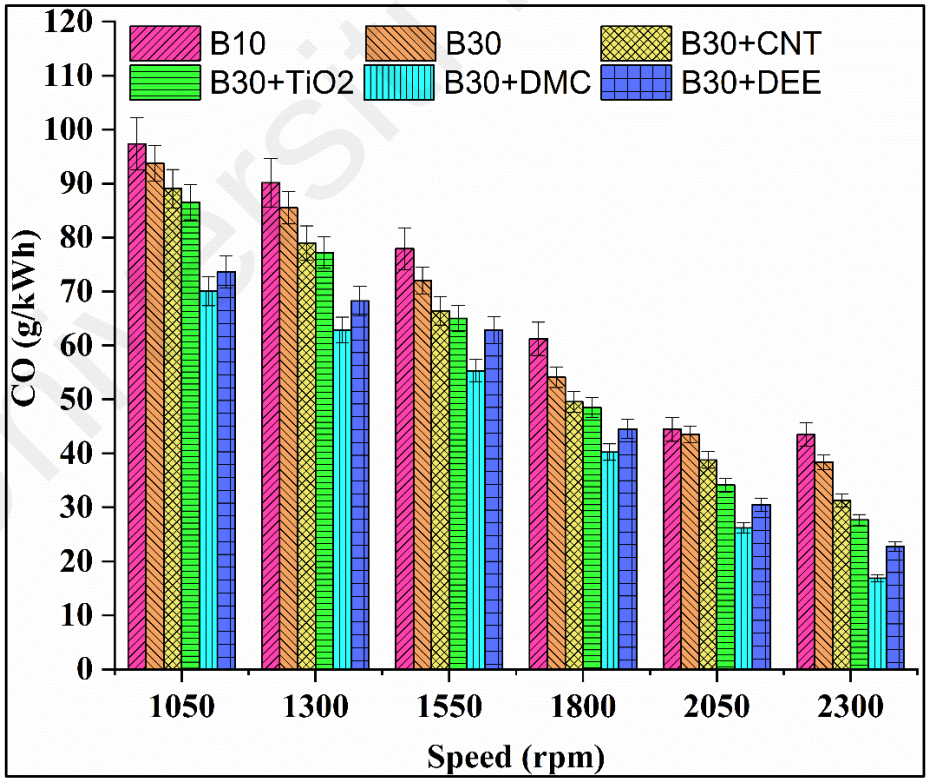

Figure 4.19: Variation of CO emissions for all tested fuels according to engine speed at full load condition

4.6.2.2 HC emissions

The variation of HC emissions with engine speed is illustrated in Figure 4.20. HC emissions are mainly dependent on fuel atomization, fuel properties, and engine operating conditions (M. Habibullah et al., 2014). The average HC emissions were 0.088, 0.0095, 0.102, 0.112, 0.128 and 0.136 g/kWh for B30+DMC, B30+DEE, B30+TiO_2, B30, B10 (commercial diesel) and B30+CNT, respectively. All ternary blends exhibited a significant reduction in HC emissions collated to B30 and B10 (commercial diesel) except B30+CNT due to the presence of carbon in its structure. On average, the ternary blends exhibited a promising reduction in HC emissions of 21.4%, 15.17%, and 8.63% for B30+DMC, B30+DEE, and B30+TiO_2, respectively compared to B30. This significant reduction in HC emissions can be attributed to the improved burning of fuel because of the large reactive surface of nanoparticles and the high oxygen content of oxygenated alcohols. (Pan et al., 2019) stated a significant reduction in HC emissions using DMC as a fuel improver collated with diesel. The HC emissions were decreased because of the high in-cylinder temperature and high heat release rate, leading to the oxidation reaction of unburned hydrocarbons. The same observations were reported by (Ghanbari et al., 2017) and (Najafi, 2018).

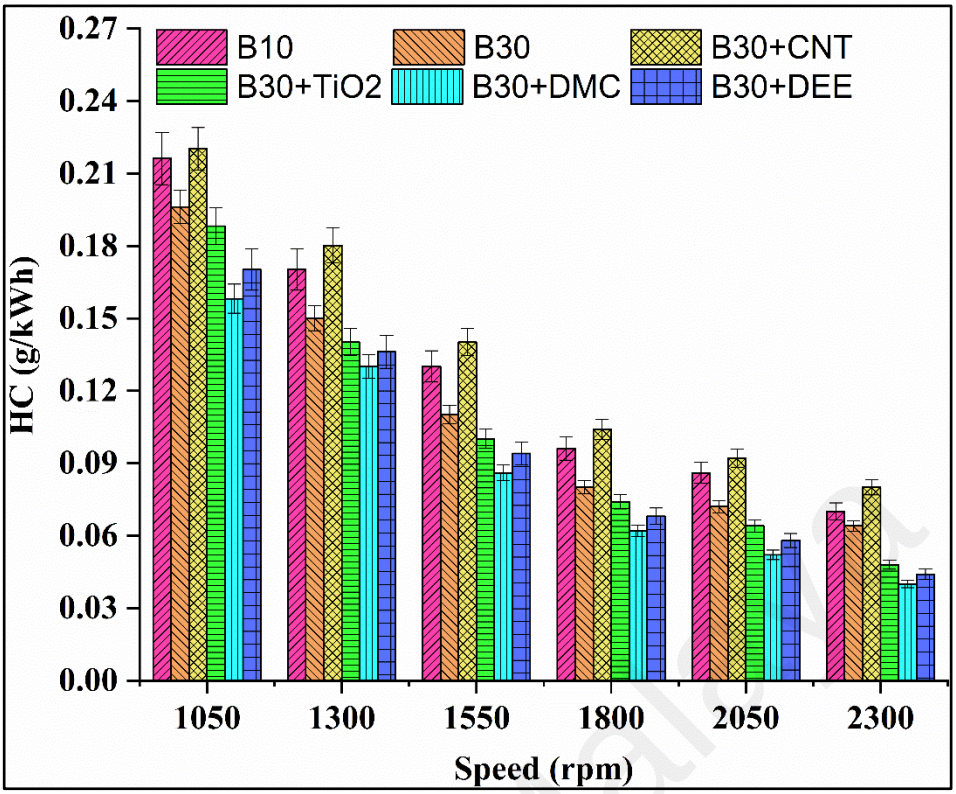

Figure 4.20: Variation of HC emissions for all tested fuels according to engine speed at full load condition

4.6.2.3 NO_x emissions

The NO_x emissions of all tested fuels are presented in Figure 4.21. The graph exhibited an increasing trend with an increase in speed for all fuel blends. The average NO_x emissions of 2.708, 2.736, 2.819, 2.871, 2.957, and 3.030 g/kWh were obtained for B30+CNT, B10 (commercial diesel), B30, B30+ TiO_2, B30+DEE, and B30+DMC, respectively. The NO_x formation is mainly caused by in-cylinder combustion temperature and pressure. High in-cylinder temperature leads to high NO_x formation because of the high cetane number and oxygen content of ternary blends (Atmanli, 2016). Compared to B30, B30+CNT showed an average NO_x emission reduction of 3.92%, while other ternary blends exhibited average increases of 1.84%, 4.90%, and 7.49% for B30+ TiO_2, B30+DEE, and B30+DMC, respectively. (Mei et al., 2019) stated a reduction in NO_x emissions using CNT (100 ppm) as a fuel additive. The presence of CNT in the fuel blend increases ignition timing and decreases the amount of mixture in premixed combustion

resulting in lower NO_x emissions. (Gad & Jayaraj, 2020) also reported a similar reduction in NO_x emissions with the use of CNT as a fuel improver. (Örs, Sarıkoç, Atabani, Ünalan, & Akansu, 2018) claimed an increase in NO_x emissions for TiO_2-diesel-biodiesel blends. This increase was due to the high in-cylinder temperature and pressure because of the improved burning of fuel using TiO_2 as a fuel additive. (Pan et al., 2019) examined the use of DMC as an oxygenated fuel improver with diesel. Their studies reported a substantial increase in NO_x emissions because of high in-cylinder temperature and pressure. High NO_x emissions are due to the high percentage of oxygen content in ternary fuel blends that leads to the complete burning of fuel and high in-cylinder temperature.

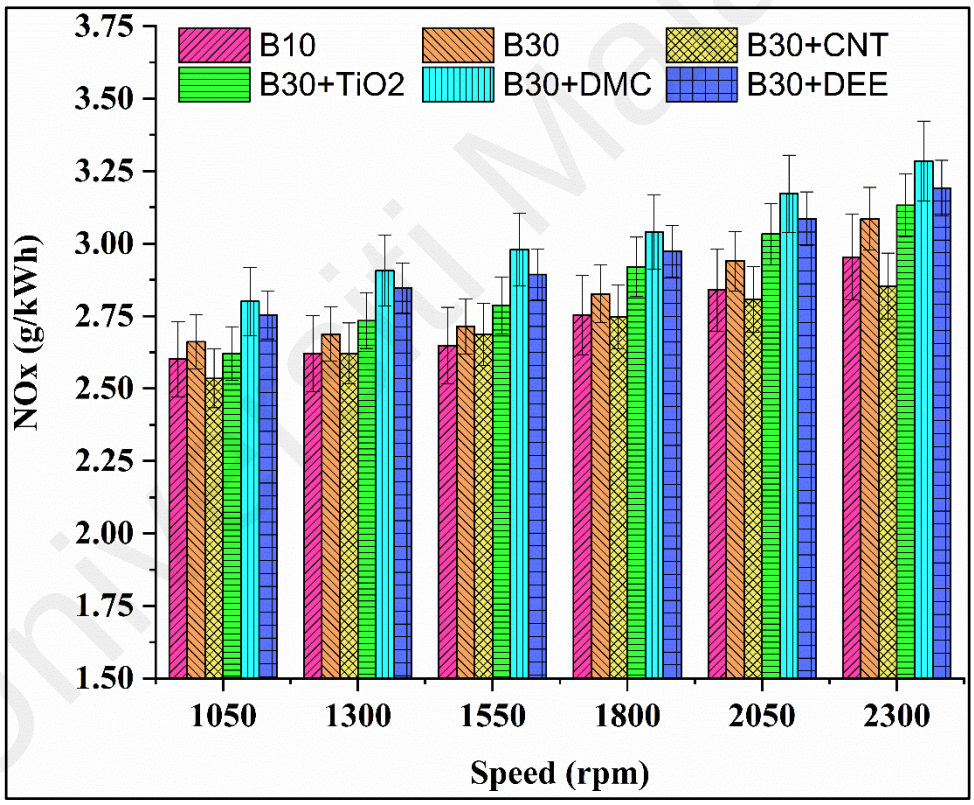

Figure 4.21: Variation of NO_x emissions for all tested fuels according to engine speed at full load condition

CHAPTER 5: CONCLUSION AND RECOMMENDATIONS

5.1 Introduction

In recent decades, biodiesel has been considered a potential candidate to overcome the dominance of petroleum diesel and mitigate environmental pollution. Biodiesel is used in existing diesel engines without any modification. Many researchers have conducted research to find different potential feedstocks for biodiesel production, and some are in the process of commercializing biodiesel. The major problem associated with biodiesel industrialization is its insufficient cold flow and oxidation stability properties. This study highlighted the potential and suitability of sesame (Sesamum indicum L.) oil for biodiesel production. The blend of sesame oil with other vegetable oil (palm oil) is used for biodiesel production to enhance the final product's cold flow and oxidation stability properties. The oxidation stability of sesame oil should be low due to high unsaturation, but the presence of natural antioxidants (Tocopherols (Vitamin E)) and naturally occurring preservatives (sesamol, sesamolin, and sesamin) restrict rancidity. Poor cold flow and oxidative stability properties of other vegetable oils (like palm oil) can be improved successfully by blending them with sesame oil in an appropriate proportion before the transesterification process.

5.2 Synthesis, optimization, and investigation of physicochemical properties of palm-sesame biodiesel blends

In this study, ultrasound-assisted transesterification was used to produce biodiesel from palm-sesame blend oil. P50S50 biodiesel yield was maximized by optimizing transesterification process variables using RSM based on Box-Behnken design and ELM coupling with a cuckoo search optimization algorithm. From the results, it could be concluded that ELM performed better compared to RSM in predicting the P50S50 yield. Maximum optimal P50S50 yield of 96.6138% was obtained using ELM coupling with cuckoo search optimization algorithm using reaction time (38.96 min), duty cycle

(59.52%), methanol-to-oil ratio (60%), and catalyst amount (0.70 wt.%). The P50S50 biodiesel had a better cloud point (7.89 °C), pour point (3.80 °C), and cold filter plugging point (1.77 °C) with better oxidative stability of 6.89 h. Physicochemical properties of the P50S50 methyl esters complied with the ranges specified for biodiesel (ASTM D6751 and EN 14214). The average COF of P50S50 biodiesel was 12.37 % lower than B10 (diesel), and WSD of P50S50 was also 21.29% lower than B10. The wear and friction characteristics of P50S50 biodiesel were also reduced compared to other tested fuels because of highly unsaturated fatty acids. Moreover, the physicochemical properties and lubricity of P50S50 biodiesel are improved compared to Palm biodiesel and B10.

5.3 Investigation of the lubricity characteristics of synthesized palm-sesame biodiesel using HFRR and fuel dilution effect using four-ball tribo tester

In the current research work, the tribological study mainly focused on diesel fuel lubricity during injection applications in diesel engines. All diesel fuel samples are tested using HFRR equipment to evaluate diesel fuel lubricity compliance with the protocol set out in ASTM standard D6079-11. After the experimental investigation, WSD, COF, and microscopic SEM images for B10 depict inferior results compared to other fuel samples. On average all fuel samples showed significant reduction in coefficient of friction 34.03%, 31.47%, 26.6%, 16.37%, 32.61% and 36.25% for B100, B30, B30+DMC, B30+Eth, B30+CNT and B30+TiO_2 respectively compared to B10. Among ternary fuel blends, B30+TiO_2 showed a promising reduction in COF. B10 (commercial diesel) exhibited very poor COF and WSD results compared to other tested fuel samples.

In the current research work, the effect of 5% palm-sesame biodiesel fuels, with alcoholic and nano-particle additives, on the tribological characteristics of lubricating oil (SAE-40) was evaluated using four-ball tribo-tester according to the ASTM D4172 standard. A considerable reduction in COF and WSD was observed for lubricant

contaminated with palm-sesame biodiesel fuel with nanoparticles, among other contaminated lubricant samples. P50S50 biodiesel fuel dilution in lubricating oil causes less degradation. On average, all contaminated lubricant fuel samples Lub+B10, Lub+B30+Ethanol, Lub+B30, Lub+B30+CNT, Lub+B30+DMC and Lub+B30+TiO_2 exhibited higher COF 42.295%, 35.81%, 31.355%, 27.56%, 27.02% and 13.78% respectively than 100% lubricant sample. Among alcoholic additives, DMC-based biodiesel fuel caused less degradation of the CI engine's lubricating oil. Lub+B30+Eth showed very high COF. While nanoparticle-based biodiesel blend (B30) caused less degradation of lubricating oil SAE-40 than alcoholic additives, nanoparticles act as a sacrificial layer between metallic contact. It is concluded that nanoparticle (TiO_2) additives in biodiesel appeared as competitive additives because it showed the least degradation of the lubricant.

5.4 Combined effect of palm-sesame biodiesel and fuel additives on diesel engine characteristics

In this work, Nanoparticles (CNT (100 ppm) and TiO_2 (100 ppm)) and oxygenated alcohols (DMC (10%) and DEE (5%)) were blended with B30 palm-sesame biodiesel-diesel fuel blends to examine their effects on engine performance and emission characteristics. The physicochemical properties of all tested fuels were determined according to ASTMD6751 standards. Engine performance and exhaust emission characteristics were obtained using a single-cylinder diesel engine with variable speed (1050-2300 rpm) at 100% engine load. Based on the results obtained, the B30+DMC fuel blend showed better engine performance and emissions, among other fuel blends.

All the values of the fuel blends are compared with the B30 fuel blend. On average, brake power and brake torque values for ternary fuel blends were higher than B30 and B10. B30+DMC showed maximum brake power, followed by B30+DEE, B30+CNT, and

B30+TiO_2. All ternary fuel blends presented an average reduction in brake-specific fuel consumption collated to B30 fuel. B30+TiO_2 exhibited a maximum reduction of up to 4.1%, followed by B30+CNT with 3.5%. All ternary fuel blends demonstrated improvement in brake thermal efficiency. B30+DMC showed an increase of 9.88%, followed by B30+TiO_2 with 5.49% compared to B30 fuel. A significant reduction of 29.9% and 21.9% in CO emissions were obtained for oxygenated ternary fuel blends B30+DMC and B30+DEE, respectively, compared to B30 fuel. The maximum reductions in HC emissions were obtained for oxygenated alcohol ternary fuel blends B30+DMC (21.4%) and B30+DEE (15.17%) compared to B30 fuel. The maximum reductions in NO_x emissions were observed for B30+CNT (3.92%), followed by B10 (2.94%) compared to B30 fuel. Other ternary fuel blends showed increased NO_x emissions due to high combustion temperature and higher oxygen content.

5.5 Recommendations

Future recommendations are discussed to make biodiesel-diesel-fuel additive blends feasible for the automotive industry. Further study and experimental work are required to make these fuel blends viable for IC engine application. Based on obtained results, the following recommended work can be proposed.

1. Investigate the effect of fuel additives with biodiesel-diesel blends on rubber components of diesel engines. The study should evaluate the compatibility of rubber materials with palm-sesame biodiesel + diesel + commercialize fuel additives (nanoparticles and oxygenated alcohols) for the automotive industry.
2. Investigate the thermal, optical physicochemical properties and tribological characteristics of palm-sesame biodiesel-diesel-fuel additives. This investigation should be carried out to study the effect of different fuel additives on the physicochemical properties of palm-sesame biodiesel-diesel fuel blends. In addition, a tribological study

should be conducted to analyze the effect of fuel additives with palm-sesame biodiesel-diesel fuel blends on the lubricity of diesel engine components (fuel pumps, cylinder liner, etc.).

REFERENCES

Absi Halabi, M., Al-Qattan, A., & Al-Otaibi, A. (2015). Application of solar energy in the oil industry—Current status and future prospects. *Renewable and Sustainable Energy Reviews, 43*, 296-314.

Agarwal, A. K. (2003a). *Lubricating oil tribology of a biodiesel-fuelled compression ignition engine.* Paper presented at the Internal Combustion Engine Division Spring Technical Conference.

Agarwal, A. K. (2003b). *Lubricating Oil Tribology of a Biodiesel-Fuelled Compression Ignition Engine.* Paper presented at the ASME 2003 Internal Combustion Engine Division Spring Technical Conference.

Aghbashlo, M., Hosseinpour, S., & Mujumdar, A. S. (2015). Application of artificial neural networks (ANNs) in drying technology: a comprehensive review. *Drying technology, 33*(12), 1397-1462.

Ahmad, M., Khan, M. A., Zafar, M., & Sultana, S. (2009). Environment-friendly Renewable Energy from Sesame Biodiesel. *Energy Sources, Part A: Recovery, Utilization, and Environmental Effects, 32*(2), 189-196.

Ahmad, M., Ullah, K., Khan, M. A., Ali, S., Zafar, M., & Sultana, S. (2011). Quantitative and Qualitative Analysis of Sesame Oil Biodiesel. *Energy Sources, Part A: Recovery, Utilization, and Environmental Effects, 33*(13), 1239-1249.

Akram, W., Singh, Y., Sharma, A., & Singh, N. K. (2019). Experimental studies on performance and exhaust emission characteristics of a diesel engine fuelled with diesel-linseed oil methyl ester (LOME) blends. *Energy Sources, Part A: Recovery, Utilization, and Environmental Effects, 43*(6), 1-15.

Al-Dawody, M. F., & Bhatti, S. (2013). Optimization strategies to reduce the biodiesel NOx effect in diesel engine with experimental verification. *Energy Conversion and Management, 68*, 96-104.

Ali, O. M., Mamat, R., Masjuki, H. H., & Abdullah, A. A. (2016). Analysis of blended fuel properties and cycle-to-cycle variation in a diesel engine with a diethyl ether additive. *Energy Conversion and Management, 108*, 511-519.

Altun, Ş., Bulut, H., & Öner, C. (2008). The comparison of engine performance and exhaust emission characteristics of sesame oil–diesel fuel mixture with diesel fuel in a direct injection diesel engine. *Renewable Energy, 33*(8), 1791-1795.

Anastopoulos, G., Lois, E., Serdari, A., Zanikos, F., Stournas, S., & Kalligeros, S. (2001). Lubrication properties of low-sulfur diesel fuels in the presence of specific types of fatty acid derivatives. *15*(1), 106-112.

Anilakumar, K. R., Pal, A., Khanum, F., & Bawa, A. S. (2010). Nutritional, medicinal and industrial uses of sesame (Sesamum indicum L.) seeds-an overview. *Agriculturae Conspectus Scientificus, 75*(4), 159-168.

Aransiola, E., Ojumu, T., Oyekola, O., Madzimbamuto, T., & Ikhu-Omoregbe, D. (2014). A review of current technology for biodiesel production: State of the art. *Biomass and Bioenergy, 61*, 276-297.

Arumugam, & Sriram, G. (2013). Synthesis and characterisation of rapeseed oil bio-lubricant–its effect on wear and frictional behaviour of piston ring–cylinder liner combination. *Proceedings of the Institution of Mechanical Engineers, Part J: Journal of Engineering Tribology, 227*(1), 3-15.

Arumugam, S., & Sriram, G. (2012). Effect of Bio-Lubricant and Biodiesel-Contaminated Lubricant on Tribological Behavior of Cylinder Liner–Piston Ring Combination. *Tribology Transactions, 55*(4), 438-445.

Arumugam, S., & Sriram, G. (2013). Preliminary study of nano-and microscale TiO2 additives on tribological behavior of chemically modified rapeseed oil. *Tribology Transactions, 56*(5), 797-805.

Atabani, Silitonga, A. S., Badruddin, I. A., Mahlia, T., Masjuki, H., & Mekhilef, S. (2012a). A comprehensive review on biodiesel as an alternative energy resource and its characteristics. *Renewable and Sustainable Energy Reviews, 16*(4), 2070-2093.

Atabani, Silitonga, A. S., Badruddin, I. A., Mahlia, T. M. I., Masjuki, H. H., & Mekhilef, S. (2012b). A comprehensive review on biodiesel as an alternative energy resource and its characteristics. *Renewable and Sustainable Energy Reviews, 16*(4), 2070-2093. doi:https://doi.org/10.1016/j.rser.2012.01.003

Atabani, A., Mahlia, T., Badruddin, I. A., Masjuki, H., Chong, W., & Lee, K. T. (2013). Investigation of physical and chemical properties of potential edible and non-edible feedstocks for biodiesel production, a comparative analysis. *Renewable Sustainable Energy Reviews, 21*, 749-755.

Atabani, A., Shobana, S., Mohammed, M., Uğuz, G., Kumar, G., Arvindnarayan, S., . . . Ala'a, H. (2019). Integrated valorization of waste cooking oil and spent coffee grounds for biodiesel production: Blending with higher alcohols, FT–IR, TGA, DSC and NMR characterizations. *Fuel, 244*, 419-430.

Atmanli, A. (2016). Comparative analyses of diesel–waste oil biodiesel and propanol, n-butanol or 1-pentanol blends in a diesel engine. *Fuel, 176*, 209-215.

Balamurugan, T., Arun, A., & Sathishkumar, G. B. (2018). Biodiesel derived from corn oil – A fuel substitute for diesel. *Renewable and Sustainable Energy Reviews, 94*, 772-778.

Banapurmath, N. R., Tewari, P. G., & Hosmath, R. S. (2008). Performance and emission characteristics of a DI compression ignition engine operated on Honge, Jatropha and sesame oil methyl esters. *Renewable Energy, 33*(9), 1982-1988.

Barbour, R., Rickeard, D., & Elliott, N. (2000). Understanding diesel lubricity. *SAE Transactions*, 1556-1566.

Betiku, E., & Adepoju, T. F. (2013). Methanolysis optimization of sesame (Sesamum indicum) oil to biodiesel and fuel quality characterization. *International Journal of Energy and Environmental Engineering, 4*(1), 9.

Bhat, K. V., Babrekar, P. P., & Lakhanpaul, S. (1999). Study of genetic diversity in Indian and exotic sesame (Sesamum indicum L.) germplasm using random amplified polymorphic DNA (RAPD) markers. *Euphytica, 110*(1), 21-34.

Borchani, C., Besbes, S., Blecker, C., & Attia, H. (2010). Chemical characteristics and oxidative stability of sesame seed, sesame paste, and olive oils. *Scientific Information Database, 12*, 585-596.

Budowski, P. (1950). Sesame oil. III. Antioxidant properties of sesamol. *Journal of the American Oil Chemists Society, 27*(7), 264-267.

Can, Ö., Öztürk, E., Solmaz, H., Aksoy, F., Çinar, C., & Yücesu, H. S. (2016). Combined effects of soybean biodiesel fuel addition and EGR application on the combustion and exhaust emissions in a diesel engine. *Applied Thermal Engineering, 95*, 115-124.

Cecrle, E., Depcik, C., Duncan, A., Guo, J., Mangus, M., Peltier, E., . . . Zhong, Y. (2012). Investigation of the effects of biodiesel feedstock on the performance and emissions of a single-cylinder diesel engine. *Energy & Fuels, 26*(4), 2331-2341.

Cetin, M., & Yüksel, F. (2007). The use of hazelnut oil as a fuel in pre-chamber diesel engine. *Applied Thermal Engineering, 27*(1), 63-67.

Chauhan, B. S., Kumar, N., & Cho, H. M. (2012). A study on the performance and emission of a diesel engine fueled with Jatropha biodiesel oil and its blends. *Energy, 37*(1), 616-622.

Chen, G., Shen, Y., Zhang, Q., Yao, M., Zheng, Z., & Liu, H. (2013). Experimental study on combustion and emission characteristics of a diesel engine fueled with 2, 5-dimethylfuran–diesel, n-butanol–diesel and gasoline–diesel blends. *Energy, 54*, 333-342.

Chhabra, M., Saini, B. S., & Dwivedi, G. (2020). Optimization of the dual stage procedure of biodiesel synthesis from Neem oil using RSM based Box Behnken design. *Energy Sources, Part A: Recovery, Utilization, Environmental Effects*, 1-24.

Chou, R., Battez, A. H., Cabello, J. J., Viesca, J. L., Osorio, A., & Sagastume, A. (2010). Tribological behavior of polyalphaolefin with the addition of nickel nanoparticles. *Tribology International, 43*(12), 2327-2332.

Christensen, E., & McCormick, R. L. (2014). Long-term storage stability of biodiesel and biodiesel blends. *Fuel Processing Technology, 128*, 339-348.

Coca, N. (2020). As palm oil for biofuel rises in Southeast Asia, tropical ecosystems shrink. Retrieved from china and the world discuss the environment website: https://www.chinadialogue.net/article/show/single/en/11957-As-palm-oil-for-biofuel-rises-in-Southeast-Asia-tropical-ecosystems-shrink

Conceição, J. N., Marangoni, B. S., Michels, F. S., Oliveira, I. P., Passos, W. E., Trindade, M. A. G., . . . Caires, A. R. L. (2019). Evaluation of molecular spectroscopy for predicting oxidative degradation of biodiesel and vegetable oil: Correlation analysis between acid value and UV–Vis absorbance and fluorescence. *Fuel Processing Technology, 183*, 1-7.

Corkwell, K. C., & Jackson, M. M. (2002). Lubricity and injector pump wear issues with E diesel fuel blends. *SAE Technical Paper*.

Dawodu, F. A., Ayodele, O. O., & Bolanle-Ojo, T. (2014). Biodiesel production from Sesamum indicum L. seed oil: An optimization study. *Egyptian Journal of Petroleum, 23*(2), 191-199.

Demirbas, A. (2005). Biodiesel production from vegetable oils via catalytic and non-catalytic supercritical methanol transesterification methods. *Progress in Energy and Combustion Science, 31*(5-6), 466-487.

Dhar, A., & Agarwal, A. K. (2014). Experimental investigations of effect of Karanja biodiesel on tribological properties of lubricating oil in a compression ignition engine. *Fuel, 130*, 112-119.

Dharma, S., Masjuki, H. H., Ong, H. C., Sebayang, A. H., Silitonga, A. S., Kusumo, F., & Mahlia, T. M. I. (2016). Optimization of biodiesel production process for mixed Jatropha curcas–Ceiba pentandra biodiesel using response surface methodology. *Energy Conversion and Management, 115*, 178-190.

Dixit, S., kanakraj, S., & Rehman, A. (2012). Linseed oil as a potential resource for bio-diesel: A review. *Renewable and Sustainable Energy Reviews, 16*(7), 4415-4421.

Dueso, C., Muñoz, M., Moreno, F., Arroyo, J., Gil-Lalaguna, N., Bautista, A., . . . Sánchez, J. L. (2018). Performance and emissions of a diesel engine using sunflower biodiesel with a renewable antioxidant additive from bio-oil. *Fuel, 234*, 276-285.

Dwivedi, G., & Sharma, M. (2015). Application of Box–Behnken design in optimization of biodiesel yield from Pongamia oil and its stability analysis. *Fuel, 145*, 256-262.

Dwivedi, G., & Sharma, M. P. (2014). Impact of cold flow properties of biodiesel on engine performance. *Renewable and Sustainable Energy Reviews, 31*, 650-656.

Echim, C., Maes, J., & Greyt, W. D. (2012). Improvement of cold filter plugging point of biodiesel from alternative feedstocks. *Fuel, 93*, 642-648.

EIA. (2019). *Annual Energy Outlook 2019*. Retrieved from https://www.eia.gov/outlooks/aeo/

EIA. (2021). *Short-Term Energy Outlook 2021*. Retrieved from USA: https://www.eia.gov/outlooks/steo/pdf/steo_full.pdf

El-Seesy, A. I., & Hassan, H. (2019). Investigation of the effect of adding graphene oxide, graphene nanoplatelet, and multiwalled carbon nanotube additives with n-

butanol-Jatropha methyl ester on a diesel engine performance. *Renewable Energy, 132*, 558-574.

El Khier, M. K. S., Ishag, K. E. A., & Yagoub, A. (2008). Chemical composition and oil characteristics of sesame seed cultivars grown in Sudan. *Research Journal of Agriculture and Biological Sciences, 4*(6), 761-766.

Elisha, O., Fauzi, A., & Anggraini, E. (2019). Analysis of Production and Consumption of Palm-Oil Based Biofuel using System Dynamics Model: Case of Indonesia.

Elleuch, M., Besbes, S., Roiseux, O., Blecker, C., & Attia, H. (2007). Quality characteristics of sesame seeds and by-products. *Food Chemistry, 103*(2), 641-650.

FAO. (2015). *Food and Agricultural Organization of the United Nations (FAO) Report*. Retrieved from http://www.fao.org/faostat/en/#data/QC

FAO. (2018). *Food and Agricultural Organization of the United Nations (FAO) Report*. Retrieved from http://www.fao.org/faostat/en/#data/QC

Farias, A. C. M. d., Medeiros, J. T. N. d., & Alves, S. M. (2014). Micro and nanometric wear evaluation of metal discs used on determination of biodiesel fuel lubricity. *Material Research, 17*, 89-99.

Fattah, I. R., Masjuki, H., Kalam, M., Mofijur, M., & Abedin, M. (2014). Effect of antioxidant on the performance and emission characteristics of a diesel engine fueled with palm biodiesel blends. *Energy Conversion and Management, 79*, 265-272.

Fazal, M., Haseeb, A., & Masjuki, H. H. (2013). Investigation of friction and wear characteristics of palm biodiesel. *Energy Conversion and Management, 67*, 251-256.

Ferdous, K., Uddin, M. R., Khan, M. R., & Islam, M. (2012). Biodiesel from Sesame oil: Base catalysed transesterification. *International Journal of Engineering & Technology, 1*(4), 420-431.

Freitas, S. V., Pratas, M. J., Ceriani, R., Lima, A. S., & Coutinho, J. A. (2010). Evaluation of predictive models for the viscosity of biodiesel. *Energy & Fuels, 25*(1), 352-358.

Fuller, D. Q. (2003). Further evidence on the prehistory of sesame. *Asian Agri-History, 7*(2), 127-137.

Gad, El-Araby, R., Abed, K. A., El-Ibiari, N. N., El Morsi, A. K., & El-Diwani, G. I. (2018). Performance and emissions characteristics of C.I. engine fueled with palm oil/palm oil methyl ester blended with diesel fuel. *Egyptian Journal of Petroleum, 27*(2), 215-219.

Gad, & Jayaraj, S. (2020). A comparative study on the effect of nano-additives on the performance and emissions of a diesel engine run on Jatropha biodiesel. *Fuel, 267*, 117168.

Gautam, A., & Agarwal, A. K. (2015). Determination of important biodiesel properties based on fuel temperature correlations for application in a locomotive engine. *Fuel, 142*, 289-302.

Geller, D. P., & Goodrum, J. W. (2004). Effects of specific fatty acid methyl esters on diesel fuel lubricity. *Fuel, 83*(17-18), 2351-2356.

Ghanbari, M., Najafi, G., Ghobadian, B., Yusaf, T., Carlucci, A., & Kiani, M. K. D. (2017). Performance and emission characteristics of a CI engine using nano particles additives in biodiesel-diesel blends and modeling with GP approach. *Fuel, 202*, 699-716.

Gharby, S., Harhar, H., Bouzoubaa, Z., Asdadi, A., El Yadini, A., & Charrouf, Z. (2017). Chemical characterization and oxidative stability of seeds and oil of sesame grown in Morocco. *Journal of the Saudi Society of Agricultural Sciences, 16*(2), 105-111.

Goff, M. J., Bauer, N. S., Lopes, S., Sutterlin, W. R., & Suppes, G. J. (2004). Acid-catalyzed alcoholysis of soybean oil. *Journal of the American Oil Chemists' Society, 81*(4), 415-420.

Gul, Shah, A. N., Aziz, U., Husnain, N., Mujtaba, M., Kousar, T., . . . Hanif, M. F. (2019). Grey-Taguchi and ANN based optimization of a better performing low-emission diesel engine fueled with biodiesel. *Energy Sources, Part A: Recovery, Utilization, and Environmental Effects*, 1-14.

Gul, Zulkifli, N., Masjuki, H., Kalam, M., Mujtaba, M., Harith, M., . . . Farooq, A. B. (2020). Effect of TMP-based-cottonseed oil-biolubricant blends on tribological behavior of cylinder liner-piston ring combinations. *Fuel, 278*, 118242.

Gul, Zulkifli, N. W. M., Kalam, M. A., Masjuki, H. H., Mujtaba, M. A., Yousuf, S., . . . Ahmad, R. (2021). RSM and Artificial Neural Networking based production optimization of sustainable Cotton bio-lubricant and evaluation of its lubricity & tribological properties. *Energy Reports, 7*, 830-839.

Gulzar, M. (2018). *Tribological Study of Nanoparticles Enriched Bio-based Lubricants for Piston Ring–Cylinder Interaction*: Springer.

Gunawan, F., Kurniawan, A., Gunawan, I., Ju, Y.-H., Ayucitra, A., Soetaredjo, F. E., & Ismadji, S. (2014). Synthesis of biodiesel from vegetable oils wastewater sludge by in-situ subcritical methanol transesterification: Process evaluation and optimization. *Biomass and Bioenergy, 69*, 28-38.

Habibullah, Masjuki, H. H., Kalam, M. A., Rizwanul Fattah, I. M., Ashraful, A. M., & Mobarak, H. M. (2014). Biodiesel production and performance evaluation of coconut, palm and their combined blend with diesel in a single-cylinder diesel engine. *Energy Conversion and Management, 87*, 250-257.

Habibullah, M., Masjuki, H. H., Kalam, M., Fattah, I. R., Ashraful, A., & Mobarak, H. (2014). Biodiesel production and performance evaluation of coconut, palm and their combined blend with diesel in a single-cylinder diesel engine. *Energy Conversion Management, 87*, 250-257.

Habibullah, M., Masjuki, H. H., Kalam, M., Zulkifli, N., Masum, B., Arslan, A., & Gulzar, M. (2015). Friction and wear characteristics of Calophyllum inophyllum biodiesel. *Industrial Crops and Products, 76*, 188-197.

Hamze, H., Akia, M., & Yazdani, F. (2015). Optimization of biodiesel production from the waste cooking oil using response surface methodology. *Process Safety and Environmental Protection, 94*, 1-10.

Hassan, M. A. (2012). Studies on Egyptian sesame seeds (Sesamum indicum L.) and its products 1-physicochemical analysis and phenolic acids of roasted Egyptian sesame seeds (Sesamum indicum L.). *World Journal of Dairy & Food Sciences, 7*(2), 195-201.

Hedayat, F., Stevanovic, S., Milic, A., Miljevic, B., Nabi, M., Zare, A., . . . Ristovski, Z. (2016). Influence of oxygen content of the certain types of biodiesels on particulate oxidative potential. *Science of The Total Environment, 545*, 381-388.

Hegde, D. M. (2012). Sesame. In *Handbook of Herbs and Spices* (pp. 449-486).

Heydari-Maleney, K., Taghizadeh-Alisaraei, A., Ghobadian, B., & Abbaszadeh-Mayvan, A. (2017). Analyzing and evaluation of carbon nanotubes additives to diesohol-B2 fuels on performance and emission of diesel engines. *Fuel, 196*, 110-123.

Hoekman, S. K., Broch, A., Robbins, C., Ceniceros, E., & Natarajan, M. (2012). Review of biodiesel composition, properties, and specifications. *Renewable and Sustainable Energy Reviews, 16*(1), 143-169.

Holman, R. T., & Elmer, O. C. (1947). The rates of oxidation of unsaturated fatty acids and esters. *Journal of the American Oil Chemists' Society, 24*(4), 127-129.

Hosseini, S. H., Taghizadeh-Alisaraei, A., Ghobadian, B., & Abbaszadeh-Mayvan, A. (2017a). Effect of added alumina as nano-catalyst to diesel-biodiesel blends on performance and emission characteristics of CI engine. *Energy, 124*, 543-552.

Hosseini, S. H., Taghizadeh-Alisaraei, A., Ghobadian, B., & Abbaszadeh-Mayvan, A. (2017b). Performance and emission characteristics of a CI engine fuelled with carbon nanotubes and diesel-biodiesel blends. *Renewable Energy, 111*, 201-213.

Hu, J., Du, Z., Li, C., & Min, E. (2005). Study on the lubrication properties of biodiesel as fuel lubricity enhancers. *Fuel, 84*(12-13), 1601-1606.

Huang, G.-B., Wang, D. H., & Lan, Y. (2011). Extreme learning machines: a survey. *International journal of machine learning and cybernetics, 2*(2), 107-122.

Ibrahim, A. (2016). Performance and combustion characteristics of a diesel engine fuelled by butanol–biodiesel–diesel blends. *Applied Thermal Engineering, 103*, 651-659.

Ighose, B. O., Adeleke, I. A., Damos, M., Junaid, H. A., Okpalaeke, K. E., & Betiku, E. (2017). Optimization of biodiesel production from Thevetia peruviana seed oil by adaptive neuro-fuzzy inference system coupled with genetic algorithm and response surface methodology. *Energy Conversion and Management, 132*, 231-240.

Imtenan, S., Masjuki, H., Varman, M., Kalam, M., Arbab, M., Sajjad, H., & Rahman, S. A. (2014). Impact of oxygenated additives to palm and jatropha biodiesel blends in the context of performance and emissions characteristics of a light-duty diesel engine. *Energy Conversion and Management, 83*, 149-158.

Imtenan, S., Masjuki, H. H., Varman, M., Fattah, I. R., Sajjad, H., & Arbab, M. (2015). Effect of n-butanol and diethyl ether as oxygenated additives on combustion–emission-performance characteristics of a multiple cylinder diesel engine fuelled with diesel–jatropha biodiesel blend. *Energy Conversion and Management, 94*, 84-94.

Ingole, S., Charanpahari, A., Kakade, A., Umare, S., Bhatt, D., & Menghani, J. (2013). Tribological behavior of nano TiO2 as an additive in base oil. *Wear, 301*(1-2), 776-785.

Ishola, N. B., Okeleye, A. A., Osunleke, A. S., & Betiku, E. (2019). Process modeling and optimization of sorrel biodiesel synthesis using barium hydroxide as a base heterogeneous catalyst: appraisal of response surface methodology, neural network and neuro-fuzzy system. *Neural Computing and Applications, 31*(9), 4929-4943.

Jayaprabakar, J., Anish, M., Beemkumar, N., Mathew, A., & Alex George, A. (2019). Effect of diethyl ether blended with neem oil methyl esters in CI engine. *International Journal of Ambient Energy, 40*(2), 116-118.

Joshi, S., Gogate, P., & Kumar, S. (2018). Intensification of ultrasound assisted esterification of karanja oil for production of biodiesel with optimization using response surface methodology. *Chemical Engineering and Processing - Process Intensification, 124*, 186-198.

Karmakar, A., Karmakar, S., & Mukherjee, S. (2010). Properties of various plants and animals feedstocks for biodiesel production. *Bioresour Technol, 101*(19), 7201-7210.

Kashyap, S. S., Gogate, P. R., & Joshi, S. M. (2019). Ultrasound assisted synthesis of biodiesel from karanja oil by interesterification: Intensification studies and optimization using RSM. *Ultrasonics Sonochemistry, 50*, 36-45.

Kaya, C., Hamamci, C., Baysal, A., Akba, O., Erdogan, S., & Saydut, A. (2009). Methyl ester of peanut (Arachis hypogea L.) seed oil as a potential feedstock for biodiesel production. *Renewable Energy, 34*(5), 1257-1260.

Khalife, E., Tabatabaei, M., Demirbas, A., & Aghbashlo, M. (2017a). Impacts of additives on performance and emission characteristics of diesel engines during steady state operation. *Progress in Energy and Combustion Science, 59*, 32-78.

Khalife, E., Tabatabaei, M., Demirbas, A., & Aghbashlo, M. (2017b). Impacts of additives on performance and emission characteristics of diesel engines during steady state operation. *Progress in energy combustion science, 59*, 32-78.

Khan, A. V., Ahmed, Q. U., Khan, M. W., & Khan, A. A. (2014). Herbal cure for poisons and poisonous bites from Western Uttar Pradesh, India. *Asian Pacific Journal of Tropical Disease, 4*, S116-S120.

Knothe, G., & Dunn, R. O. (2003). Dependence of oil stability index of fatty compounds on their structure and concentration and presence of metals. *Journal of the American Oil Chemists' Society, 80*(10), 1021-1026.

Knothe, G., & Steidley, K. R. (2005). Lubricity of components of biodiesel and petrodiesel. The origin of biodiesel lubricity. *Energy & Fuels, 19*(3), 1192-1200.

Konishi, T., Klaus, E., & Duda, J. (1996). Wear characteristics of aluminum-silicon alloy under lubricated sliding conditions. *Tribology Transactions, 39*(4), 811-818.

Kumar, N. (2017). Oxidative stability of biodiesel: Causes, effects and prevention. *Fuel, 190*, 328-350.

Kumar, R., Tiwari, P., & Garg, S. (2013). Alkali transesterification of linseed oil for biodiesel production. *Fuel, 104*, 553-560.

Kumar, S., Dinesha, P., Ajay, C., & Kabbur, P. (2020). Combined effect of oxygenated liquid and metal oxide nanoparticle fuel additives on the combustion characteristics of a biodiesel engine operated with higher blend percentages. *Energy, 197*, 117194.

Kurtgoz, Y., Karagoz, M., & Deniz, E. (2017). Biogas engine performance estimation using ANN. *Engineering Science and Technology, an International Journal, 20*(6), 1563-1570.

Kuszewski, H., Jaworski, A., & Ustrzycki, A. (2017). Lubricity of ethanol–diesel blends–Study with the HFRR method. *Fuel, 208*, 491-498.

Laad, M., & Jatti, V. K. S. (2018). Titanium oxide nanoparticles as additives in engine oil. *Journal of King Saud University - Engineering Sciences, 30*(2), 116-122.

Lam, M. K., Tan, K. T., Lee, K. T., & Mohamed, A. R. (2009). Malaysian palm oil: Surviving the food versus fuel dispute for a sustainable future. *Renewable and Sustainable Energy Reviews, 13*(6-7), 1456-1464.

Lanjekar, R. D., & Deshmukh, D. (2016). A review of the effect of the composition of biodiesel on NOx emission, oxidative stability and cold flow properties. *Renewable and Sustainable Energy Reviews, 54*, 1401-1411.

Lapuerta, M., Armas, O., & Rodriguez-Fernandez, J. (2008). Effect of biodiesel fuels on diesel engine emissions. *Progress in energy combustion science, 34*(2), 198-223.

Lapuerta, M., Garcia-Contreras, R., & Agudelo, J. R. (2010). Lubricity of ethanol-biodiesel-diesel fuel blends. *Energy & Fuels, 24*(2), 1374-1379.

Latiff, R. (2020). Malaysia to implement B30 biodiesel mandate in transport sector before 2025 [Press release]. Retrieved from https://www.reuters.com/article/us-

malaysia-palmoil-biodiesel/malaysia-to-implement-b30-biodiesel-mandate-in-transport-sector-before-2025-idUSKBN20F0D8

Lee, J., Lee, Y., & Choe, E. (2008). Effects of sesamol, sesamin, and sesamolin extracted from roasted sesame oil on the thermal oxidation of methyl linoleate. *LWT-Food Science and Technology, 41*(10), 1871-1875.

Liu, W., Lu, G., Yang, G., & Bi, Y. (2019). Improving oxidative stability of biodiesel by cis-trans isomerization of carbon-carbon double bonds in unsaturated fatty acid methyl esters. *Fuel, 242*, 133-139.

Ma, F., & Hanna, M. A. (1999). Biodiesel production: a review. *Bioresource Technology, 70*(1), 1-15.

Maddikeri, G. L., Pandit, A. B., & Gogate, P. R. (2013). Ultrasound assisted interesterification of waste cooking oil and methyl acetate for biodiesel and triacetin production. *Fuel Processing Technology, 116*, 241-249.

Mahlia, T., Syazmi, Z., Mofijur, M., Abas, A. P., Bilad, M., Ong, H. C., & Silitonga, A. (2020). Patent landscape review on biodiesel production: Technology updates. *Renewable and Sustainable Energy Reviews, 118*, 109526.

Maleque, M. A., Masjuki, H. H., & Haseeb, A. (2000). Effect of mechanical factors on tribological properties of palm oil methyl ester blended lubricant. *Wear, 239*(1), 117-125.

Maran, J. P., Manikandan, S., Nivetha, C. V., & Dinesh, R. (2017). Ultrasound assisted extraction of bioactive compounds from Nephelium lappaceum L. fruit peel using central composite face centered response surface design. *Arabian Journal of Chemistry, 10*, S1145-S1157.

Maran, J. P., Sivakumar, V., Sridhar, R., & Immanuel, V. P. (2013). Development of model for mechanical properties of tapioca starch based edible films. *Industrial Crops and Products, 42*, 159-168.

Martinez-Guerra, E., & Gude, V. G. (2014). Transesterification of used vegetable oil catalyzed by barium oxide under simultaneous microwave and ultrasound irradiations. *Energy Conversion and Management, 88*, 633-640.

Martinez-Guerra, E., & Gude, V. G. (2016). Determining optimum pulse mode for ultrasound enhanced biodiesel production. *Journal of Industrial and Engineering Chemistry, 35*, 14-19.

Marwaha, A., Rosha, P., Mohapatra, S. K., Mahla, S. K., & Dhir, A. (2019). Biodiesel production from Terminalia bellerica using eggshell-based green catalyst: An optimization study with response surface methodology. *Energy Reports, 5*, 1580-1588.

Mat Yasin, M. H., Mamat, R., Najafi, G., Ali, O. M., Yusop, A. F., & Ali, M. H. (2017). Potentials of palm oil as new feedstock oil for a global alternative fuel: A review. *Renewable and Sustainable Energy Reviews, 79*, 1034-1049.

Mehmood, S., Saeed, D. A., Rizwan, M., Khan, M. N., Aziz, O., Bashir, S., . . . Shaheen, A. (2018). Impact of different amendments on biochemical responses of sesame (Sesamum indicum L.) plants grown in lead-cadmium contaminated soil. *Plant Physiology and Biochemistry, 132*, 345-355.

Mei, D., Zuo, L., Adu-Mensah, D., Li, X., & Yuan, Y. (2019). Combustion characteristics and emissions of a common rail diesel engine using nanoparticle-diesel blends with carbon nanotube and molybdenum trioxide. *Applied Thermal Engineering, 162*, 114238.

Milano, J., Ong, H. C., Masjuki, H. H., Silitonga, A. S., Chen, W.-H., Kusumo, F., . . . Sebayang, A. H. (2018). Optimization of biodiesel production by microwave irradiation-assisted transesterification for waste cooking oil-Calophyllum inophyllum oil via response surface methodology. *Energy Conversion and Management, 158*, 400-415.

Moazzami, A., & Kamal-Eldin, A. (2009). 8 - Sesame Seed Oil. In R. A. Moreau & A. Kamal-Eldin (Eds.), *Gourmet and Health-Promoting Specialty Oils* (pp. 267-282): AOCS Press.

Morris, J. B. (2002). Food, industrial, nutraceutical, and pharmaceutical uses of sesame genetic resources. *Trends in new crops and new uses*, 153-156.

Moser, B. R. (2009). Comparative oxidative stability of fatty acid alkyl esters by accelerated methods. *Journal of the American Oil Chemists' Society, 86*(7), 699-706.

Mubashir, G. (2017). *Tribological study of nanoparticles enrichedbio-based lubricants for engine piston ring–cylinder interaction.* (PhD), University of Malaya, Malaysia.

Murcak, A., Haşimoğlu, C., Çevik, İ., Karabektaş, M., & Ergen, G. (2013). Effects of ethanol–diesel blends to performance of a DI diesel engine for different injection timings. *Fuel, 109*, 582-587.

Muthukumaran, C., Praniesh, R., Navamani, P., Swathi, R., Sharmila, G., & Kumar, N. M. (2017). Process optimization and kinetic modeling of biodiesel production using non-edible Madhuca indica oil. *Fuel, 195*, 217-225.

Nadeem, M., Rangkuti, C., Anuar, K., Haq, M., Tan, I., & Shah, S. (2006). Diesel engine performance and emission evaluation using emulsified fuels stabilized by conventional and gemini surfactants. *Fuel, 85*(14-15), 2111-2119.

Nagaraja, S., Soorya Prakash, K., Sudhakaran, R., & Sathish Kumar, M. (2016). Investigation on the emission quality, performance and combustion characteristics of the compression ignition engine fueled with environmental friendly corn oil methyl ester – Diesel blends. *Ecotoxicology and Environmental Safety, 134*, 455-461.

Naik, N. S., & Balakrishna, B. (2018). A comparative study of B10 biodiesel blends and its performance and combustion characteristics. *International Journal of Ambient Energy, 39*(3), 257-263.

Najafi, G. (2018). Diesel engine combustion characteristics using nano-particles in biodiesel-diesel blends. *Fuel, 212*, 668-678.

Nanthagopal, K., Ashok, B., Garnepudi, R. S., Tarun, K. R., & Dhinesh, B. (2019). Investigation on diethyl ether as an additive with Calophyllum Inophyllum biodiesel for CI engine application. *Energy Conversion and Management, 179*, 104-113.

Nanthagopal, K., Ashok, B., Tamilarasu, A., Johny, A., & Mohan, A. (2017). Influence on the effect of zinc oxide and titanium dioxide nanoparticles as an additive with Calophyllum inophyllum methyl ester in a CI engine. *Energy Conversion and Management, 146*, 8-19.

Nayak, M. G., & Vyas, A. P. (2019). Optimization of microwave-assisted biodiesel production from Papaya oil using response surface methodology. *Renewable Energy, 138*, 18-28.

Nguyen, T., Pham, M., & Le Anh, T. (2020). Spray, combustion, performance and emission characteristics of a common rail diesel engine fueled by fish-oil biodiesel blends. *Fuel, 269*, 117108.

Niju, S., Rabia, R., Devi, K. S., Kumar, M. N., & Balajii, M. (2020). Modified Malleus Malleus shells for biodiesel production from waste cooking oil: An optimization study using box–behnken design. *Waste Biomass Valorization, 11*(3), 793-806.

Nzikou, J., Matos, L., Bouanga-Kalou, G., Ndangui, C., Pambou-Tobi, N., Kimbonguila, A., . . . Desobry, S. (2009). Chemical composition on the seeds and oil of sesame (Sesamum indicum L.) grown in Congo-Brazzaville. *Advance Journal of Food Science and Technology, 1*(1), 6-11.

Okoye, P. U., Wang, S., Khanday, W. A., Li, S., Tang, T., & Zhang, L. (2020). Box-Behnken optimization of glycerol transesterification reaction to glycerol carbonate over calcined oil palm fuel ash derived catalyst. *Renewable Energy, 146*, 2676-2687.

Ong, H. C., Masjuki, H., Mahlia, T., Silitonga, A., Chong, W., & Yusaf, T. (2014a). Engine performance and emissions using Jatropha curcas, Ceiba pentandra and Calophyllum inophyllum biodiesel in a CI diesel engine. *Energy, 69*, 427-445.

Ong, H. C., Masjuki, H., Mahlia, T. I., Silitonga, A., Chong, W., & Yusaf, T. (2014b). Engine performance and emissions using Jatropha curcas, Ceiba pentandra and Calophyllum inophyllum biodiesel in a CI diesel engine. *Energy, 69*, 427-445.

Ong, H. C., Milano, J., Silitonga, A. S., Hassan, M. H., Shamsuddin, A. H., Wang, C.-T., . . . Sutrisno, J. (2019). Biodiesel production from Calophyllum inophyllum-Ceiba pentandra oil mixture: Optimization and characterization. *Journal of Cleaner Production, 219*, 183-198.

Onoji, S. E., Iyuke, S. E., Igbafe, A. I., & Nkazi, D. B. (2016). Rubber seed oil: A potential renewable source of biodiesel for sustainable development in sub-Saharan Africa. *Energy Conversion and Management, 110*, 125-134.

Örs, I., Sarıkoç, S., Atabani, A., Ünalan, S., & Akansu, S. (2018). The effects on performance, combustion and emission characteristics of DICI engine fuelled with TiO2 nanoparticles addition in diesel/biodiesel/n-butanol blends. *Fuel, 234*, 177-188.

Özener, O., Yüksek, L., Ergenç, A. T., & Özkan, M. (2014). Effects of soybean biodiesel on a DI diesel engine performance, emission and combustion characteristics. *Fuel, 115*, 875-883.

Pan, Qian, W., Zheng, Z., Huang, R., Zhou, X., Huang, H., & Li, M. (2019). The potential of dimethyl carbonate (DMC) as an alternative fuel for compression ignition engines with different EGR rates. *Fuel, 257*, 115920.

Pan, Qu, W., Ma, H., Atungulu, G. G., & McHugh, T. H. (2011). Continuous and pulsed ultrasound-assisted extractions of antioxidants from pomegranate peel. *Ultrasonics Sonochemistry, 18*(5), 1249-1257.

Park, J.-Y., Kim, D.-K., Lee, J.-P., Park, S.-C., Kim, Y.-J., & Lee, J.-S. (2008). Blending effects of biodiesels on oxidation stability and low temperature flow properties. *Bioresource Technology, 99*(5), 1196-1203.

Patel, R. L., & Sankhavara, C. D. (2017). Biodiesel production from Karanja oil and its use in diesel engine: A review. *Renewable and Sustainable Energy Reviews, 71*, 464-474.

Patil, P. D., & Deng, S. (2009). Optimization of biodiesel production from edible and non-edible vegetable oils. *Fuel, 88*(7), 1302-1306.

Prakash Maran, J., Manikandan, S., Vigna Nivetha, C., & Dinesh, R. (2017). Ultrasound assisted extraction of bioactive compounds from Nephelium lappaceum L. fruit peel using central composite face centered response surface design. *Arabian Journal of Chemistry, 10*, S1145-S1157.

Prakash Maran, J., Mekala, V., & Manikandan, S. (2013). Modeling and optimization of ultrasound-assisted extraction of polysaccharide from Cucurbita moschata. *Carbohydrate polymers, 92*(2), 2018-2026.

Pullen, J., & Saeed, K. (2012). An overview of biodiesel oxidation stability. *Renewable and Sustainable Energy Reviews, 16*(8), 5924-5950. doi:https://doi.org/10.1016/j.rser.2012.06.024

Pullen, J., & Saeed, K. (2014). Experimental study of the factors affecting the oxidation stability of biodiesel FAME fuels. *Fuel Processing Technology, 125*, 223-235.

Qi, D. H., Chen, H., Geng, L. M., & Bian, Y. Z. (2011). Effect of diethyl ether and ethanol additives on the combustion and emission characteristics of biodiesel-diesel blended fuel engine. *Renewable Energy, 36*(4), 1252-1258.

Rabinowicz, E. (1984). The least wear. *Wear, 100*(1-3), 533-541.

Raju, V. D., Kishore, P., Nanthagopal, K., & Ashok, B. (2018). An experimental study on the effect of nanoparticles with novel tamarind seed methyl ester for diesel engine applications. *Energy conversion management, 164*, 655-666.

Rakopoulos, D. C., Rakopoulos, C. D., Giakoumis, E. G., Papagiannakis, R. G., & Kyritsis, D. C. (2014). Influence of properties of various common bio-fuels on the combustion and emission characteristics of high-speed DI (direct injection) diesel engine: Vegetable oil, bio-diesel, ethanol, n-butanol, diethyl ether. *Energy, 73*, 354-366.

Ramírez-Verduzco, L. F., Rodríguez-Rodríguez, J. E., & del Rayo Jaramillo-Jacob, A. (2012). Predicting cetane number, kinematic viscosity, density and higher heating value of biodiesel from its fatty acid methyl ester composition. *Fuel, 91*(1), 102-111.

Ramírez Verduzco, L. F. (2013). Density and viscosity of biodiesel as a function of temperature: Empirical models. *Renewable and Sustainable Energy Reviews, 19*, 652-665.

Ramos, M. J., Fernández, C. M., Casas, A., Rodríguez, L., & Pérez, Á. (2009). Influence of fatty acid composition of raw materials on biodiesel properties. *Bioresource Technology, 100*(1), 261-268.

Rashed, M. M., Kalam, M. A., Masjuki, H. H., Mofijur, M., Rasul, M. G., & Zulkifli, N. W. M. (2016). Performance and emission characteristics of a diesel engine fueled with palm, jatropha, and moringa oil methyl ester. *Industrial Crops and Products, 79*, 70-76.

REN21. (2018). *Renewables 2018 Global Status Report* (978-3-9818911-3-3). Retrieved from Paris: https://www.ren21.net/gsr-2018/chapters/chapter_01/chapter_01/

REN21. (2019). *Renewables 2019 Global Status Report* (978-3-9818911-3-3). Retrieved from Paris: https://www.ren21.net/gsr-2019/chapters/chapter_01/chapter_01/#sub_1_1

REN21. (2020). *Renewables 2020 Global Status Report* (978-3-948393-00-7). Retrieved from Paris: https://www.ren21.net/gsr-2020/chapters/chapter_01/chapter_01/#sub_4

Rounce, P., Tsolakis, A., Leung, P., & York, A. (2010). A comparison of diesel and biodiesel emissions using dimethyl carbonate as an oxygenated additive. *Energy Fuels, 24*(9), 4812-4819.

S Gavhane, R., M Kate, A., Pawar, A., Safaei, M. R., M Soudagar, M. E., Mujtaba Abbas, M., . . . Badruddin, I. A. (2020). Effect of Zinc Oxide Nano-Additives and Soybean Biodiesel at Varying Loads and Compression Ratios on VCR Diesel Engine Characteristics. *Symmetry, 12*(6), 1042.

Sajjadi, B., Raman, A. A. A., & Arandiyan, H. (2016). A comprehensive review on properties of edible and non-edible vegetable oil-based biodiesel: Composition, specifications and prediction models. *Renewable and Sustainable Energy Reviews, 63*, 62-92.

Saloua, F., Eddine, N. I., & Hedi, Z. (2009). Chemical composition and profile characteristics of Osage orange Maclura pomifera (Rafin.) Schneider seed and seed oil. *Industrial Crops and Products, 29*(1), 1-8.

Sarve, Sonawane, S. S., & Varma, M. N. (2015). Ultrasound assisted biodiesel production from sesame (Sesamum indicum L.) oil using barium hydroxide as a heterogeneous catalyst: Comparative assessment of prediction abilities between response surface methodology (RSM) and artificial neural network (ANN). *Ultrasonics Sonochemistry, 26*, 218-228.

Saxena, V., Kumar, N., & Saxena, V. K. (2017). A comprehensive review on combustion and stability aspects of metal nanoparticles and its additive effect on diesel and biodiesel fuelled CI engine. *Renewable Sustainable Energy Reviews, 70*, 563-588.

Saxena, V., Kumar, N., & Saxena, V. K. (2019). Multi-objective optimization of modified nanofluid fuel blends at different TiO2 nanoparticle concentration in diesel engine: Experimental assessment and modeling. *Applied Energy, 248*, 330-353.

Saydut, Duz, M. Z., Kaya, C., Kafadar, A. B., & Hamamci, C. (2008). Transesterified sesame (Sesamum indicum L.) seed oil as a biodiesel fuel. *Bioresour Technology, 99*(14), 6656-6660.

Saydut, A., Erdogan, S., Kafadar, A. B., Kaya, C., Aydin, F., & Hamamci, C. (2016). Process optimization for production of biodiesel from hazelnut oil, sunflower oil and their hybrid feedstock. *Fuel, 183*, 512-517.

Sendzikiene, E., Makareviciene, V., & Janulis, P. (2005). Oxidation Stability of Biodiesel Fuel Produced from Fatty Wastes. *Polish Journal of Environmental Studies, 14*(3).

Shahnazar, S., Bagheri, S., & Abd Hamid, S. B. (2016). Enhancing lubricant properties by nanoparticle additives. *International Journal of Hydrogen Energy, 41*(4), 3153-3170.

Shanmugaprakash, M., & Sivakumar, V. (2013). Development of experimental design approach and ANN-based models for determination of Cr (VI) ions uptake rate from aqueous solution onto the solid biodiesel waste residue. *Bioresource Technology, 148*, 550-559.

Sharon, H., Ram, P. J. S., Fernando, K. J., Murali, S., & Muthusamy, R. (2013). Fueling a stationary direct injection diesel engine with diesel-used palm oil–butanol blends–an experimental study. *Energy Conversion and Management, 73*, 95-105.

Silitonga, A. S., Mahlia, T. M. I., Kusumo, F., Dharma, S., Sebayang, A. H., Sembiring, R. W., & Shamsuddin, A. H. (2019). Intensification of Reutealis trisperma biodiesel production using infrared radiation: Simulation, optimisation and validation. *Renewable Energy, 133*, 520-527.

Silitonga, A. S., Masjuki, H. H., Mahlia, T. M. I., Ong, H. C., Chong, W. T., & Boosroh, M. H. (2013). Overview properties of biodiesel diesel blends from edible and non-edible feedstock. *Renewable and Sustainable Energy Reviews, 22*, 346-360.

Silitonga, A. S., Shamsuddin, A. H., Mahlia, T. M. I., Milano, J., Kusumo, F., Siswantoro, J., . . . Ong, H. C. (2020). Biodiesel synthesis from Ceiba pentandra oil by microwave irradiation-assisted transesterification: ELM modeling and optimization. *Renewable Energy, 146*, 1278-1291.

Singh, S. P., & Singh, D. (2010). Biodiesel production through the use of different sources and characterization of oils and their esters as the substitute of diesel: A review. *Renewable and Sustainable Energy Reviews, 14*(1), 200-216.

Singh, Y., Singla, A., Kumar, A., & Kumar, D. (2016). Friction and wear characteristics of jatropha oil-based biodiesel blended lubricant at different loads. *Energy Sources, Part A: Recovery, Utilization, and Environmental Effects, 38*(18), 2749-2755.

Singh, Y., Singla, A., & Singh, A. K. (2017). Sustainability of Moringa-oil–based biodiesel blended lubricant. *Energy Sources, Part A: Recovery, Utilization, and Environmental Effects, 39*(3), 313-319.

Soudagar, Nik-Ghazali, N.-N., Abul Kalam, M., Badruddin, I. A., Banapurmath, N. R., & Akram, N. (2018). The effect of nano-additives in diesel-biodiesel fuel blends: A comprehensive review on stability, engine performance and emission characteristics. *Energy Conversion and Management, 178*, 146-177.

Soudagar, M. E. M., Banapurmath, N. R., Afzal, A., Hossain, N., Abbas, M. M., Haniffa, M. A. C. M., . . . Mubarak, N. M. (2020). Study of diesel engine characteristics by adding nanosized zinc oxide and diethyl ether additives in Mahua biodiesel–diesel fuel blend. *Scientific Reports, 10*(1), 15326.

Soudagar, M. E. M., Nik-Ghazali, N.-N., Kalam, M., Badruddin, I. A., Banapurmath, N., Ali, M. A. B., . . . Akram, N. (2020). An investigation on the influence of aluminium oxide nano-additive and honge oil methyl ester on engine performance, combustion and emission characteristics. *Renewable Energy, 146*, 2291-2307.

Soudagar, M. E. M., Nik-Ghazali, N.-N., Kalam, M., Badruddin, I. A., Banapurmath, N., Khan, T. Y., . . . Afzal, A. (2019). The effects of graphene oxide nanoparticle additive stably dispersed in dairy scum oil biodiesel-diesel fuel blend on CI engine: performance, emission and combustion characteristics. *Fuel, 257*, 116015.

Sperring, T., & Nowell, T. (2005). SYCLOPS—a qualitative debris classification system developed for RAF early failure detection centres. *Tribology International, 38*(10), 898-903.

Strömberg, N., Saramat, A., & Eriksson, H. (2013). Biodiesel degradation rate after refueling. *Fuel, 105*, 301-305.

Subhedar, P. B., & Gogate, P. R. (2016). Ultrasound assisted intensification of biodiesel production using enzymatic interesterification. *Ultrasonics Sonochemistry, 29*, 67-75.

Sulek, M., Kulczycki, A., & Malysa, A. (2010). Assessment of lubricity of compositions of fuel oil with biocomponents derived from rape-seed. *Wear, 268*(1-2), 104-108.

Taha-Tijerina, J., Shaji, S., Sharma Kanakkillam, S., Mendivil Palma, M. I., & Aviña, K. (2020). Tribological and Thermal Transport of Ag-Vegetable Nanofluids Prepared by Laser Ablation. *10*(5), 1779.

Tan, S. X., Lim, S., Ong, H. C., & Pang, Y. L. (2019). State of the art review on development of ultrasound-assisted catalytic transesterification process for biodiesel production. *Fuel, 235*, 886-907.

Ünal, M. K., & Yalçın, H. (2008). Proximate composition of Turkish sesame seeds and characterization of their oils. *Grasas y aceites, 59*(1), 23-26.

Uusitalo, V., Leino, M., Kasurinen, H., & Linnanen, L. (2017). Transportation biofuel efficiencies from cultivated feedstock in the boreal climate zone: Case Finland. *Biomass and Bioenergy, 99*, 79-89.

Valihesari, M., Pirouzfar, V., Ommi, F., & Zamankhan, F. (2019). Investigating the effect of Fe2O3 and TiO2 nanoparticle and engine variables on the gasoline engine performance through statistical analysis. *Fuel, 254*, 115618.

Vardoulakis, S., Dimitroulopoulou, C., Thornes, J., Lai, K.-M., Taylor, J., Myers, I., . . . Chalabi, Z. (2015). Impact of climate change on the domestic indoor environment and associated health risks in the UK. *Environment International, 85*, 299-313.

Viesca, J. L., Hernández Battez, A., González, R., Chou, R., & Cabello, J. J. (2011). Antiwear properties of carbon-coated copper nanoparticles used as an additive to a polyalphaolefin. *Tribology International, 44*(7), 829-833.

Wadumesthrige, K., Ara, M., Salley, S. O., & Ng, K. Y. S. (2009). Investigation of Lubricity Characteristics of Biodiesel in Petroleum and Synthetic Fuel. *Energy & Fuels, 23*(4), 2229-2234.

Wakil, Kalam, M., Masjuki, H., Fattah, I. R., & Masum, B. (2014). Evaluation of rice bran, sesame and moringa oils as feasible sources of biodiesel and the effect of blending on their physicochemical properties. *RSC Advances, 4*(100), 56984-56991.

Wakil, Kalam, M. A., Masjuki, H. H., Atabani, A. E., & Rizwanul Fattah, I. M. (2015). Influence of biodiesel blending on physicochemical properties and importance of mathematical model for predicting the properties of biodiesel blend. *Energy Conversion and Management, 94*, 51-67.

Wakil, Masjuki, H. H., Kalam, M., Teoh, Y., How, H., & Imtenan, S. (2015). Influence of engine operating variable on combustion to reduce exhaust emissions using various biodiesels blend. *RSC Advances, 5*(122), 100674-100681.

Wang, D., Wang, P., & Ji, Y. (2015). An oscillation bound of the generalization performance of extreme learning machine and corresponding analysis. *Neurocomputing, 151*, 883-890.

Were, B. A., Onkware, A. O., Gudu, S., Welander, M., & Carlsson, A. S. (2006). Seed oil content and fatty acid composition in East African sesame (Sesamum indicum L.) accessions evaluated over 3 years. *Field Crops Research, 97*(2-3), 254-260.

Wong, K. I., Wong, P. K., Cheung, C. S., & Vong, C. M. (2013). Modeling and optimization of biodiesel engine performance using advanced machine learning methods. *Energy, 55*, 519-528.

Wu, Tsui, W. C., & Liu, T. C. (2007). Experimental analysis of tribological properties of lubricating oils with nanoparticle additives. *Wear, 262*(7), 819-825.

Yamane, K., Kawasaki, K., Sone, K., Hara, T., & Prakoso, T. (2007). Oxidation stability of biodiesel and its effects on diesel combustion and emission characteristics. *International Journal of Engine Research, 8*(3), 307-319.

Yang, Z., Hollebone, B. P., Wang, Z., Yang, C., & Landriault, M. (2013). Factors affecting oxidation stability of commercially available biodiesel products. *Fuel Processing Technology, 106*, 366-375.

Yasin, M. M., Yusaf, T., Mamat, R., & Yusop, A. F. (2014). Characterization of a diesel engine operating with a small proportion of methanol as a fuel additive in biodiesel blend. *Applied Energy, 114*, 865-873.

Younis, K. A., Gardy, J., & Barzinji, K. S. (2014). Production and characterization of biodiesel from locally sourced sesame seed oil, used cooking oil and other commercial vegetable oils in Erbil-Iraqi Kurdistan. *American Journal of Applied Chemistry., 2*, 105.

Yusup, S., & Khan, M. (2010). Basic properties of crude rubber seed oil and crude palm oil blend as a potential feedstock for biodiesel production with enhanced cold flow characteristics. *Biomass and Bioenergy, 34*(10), 1523-1526.

Zhang, J., Niu, S., Zhang, Y., Tang, C., Jiang, X., Hu, E., & Huang, Z. (2013). Experimental and modeling study of the auto-ignition of n-heptane/n-butanol mixtures. *Combustion Flame, 160*(1), 31-39.

Zhang, Z., Lu, Y., Wang, Y., Yu, X., Smallbone, A., Dong, C., & Roskilly, A. P. (2019). Comparative study of using multi-wall carbon nanotube and two different sizes of cerium oxide nanopowders as fuel additives under various diesel engine conditions. *Fuel, 256*, 115904.

Zulkifli, N. W. M., Kalam, M. A., Masjuki, H. H., Shahabuddin, M., & Yunus, R. (2013). Wear prevention characteristics of a palm oil-based TMP (trimethylolpropane) ester as an engine lubricant. *Energy, 54*, 167-173.

LIST OF PUBLICATIONS

1. **Mujtaba, M. A.**, et al. (2020). Critical review on sesame seed oil and its methyl ester on cold flow and oxidation stability. **Energy Reports**. https://doi.org/10.1016/j.egyr.2019.11.160 **(ISI Indexed, Q1 Published)**

2. **Mujtaba, M. A.**, et al. (2020). Ultrasound-assisted process optimization and tribological characteristics of biodiesel from palm-sesame oil via response surface methodology and extreme learning machine - Cuckoo search. **Renewable Energy**. https://doi.org/10.1016/j.renene.2020.05.158 **(ISI Indexed, Q1 Published)**

3. **Mujtaba M.A.**, et al. (2020). Comparative study of nanoparticles and alcoholic fuel additives-biodiesel-diesel blend for performance and emission improvements. **Fuel**. https://doi.org/10.1016/j.fuel.2020.118434 2020;279:118434 **(ISI Indexed, Q1 Published)**

4. **Mujtaba, M. A.**, et al. (2020). Effect of alcoholic and nano-particles additives on tribological properties of diesel-palm-sesame-biodiesel blends. **Energy Reports**. https://doi.org/10.1016/j.egyr.2020.12.009 **(ISI Indexed, Q1 Published)**

5. **Mujtaba, M. A.**, et al. (2021) Effect of palm-sesame biodiesel fuels with alcoholic and nanoparticle additives on tribological characteristics of lubricating oil by four ball tribo-tester. **Alexandria Engineering**. https://doi.org/10.1016/j.aej.2021.03.017 **(ISI Indexed, Q1)**

6. **Mujtaba M.A.**, et al. (2020) Effect of Additivized Biodiesel Blends on Diesel Engine Performance, Emission, Tribological Characteristics, and Lubricant Tribology. **Energies**. https://doi.org/10.3390/en13133375 **(ISI Indexed, Q3 Published)**

7. **Mujtaba M.A.**, et al. (2021) Effect of primary and secondary alcohols as oxygenated additives on the performance and emission characteristics of diesel engine. **Energy Reports**. https://doi.org/10.1016/j.egyr.2020.12.008 **(ISI Indexed, Q1 Published)**

8. **Mujtaba M.A.**, et al. (2021) Development of empirical correlations for density and viscosity estimation of ternary biodiesel blends. **Renewable Energy**. https://doi.org/10.1016/j.renene.2021.07.121 **(ISI Indexed, Q1 Published)**